APPENDIX N° 1
TO THE FINAL TECHNICAL REPORT,
CONTRACT DAJA 45-90-C-0052
(October, 1992)

APPROXIMATE ANALYSIS ON STRAIN RATE EFFECTS AND BEHAVIOR OF STRESS AND STRAIN FIELDS AT THE CRACK TIP IN MODE II IN METALLIC MATERIALS

b y

I.V. VARFOLOMEYEV

and

J.R. KLEPACZKO

LABORATOIRE DE PHYSIQUE ET
MECANIQUE DES MATERIAUX
U.R.A. C.N.R.S. N° 1215

INSTITUT SUPERIEUR DE GENIE MECANIQUE
ET PRODUCTIQUE

DISTRIBUTION UNLIMITED

UNIVERSITE DE METZ

CONTENTS

1. Introduction

Analysis of conditions for crack initiation and fracture toughness in the case of metallic materials under various loading rates are the problems of great interest in fracture mechanics. For Mode I and Mode III several investigations have been carried out to reveal the loading rate effect ($\dot{K}_I$, $\dot{K}_{III}$) on fracture toughness (K_{IC}, K_{IIIC}). At the same time, systematic analyses have been performed for majority of structural materials to study strain rate ($\dot{\varepsilon}$) effect on the yield stress (σ_Y), ultimate stress (σ_u), material strain hardening, etc. Using of such data, some correlations between fracture toughness and parameters of stress-strain diagram at different strain rates have been derived (Klepaczko, 1990). The theoretical background of such correlations consists of solutions for elastic and elastic-plastic stress-strain fields near a crack tip, such as Williams' (1957) linear-elastic solution for crack tip fields at a stationary crack; approximate analyses of Irwin (1960), Dugdale (1960) (often refered to as the Barenblatt-Dugdale-Bilby-Cottrell-Swinden model), Duffy (1969) for the size and shape of the crack tip plastic zone; solutions of Tuba (1966) as well as Hutchinson (1968a) and Rice and Rosengren (1968) (refered to as the HRR-solution) for crack tip fields in elastic-plastic materials. Analyses of stress distribution at the tip of a stationary crack under dynamic loading have been performed by Freund (1990) and Lee and Freund (1990).

Application of the HRR-solution and criterion of cleavage fracture in the form (Ritchie *et al.*, 1973)

$$K_I = K_{IC} \quad \text{when} \quad \sigma_{yy} = \sigma_F \text{ at } x = l_F$$

results in the following relationship

$$K_{IC} = \sigma_Y \left(\frac{\sigma_F}{\sigma_Y}\right)^{(N+1)/2} \left[\frac{\alpha \; I(N) \; l_F}{(1-\nu^2)\Sigma_{yy}^{N+1}}\right]^{1/2} \tag{1.1}$$

where σ_F is the critical cleavage stress; l_F is characteristic distance ahead of the crack tip; σ_{yy} is the stress component in Cartesian coordinates (x,y) with the origin at the crack tip (Fig.1); α and N are material constants in the Ramberg-Osgood equation

$$\frac{\varepsilon}{\varepsilon_Y} = \frac{\sigma}{\sigma_Y} + \alpha \left(\frac{\sigma}{\sigma_Y}\right)^N \tag{1.2}$$

with $\varepsilon_Y = \sigma_Y/E$; E and ν are Young's modulus and Poisson's ratio; Σ_{yy} and $I(N)$

are coordinate function and numerical factor in the HRR-solution (see Chapter 3).

Another important application of fracture mechanics arises from a relationship between loading rate and specimen thickness for fracture

toughness measurements, i.e. $B=f(\dot{K}_I)$. The reason for limitations on the B value turns out from requirements of small scale yielding or, equivalently, restrictions on the crack tip plastic zone size, r_p. Thus, making use of Irwin's (1960) correction for plane strain, one finds

$$r_p = \frac{1}{3\pi} \left(\frac{K_I}{\sigma_Y}\right)^2 \qquad (1.3)$$

The well-known ASTM limiting condition

$$B \geq 2.5 \, (K_{IC}/\sigma_Y)^2 \qquad (1.4)$$

is found to be equivalent to the following one

$$B \geq 24 r_p \qquad (1.5)$$

Since the r_p value is diminishing with increasing the loading rate, specimens smaller in dimensions can be employed in K_{IC} tests at high

loading rates. An example of correlation between B and $\dot{K}_I$ is given by Klepaczko (1990).

It should be noted that the majority of experimental and theoretical results on rate sensitivity of fracture toughness are obtained for cracks in Mode I and Mode III (see Klepaczko, 1990). For in-plane shear cracks (Mode II) such solutions are not available. No much progress is achieved in experimental techniques for measurements of fracture toughness (K_{IIC}, J_{IIC}) in Mode II. Only a few works are known on experimental studies of Mode II crack behavior at quasi-static case (Banks-Sills and Arcan, 1986; Banks-Sills and Sherman, 1991; Davies et al., 1985; Hoyniak and Conway, 1979; Maccagno and Knott, 1992; Mall and Mol, 1991; Tohgo et al., 1989; Tohgo and Ishii, 1992) and dynamic case (Kalthoff and Winkler, 1987; Mason et al., 1992). Some important features of crack behavior in Mode II which follow from those works are outlined below:

(1) Difficulties in creating pure Mode II conditions. Only in quasi-static loading, pure Mode II can be expected to occur for some specimens and load schemes. More often, mixed Mode I-II crack tip deformation ($K_I>0$) or crack surfaces contact ($K_I<0$) are observed. In the latter case, application of the J-integral and HRR-solution for characterization of crack tip fields becomes questionable.

(2) Different character of fracture initiation for specimens of different materials and with different load schemes. Thus, some authors observe crack initiation in direction of about 70...80° with respect to the initial crack line, which is usually refered to as brittle fracture mechanism (Sih,

1973; 1974); in this case the crack initiation angle can be predicted by criteria of maximum tensile stress or minimum strain energy density. In the majority of investigations (Banks-Sills and Sherman, 1991; Maccagno and Knott, 1992; Tohgo and Ishii, 1992) crack propagates in direction close to the original crack (or notch) plane, which is refered to as ductile fracture mechanism.

(3) Transition in fracture mechanism with increasing loading rates. It has been observed by Kalthoff and Winkler (1987) in dynamic tests of steel that after certain limit of the loading rate the change in the crack initiation angle (from 70° with respect to the ligament at lower loading rate to about 10° at higher loading rate) occured. This transition has been supposed to occure due to formation of localized shear bands.

Also some difficulties arise in numerical simulation of crack behavior at high loading rates. An analytic solution for the stress field at a stationary crack tip in Mode I and II under dynamic loading has been derived by Lee and Freund (1990) for the case of linear-elastic material and idealized geometry of a cracked body, i.e. an edge crack in a half-plane. Similar analysis for specimens of finite size and elastic-plastic material seams to be very complicated with prime attention paid to use adequate stress-strain, strain-rate, temperature constitutive relations governing material behavior at the crack tip in high strain rates (see Klepaczko, 1987).

As an alternative to exact solution of elastic-plastic stress-strain fields at a crack tip under dynamic loading, an approximate quasi-static approach can be applied as follows. Equations (1.1),(1.3),(1.4), as well as other solutions for evaluation of K_{IC}, r_p, B and stress and strain components, involve material parameters (σ_Y,α,N) which are in general rate sensitive. Since those material parameters can be found for certain material as functions of strain rate, their introduction into equations for fracture mechanics parameters leads to approximate assessments of material behavior at a crack tip for different loading rates. It is obvious that such a quasi-static analysis takes no account of inertia effect, temperature and strain rate redistribution due to presence of a crack. In fact, when an exact analysis cannot be avoided, more general constitutive relations are to be used along with numerical methods.

In the present report, the quasi-static analysis is carried out to study strain rate effect on elastic-plastic stress-strain fields at a crack tip in Mode II for materials with different rate sensitivity: mild steel, titanium alloy and aluminum alloy. Evolution of the crack tip plastic zone size and shape with increasing the strain rate from 10^{-4} to 10^3 s^{-1} is analysed. Also a brief review of solutions on elastic and elastic-plastic crack tip fields in Mode II and results of K_{IIC} or J_{IIC} measurements are presented.

2. Characterization of Stress and Strain Fields and Plastic Zone at the Crack Tip in Mode II Via Small Scale Yielding Approximation

The small scale yielding (SSY) concept is succesfully applied to fracture mechanics for approximate analysis of plasticity effects on crack behavior. If the SSY concept is considered, a small plastic zone of radius $r=r_p$ is supposed to occur at the crack tip with a stress field within and near the plastic zone $(r < r_p+\delta)$ determined from the general elastic-plastic solution, while at the distance $r > r_p+\delta$ from the crack tip the stress components are governed by the asymptotic linear-elastic representation (Williams, 1957; Irwin, 1958)

$$\sigma_{ij}^{(\beta)} = \frac{K_\beta}{\sqrt{2\pi r}} \Sigma_{ij}^{(\beta)} (\theta) + O(r^0) \qquad (2.1)$$

Here $\sigma_{ij}^{(\beta)}$ are the stress components in Cartesian coordinates (x,y) with the origin at the crack tip (Fig.1); (r,θ) are the polar coordinates with the origin at the crack tip (Fig.1); $\Sigma_{ij}^{(\beta)}$ are specified functions of the polar angle; index "β" is refered to the crack tip deformation mode, β = I,II,III (I - opening mode, II - in-plane shear mode, III - anti-plane deformation); K_β is the stress intensity factor for corresponding deformation mode. The second term in the right side of eq.(2.1) is limited at $r \to 0$.

Evidently, the necessary condition for validity of the SSY approximation is the requirement of small size of the plastic zone in comparison to the crack length a, body thickness B, ligament size H=W-a (W being the width of a cracked section), i.e.

$$r_p \ll a , \quad r_p \ll B , \quad r_p \ll H$$

Practically, in measuring the plane strain fracture toughness, the conditions discussed above are satisfied with the ASTM requirement

$$B \geq 2.5 \, (K_{IC}/\sigma_Y)^2$$

which corresponds to $r_p \leq 0.04B$, when Irwin's plasticity correction is taken.

The use of the SSY approximation allows for linear-elastic fracture mechanics methods and criteria (e.g., $K_\beta = K_{\beta C}$) be extended to analyse the elastic-plastic material behavior. In particular, within the SSY approximation some efficient solutions for the crack tip plastic zone size and shape have been derived (Irwin, 1960; Dugdale, 1960; Duffy et al., 1969; Larsson and Carlsson, 1973; Rice, 1974). Some approximate assessments of the crack tip plastic zone in Mode II are discussed below with prime attention paid to the change of r_p due to variation of the applied stress level, τ_{appl}/τ_Y, which makes it possible to incorporate the rate sensitivity of the yield stress, τ_Y, into analysis which follows.

2.1. Mode II Crack Tip Stress Field in Small Scale Yielding

Asymptotic terms of the linear-elastic stress field at the crack tip in Mode II are given by (Williams, 1957; Irwin, 1957; Broek, 1987; Kanninen and Popelar, 1985)

$$\sigma_{ij} = \frac{K_{II}}{\sqrt{2\pi r}} \Sigma_{ij}(\theta)$$

In Cartesian coordinates one has

$$\Sigma_{xx} = - \sin\frac{\theta}{2} (2 + \cos\frac{\theta}{2} \cos\frac{3\theta}{2}) ,$$

$$\Sigma_{yy} = \sin\frac{\theta}{2} \cos\frac{\theta}{2} \cos\frac{3\theta}{2} ,$$

$$\Sigma_{xy} = \cos\frac{\theta}{2} (1 - \sin\frac{\theta}{2} \sin\frac{3\theta}{2}) ,$$

$$\Sigma_{zz} = \nu(\Sigma_{xx} + \Sigma_{yy}) \qquad \text{for plane strain,}$$

$$\Sigma_{zz} = 0 \qquad \text{for plane stress,}$$

$$\Sigma_{yz} = \Sigma_{zx} = 0 ;$$

(2.2)

in cylindrical coordinates

$$\Sigma_{rr} = \sin\frac{\theta}{2} (3\cos^2\frac{\theta}{2} - 2) ,$$

$$\Sigma_{\theta\theta} = - 3\sin\frac{\theta}{2} \cos^2\frac{\theta}{2} ,$$

$$\Sigma_{r\theta} = \cos\frac{\theta}{2} (3\cos^2\frac{\theta}{2} - 2) ,$$

$$\Sigma_{zz} = \nu(\Sigma_{rr} + \Sigma_{\theta\theta}) \qquad \text{for plane strain,}$$

$$\Sigma_{zz} = 0 \qquad \text{for plane stress,}$$

$$\Sigma_{\theta z} = \Sigma_{zr} = 0 ;$$

(2.3)

the principal stresses are

$$\sigma_{1,2} = \frac{K_{II}}{\sqrt{2\pi r}} (-\sin\frac{\theta}{2} \pm \sqrt{1-(3/4)\sin^2\theta}) ,$$

$$\sigma_3 = -2\nu \frac{K_{II}}{\sqrt{2\pi r}} \sin\frac{\theta}{2} \qquad \text{for plane strain,}$$

$$\sigma_3 = 0 \qquad \text{for plane stress}$$

(2.4)

The stress intensity factor, K_{II} , is a measure of the amplitude of the crack tip stress field. In the presence of plasticity, the J-integral (Cherepanov, 1979; Rice, 1968a) is found to be an adequate parameter characterizing the crack tip field amplitude (Hutchinson, 1968a). According to Rice (1968a), the J-integral is represented by

$$J = \int_{\Gamma} (W dy - \sigma_{ij} n_j \frac{\partial u_i}{\partial x}) ds \qquad (2.5)$$

where Γ is an arbitrary contour surrounding the crack tip with the origin and end at lower and upper crack surfaces respectively, n_j are components of the outer normal to Γ, u_i are displacement components $(x_1 = x, x_2 = y)$; W is the strain energy density,

$$W = \int_0^{\epsilon_{ij}} \sigma_{ij} d\epsilon_{ij} \qquad (2.6)$$

Under conditions of traction-free crack surfaces and absence of body forces, the J-integral is path-independent. This property is employed to derive several fracture mechanics solutions both in the elastic and elastic-plastic cases. The J-integral was introduced into the elastic-plastic crack tip field solutions (Hutchinson, 1968a; Rice and Rosengren, 1968) and, thus, used as a fracture criterion when plasticity induced effects are significant.

If the SSY approximation is assumed, the J-integral and stress intensity factor for Mode II are related by

$$J_{II} = \frac{1-\nu^2}{E} K_{II}^2 \qquad \text{for plane strain,}$$

$$\qquad (2.7)$$

$$J_{II} = \frac{1}{E} K_{II}^2 \qquad \text{for plane stress.}$$

2.2. Irwin's Plastic Zone Correction

Consider crack of length a subjected to in-plane shear by stresses τ_{appl} at infinity (Fig.2). The presence of the plastic zone of size r_p ahead of the crack tip can be taken into account, according to Irwin (1960), by increasing compliance of the cracked body. To introduce plasticity, an effective crack of length $a_{eff} = a + \delta_1$ is considered (Fig.2) with the stress intensity factor equal to $K_{II,eff}$. Following the SSY approximation, the stress at a distance $x > \delta_2$ ahead of the effective crack tip is expressed by

$$\tau_{xy} = \frac{K_{II,eff}}{\sqrt{2\pi x}}$$

The distance δ_2 is found by equating $\tau_{xy} = \tau_Y$ (with τ_Y be the yield stress in shear)

$$\delta_2 = \frac{1}{2\pi} \left(\frac{K_{II,eff}}{\tau_Y}\right)^2$$

Equilibrium condition (equality of areas S_1 and S_2 in Fig.2) leads to

$$r_p = 2\sqrt{\frac{\delta_2}{2\pi}} \frac{K_{II,eff}}{\tau_Y} = \frac{1}{\pi} \left(\frac{K_{II,eff}}{\tau_Y}\right)^2$$

The SSY requirement $r_p \ll a$ is equivalent to $K_{II,eff} \approx K_{II}$ and, thus, one can finally find

$$r_p = \frac{1}{\pi} \left(\frac{K_{II}}{\tau_Y} \right)^2 \tag{2.8}$$

Formula (2.8) may be applied to approximate assessment of the plastic zone size ahead of the crack tip in Mode II both in plane stress and plane strain. Indeed, analysis of plastic constraint factor (p.c.f.) (Broek, 1987) results in

$$p.c.f. = 1/\sqrt{3}$$

for both plane stress and plane strain conditions, expecting $r_p(\theta=0)$ be independent of the stress state. Note that this feature of the crack tip plastic zone behavior in Mode II differes substantially from that in Mode I. For the latter an effective yield stress in plane strain is three times of that in plane stress (Broek, 1987). Further analysis of Irwin (1960) has revealed the ratio of p.c.f. values for plane strain and plane stress be equal to $\sqrt[4]{8}$ which leads to the following approximate assessments

$$r_p = \frac{1}{\pi} \left(\frac{K_I}{\sigma_Y} \right)^2 \quad \text{in plane stress,}$$

$$r_p = \frac{1}{3\pi} \left(\frac{K_I}{\sigma_Y} \right)^2 \quad \text{in plane strain.}$$

As a result, the area of plastic zone for Mode I in plane strain is one order smaller that in plane stress. In contrast, plane stress/plane strain transition does not affect significantly the size and area of the crack tip plastic zone in Mode II.

2.3. The Dugdale Model

This model has been originally applied to approximate evaluation of the plastic zone size ahead of a Mode I crack tip in plane stress (Dugdale, 1960). With notes made above, there is no significant difference in plastic zone size for Mode II crack in plane stress and plane strain.

As in Irwin's approach, the effective crack length $a_{eff}=a+r_p$ is considered under actual load or under stresses τ_{appl} applied to crack surfaces, as it follows from the superposition principle (Bueckner, 1958). At the surfaces of the effective crack, in small vicinity of its tip, $0 \leq r \leq r_p$, compressive stresses $-\sigma_Y$ (for opening mode crack) or shear stresses $-\tau_Y$ (for in-plane shear mode) are applied to restrict respectively crack opening or sliding. The length r_p which is associated with the plastic zone size is determined from the condition of no singularity, i.e. $K_\beta=0$. For a crack in Mode II it implies that

$$K_{IIa} + K_{IIb} = 0 ,$$

where K_{IIa} and K_{IIb} are stress intensity factors for the effective crack under actual stresses τ_{appl} (index "a") and stresses $-\tau_Y$ acting within the distance r_p at the crack tip (index "b").

Making use of reference solutions for stress intensity factor (Tada et $al.$. 1973; Savruk. 1988), one can find r_p for some crack geometries in Mode II:

(1) *Through crack of length $2a$ in an infinite plate:*

$$\frac{r_p}{a} = \sec\left(\frac{\pi}{2}\frac{\tau_{appl}}{\tau_Y}\right) - 1 \qquad (2.9)$$

(2) *Semi-infinite crack in an infinite plate:*

$$\frac{r_p}{a} = \frac{(\tau_{appl}/\tau_Y)^2}{1-(\tau_{appl}/\tau_Y)^2} \qquad (2.10)$$

Here the plastic zone size is normalized by the crack length, which is finite for a physical crack.

(3) *Edge crack of length a in a semi-infinite plate.*

In this case the size of plastic zone depends on the applied load by the following relationship

$$\frac{\tau_{appl}}{\tau_Y} = \frac{2}{1.1215\pi} I\left(\frac{a}{a+r_p}\right) \qquad (2.11)$$

with

$$I(\xi) = \int_{\xi}^{1} (1-\eta^2)^{-1/2}\{1+(1-\eta^2)(0.2945-0.3912\eta^2+0.7685\eta^4-0.9942\eta^6+0.5094\eta^8)\}d\eta$$

In deriving eq.(2.11) Green's function for K_{II} obtained by Hartranft and Sih (1973) is used.

Note an important difference in results following from Irwin's and Dugdale's models. With the dimensionless parameter R_p defined as

$$R_p = r_p\left(\frac{\tau_Y}{K_{II}}\right)^2,$$

the Irwin solution yields

$$R_p = \frac{1}{\pi}$$

with constant R_p-value for any load level, τ_{appl}/τ_Y, and independent of crack geometry. In Fig.3 comparison is made of Dugdale's and Irwin's solutions for R_p at a tip of a semi-infinite crack in an infinite plane and an edge crack in a half-plane. One can see that Dugdale's solution strongly depends on the stress level, while R_p-values for different crack geometries nearly coincide. More realistic prediction of the plastic zone size based on Dugdale's model, comparing to Irwin's solution, has been noticed by Broek (1987) for the Mode I conditions.

Both Irwin's and Dugdale's approaches allow for determination of r_p only ahead of the crack tip. To find the shape of plastic zone, i.e. r_p as a function of the polar angle θ, the linear-elastic stress field in the form of

solution (2.2)-(2.4) and appropriate yield criterion can be employed within the SSY approximation. The yield criterion is usually expressed as the Huber-Mises condition.

$$(\sigma_1-\sigma_2)^2 + (\sigma_2-\sigma_3)^2 + (\sigma_3-\sigma_1)^2 = 2\sigma_Y^2 \qquad \text{with} \quad \sigma_Y=\sqrt{3}\,\tau_Y \ . \qquad (2.12)$$

or the Tresca condition,

$$2\tau_{max} = \max \{ \ |\sigma_1-\sigma_2| \ , \ |\sigma_2-\sigma_3| \ , \ |\sigma_3-\sigma_1| \ \} \ = \ \sigma_Y \quad \text{with} \quad \sigma_Y=2\tau_Y \qquad (2.13)$$

In what follows, some approximate solutions for the plastic zone at the crack tip in Mode II are considered which are based on yield criteria (2.12) and (2.13).

2.4. Plastic Zone Geometry in Mode II Based on the Asymptotic Linear-Elastic Stress Field

Consider a crack of Mode II in plane strain. Making use of the Huber-Mises yield condition (2.12) and expressions (2.4) for principal stresses, one can find the following equation governing the plastic zone geometry near the crack tip

$$r_p(\theta) = \frac{1}{6\pi}\left(\frac{K_{II}}{\tau_Y}\right)^2\left[3 + \sin^2\frac{\theta}{2} - \frac{9}{4}\sin^2\theta - 4v(1-v)\sin^2\frac{\theta}{2} \right] \qquad (2.14)$$

If the J-integral instead of the stress intensity factor is employed to characterize the crack tip stress field, then eq.(2.14) takes the form

$$r_p(\theta) = \frac{1}{6\pi(1-v^2)} \frac{J_{II}E}{\tau_Y^2} \left[3 + \sin^2\frac{\theta}{2} - \frac{9}{4}\sin^2\theta - 4v(1-v)\sin^2\frac{\theta}{2} \right] \qquad (2.14a)$$

with J_{II} and K_{II} being related by eq.(2.7).

When the Tresca yield criterion (2.13) is used. it is necessary to note that according to eqs (2.4)

$$\sigma_2 < \sigma_1 \ , \quad \sigma_2 < \sigma_3 \ ;$$

at the same time one of the conditions

$$\sigma_1 > \sigma_3 \quad \text{or} \quad \sigma_1 < \sigma_3$$

must hold depending upon the values of v and θ. Thus, the yielding occures if one of the following conditions is satisfied:

$$\frac{1}{2}(\sigma_1 - \sigma_2) = \tau_Y \quad \text{or} \quad \frac{1}{2}(\sigma_3 - \sigma_2) = \tau_Y$$

These result in

$$r_p = \max \{r_{p1}; r_{p2}\}$$

with

$$r_{p1} = \frac{1}{2\pi} \left(\frac{K_{II}}{\tau_Y}\right)^2 (1 - \frac{3}{4} \sin^2 \theta)$$

(2.15)

$$r_{p1} = \frac{1}{8\pi} \left(\frac{K_{II}}{\tau_Y}\right)^2 \left[\sqrt{1-(3/4)\sin^2 \theta} + (1-2v)\sin\frac{\theta}{2}\right]$$

or, in terms of the J-integral,

$$r_{p1} = \frac{1}{2\pi(1-v^2)} \frac{J_{II}E}{\tau_Y^2} (1 - \frac{3}{4} \sin^2 \theta)$$

(2.15a)

$$r_{p1} = \frac{1}{8\pi(1-v^2)} \frac{J_{II}E}{\tau_Y^2} \left[\sqrt{1-(3/4)\sin^2 \theta} + (1-2v)\sin\frac{\theta}{2}\right]$$

The results of calculations of the plastic zone shape in plane strain based on the Huber-Mises and the Tresca yield criteria, eqs (2.14) and (2.15), are presented in Fig.4 for Poisson's ratio ranging from 0 to C.5. (Since the plastic zone is symmetrical with respect to the crack line, only its variation at $0 \le \theta \le \pi$ is analysed throughout this report.) The Huber-Mises yield criterion predicts (Fig.4a) a smaller plastic zone size ahead of the crack than behind the tip, with the condition $r_p(\theta=0)=r_p(\theta=\pi)$ valid only at $v=0.5$. One can conclude from Fig.4a that only slight differences in the plastic zone shape ahead of the crack tip exist with variation of Poisson's ratio; also, if $v>0.3$ the plastic zone is nearly symmetrical with respect to the y-axis ($\theta=\pi/2$). The Tresca yield criterion predicts (Fig.4b) symmetrical plastic zone shape with respect to the y-axis for all v-values greater than 0.3; this case corresponds in Fig.4b to the curve with $v=0.33$. If $v<0.3$, only slight dependence of the plastic zone shape on Poisson's ratio in the range of polar angle from about $2\pi/5$ to π is observed.

In accordance to eqs (2.4) for principal stresses, the plastic zone geometry in plane stress can be obtained from eqs (2.14)-(2.15a) putting Poisson's ratio equal $v=0$. Thus, the curves in Fig.4a,b corresponding to $v=0$ can be considered at the same time as plane stress solutions.

Since the stress intensity factor, K_{II}, is proportional to the applied stress, τ_{appl}, the plastic zone size in formulae (2.14) and (2.15) is proportional to $(\tau_{appl}/\tau_Y)^2$. Consequently, decreasing the stress level (due to increase of τ_Y with τ_{appl}=const or decrease of τ_{appl} with τ_Y=const) leads to diminishing the plastic zone proportionally to $(\tau_{appl}/\tau_Y)^2$, without any changes in its shape. This conclusion is in contradiction to the finite-element results by Banks-Sills and Sherman (1990) which demonstrate changes in the shape of plastic zone with increasing load level; namely, a significant decrease in the ratio of $r_p(\theta=\pi)$ to $r_p(\theta=0)$ with increase of the load level has been observed.

2.5. Influence of Non-Singular Terms in the Elastic Crack Tip Stress Field on the Plastic Zone Geometry

The SSY approximation, as discussed at the beginning of this chapter, is valid only in a limited range of the level of applied load, τ_{appl}/τ_Y. Larsson and Carlsson (1973) and Rice (1974) have found that neglecting non-singular terms in the series expansion (2.1) of the stress field near a crack tip leads to significant errors in evaluation of the plastic zone size. For Mode I, a two-parameter crack tip field characterization has been suggested in those papers

$$\sigma_{ij}^{(I)}(r,\theta) = \frac{K_I}{\sqrt{2\pi r}} \Sigma_{ij}^{(I)}(\theta) + T_{ij}(\theta) \ ,$$

with $T_{xx} = T \neq 0$, $T_{xy} = T_{yy} = 0$ (Williams, 1957; Irwin, 1957; Kanninen and Popelar, 1985). The T-effect has appeared to be different for various geometries of cracked specimens resulting in different configurations of the plastic zone (Larsson and Carlsson, 1973). At the same time, no T-effect on the J-integral has been found by Rice (1974). Another important piece of information which follows from Rice's (1974) analysis is that, when T-effect being taken into account, deviation of the plastic zone size from the SSY solution of Irwin (1960) is proportional to σ_{appl}/σ_Y , while the difference is proportional to $(\sigma_{appl}/\sigma_Y)^2$ with T-stresses being neglected (e.g., Dugdale's model). Thus, the two-parameter solution of Larsson and Carlsson (1973) and Rice (1974) predicts more rapid increase of the plastic zone size with the load level than previous models. With T-effect taken into account, the boundary layer formulation has been modified and some important corrections to elastic and elastic-plastic crack tip fields have been obtained for both pure Mode I and mixed Mode I-II conditions (Larsson and Carlsson,1973; Du and Hancock, 1991; Betegon and Hancock, 1991; Du et al., 1991).

To study the effect of non-singular stress components on plastic zone behavior in Mode II, let us represent the crack tip stress field as follows (Williams, 1957; Irwin, 1957; Kanninen and Popelar, 1985)

$$\sigma_{ij}(r,\theta) = \frac{K_{II}}{\sqrt{2\pi r}} \Sigma_{ij}(\theta) + T_{ij}(\theta) + \frac{\tau_{appl}}{\sqrt{H}} \sqrt{r} \, A\Psi_{ij}(\theta) + \ldots \qquad (2.16)$$

where $\Sigma_{ij}(\theta)$ functions are determined from eqs (2.2),(2.3). To specify functions $T_{ij}(\theta)$ and $\Psi_{ij}(\theta)$, consider formulation of the plane problem in terms of Airy's stress function of complex variable $\bar{z} = x + iy = re^{i\theta}$. Following to Kanninen and Popelar (1985), one can write

$$\sigma_{xx} + \sigma_{yy} = 2[\Omega'(z) + \bar{\Omega}'(\bar{z})] \ , \qquad (2.17)$$

$$\sigma_{yy} - \sigma_{xx} - 2i\tau_{xy} = 2[z\bar{\Omega}''(\bar{z}) + \bar{\omega}''(\bar{z})] \ ,$$

where $\Omega(z)$ and $\omega(z)$ are holomorphic functions, the overbar denotes the complex conjugate. For Mode II, the stress function is an odd one of the y-coordinate, and Ω and ω' take the form (Kanninen and Popelar,1985)

$$\Omega(z) = iaz^{\lambda+1} \quad , \quad \omega'(z) = ibz^{\lambda+1} \tag{2.18}$$

where a, b and λ are real constants to be determined from the boundary conditions; $\lambda > -1$.

After substitution of eqs (2.18) into eqs (2.17), one can find

$$\sigma_{xx} + \sigma_{yy} = -4a(\lambda+1)\, r^{\lambda} \sin \lambda\theta , \tag{2.19}$$

$$\sigma_{yy} - i\tau_{xy} = -(\lambda+1)\, r^{\lambda} \{ (2a+b)\sin \lambda\theta + a\lambda \sin (\lambda-2)\theta$$
$$+ i [\, a\lambda \cos (\lambda-2)\theta + b \cos \lambda\theta \,] \} \tag{2.20}$$

For traction-free crack surfaces, eq.(2.20) yields the boundary conditions

$$(2a + b + a\lambda) \sin \lambda\pi = 0 ,$$

$$(a\lambda + b) \cos \lambda\pi = 0 , \tag{2.21}$$

which result in eigenvalue solutions of the boundary value problem as

$$\sin \lambda\pi = 0 \quad \text{or} \quad \cos \lambda\pi = 0 ,$$

or, equivalently,

$$\lambda = n/2 \quad \text{with} \quad n = -1, 0, 1, 2, \ldots$$

For the first eigenvalue, $\lambda = -1/2$, eqs (2.19)-(2.21) lead to the singular stress field given by eqs (2.2). The second eigenvalue, $\lambda = 0$, corresponds to the case in which all stress components vanish, i.e.

$$T_{xx} = T_{yy} = T_{xy} = 0 \tag{2.22}$$

Thus, in contrast to Mode I, the crack tip stress field in Mode II does not contain constant value terms (T-terms).

Substituting $\lambda = 1/2$ into eqs (2.19)-(2.21), one can find Ψ-terms:

$$\Psi_{xx} = \sin\frac{\theta}{2} (2 + \cos^2\frac{\theta}{2}) ,$$

$$\Psi_{yy} = - \sin\frac{\theta}{2} \cos^2 \frac{\theta}{2} , \tag{2.23}$$

$$\Psi_{xy} = \cos\frac{\theta}{2} (1 + \sin^2 \frac{\theta}{2}) ,$$

or, in polar coordinates,

$$\Psi_{rr} = \sin\frac{\theta}{2} (2 + 5 \cos\frac{\theta}{2} \cos\frac{3\theta}{2}) ,$$

$$\Psi_{\theta\theta} = -5\sin\frac{\theta}{2} \cos\frac{\theta}{2} \cos\frac{3\theta}{2} , \tag{2.23a}$$

$$\Psi_{r\theta} = \frac{5}{2} \cos\theta \cos\frac{3\theta}{2} - \frac{3}{2} \cos\frac{\theta}{2}$$

For certain geometry and loading conditions the amplitude A of non-singular Ψ-components of the stress field (2.16) can be determined from results of numerical treatment of a boundary value problem. For example,

by analogy with approach of Larsson and Carlsson (1973), one can write

$$A = lim_{r \to 0} \sqrt{\frac{H}{r}} \frac{1}{\tau_{appl}} [\tau_{xy}^{act} (r,\theta=0) - \tau_{xy}^{BLF} (r,\theta=0)]$$

where τ_{xy}^{act} and τ_{xy}^{BLF} are stress components for the actual geometry of a cracked body and for geometry corresponding to the boundary layer formulation with one-parameter (K_{II}) characterization of the crack tip fields.

An approximate assessment of the Ψ-stress amplitude can be obtained for particular crack geometries as follows. Consider a plate of width W containing an edge crack of length a; let H=W-a be a ligament size. The plate is subjected to shear stresses τ_{appl} acting parallel to the crack line. With terms of order r^1 be omitted in eq.(2.16), the equilibrium condition yields

$$\int_{0}^{H} \tau_{xy} (r,\theta=0) \, d\theta = \tau_{appl} W ,$$

and, after integrating,

$$A = \frac{3}{2} \left(\frac{W}{H} - \frac{K_{II}}{\tau_{appl}} \sqrt{\frac{2}{\pi H}} \right)$$

Making use of conventional representation of the stress intensity factor in the form

$$K_{II} = Y_{II} \ \tau_{appl} \sqrt{\pi a}$$

where Y_{II} is a geometrical factor, we get finally

$$A = \frac{3}{2} \left(\frac{W}{H} - Y_{II} \sqrt{\frac{2a}{H}} \right) \tag{2.24}$$

Consider two examples of calculating the non-singular stress term amplitude for different crack geometries in Mode II.

(1) *Edge crack of length a=H=W/2 in a plate.*
According to results published by Tada et al. (1973),
$$Y_{II} = 1.252 ,$$
and formula (2.24) yields
$$A = 0.344$$

(2) *Semi-infinite crack in an infinite plate.*
This example is a limiting case of the previous one with $a \to \infty$. The geometrical factor equals (Savruk, 1988)

$$Y_{II} = \frac{2\sqrt{2}}{\pi} ,$$

and one can find from eq.(2.24)
$$A = 1.09$$

For the latter geometry an analysis of the plastic zone evolution with variation of the stress level is performed below. The Huber-Mises yield condition (2.12) can be rewriten in the form

$$\frac{1}{2}[(\sigma_{xx} - \sigma_{yy})^2 + (\sigma_{yy} - \sigma_{zz})^2 + (\sigma_{zz} - \sigma_{xx})^2] + 3\tau_{xy}^2 = 3\tau_Y^2, \qquad (2.12a)$$

or, equivalently, for plane strain conditions

$$(1 - \nu + \nu^2)(\sigma_{xx} + \sigma_{yy})^2 - 3(\sigma_{xx}\sigma_{yy} - \tau_{xy}^2) = 3\tau_Y^2 \qquad (2.12b)$$

As it is mentioned above, the yield condition for plane stress may be derived after that for plane strain, eq.(2.12b), putting $\nu=0$.

Introducing dimensionless parameters

$$\overline{\sigma}_{ij} = \sigma_{ij}/\tau_Y, \quad R = r(\tau_Y/K_{II})^2,$$

the stress components and the yield criterion are of the form

$$\overline{\sigma}_{ij}(R,\theta) = \frac{1}{\sqrt{2\pi R}}\Sigma_{ij}(\theta) + AY_{II}(\frac{\tau_{appl}}{\tau_Y})^2\sqrt{2\pi R}\,\Psi_{ij}(\theta), \qquad (2.25)$$

$$(1 - \nu + \nu^2)(\overline{\sigma}_{xx} + \overline{\sigma}_{yy})^2 - 3(\overline{\sigma}_{xx}\overline{\sigma}_{yy} - \overline{\tau}_{xy}^2) = 3 \qquad (2.26)$$

Equations (2.25) and (2.26) predict dependence of the dimensionless radius of the plastic zone,

$$R_p = r_p(\tau_Y/K_{II})^2,$$

on the applied stress level; this conclusion is in agreement with the results of Larsson and Carlsson (1973) and Rice (1974) on Mode I.

The closed form solution of eqs (2.25) and (2.26) for R_p is rather complicated, variation of $R_p(\theta)$ has been derived by numerical treatment of eqs (2.25) and (2.26) for different stress levels and two values of Poisson's ratio: $\nu=0$ and $\nu=0.33$. Results for both plane stress ($\nu=0$), Fig.5a, and plane strain ($\nu=0.33$), Fig.5b, indicate significant change in the shape of plastic zone as compared to shapes derived from the model with one-parameter characterization of the stress field near a crack tip (Fig.4). The present two-parameter solution predicts more rapid growth of the plastic zone ahead of the crack tip than behind it. With increasing the load level, the major plastic zone area concentrates ahead of the crack tip, which is more characteristic of the plane strain case. For the latter the plastic zone hight ahead of the crack tip is larger that behind. These features of the plastic zone behavior at the crack tip in Mode II differ from those predicted by the one-parameter model (Fig.4) and agree with the finite-element results by Banks-Sills and Sherman (1990).

Note that previous solutions for the plastic zone geometry do not incorporate Irwin's correction for plasticity. Since conditions $\sigma_{xx} = \sigma_{yy} = 0$,

$\tau_{xy} \neq 0$ are hold at $\theta=0$, Irwin's approach is directly applied to evaluation of the plastic zone size ahead of the crack tip. This results in the value of $r_p(\theta=0)$ twice larger than predicted before (Figs 4,5), while the values of $r_p(\theta=\pi)$ and the plastic zone hight do not change. It is briefly discussed in Chapter 6 which assessments of the plastic zone size and shape are more realistic.

2.6. Stress Intensity Factors for Cracks Subjected to In-Plane Shear Loading

Within the SSY approximation, the size and shape of plastic zone near a crack tip are expressed via the stress intensity factor. Some reference K_{II}-solutions for plane crack problems are summarized in this section. Note that in stress intensity factor analyses actual boundary conditions are often formulated, according to the superposition principle (Bueckner, 1958), in terms of self-equilibrium stresses applied to crack surfaces. With such transformation the formulation of a boundary value problem is simplified and some efficient techniques for calculation of the stress intensity factors can be employed (e.g., Green's, or weight function, method).

(1) <u>Central crack of length $2a$ in an infinite plate (Fig.6.1).</u>

For arbitrary stress distribution on crack surfaces, $\tau(\xi)$, stress intensity factors at right (+) and left (-) crack tips are determined as follows (Savruk, 1988)

$$K_{II}^{+} = \frac{1}{\sqrt{\pi a}} \int_{-a}^{a} \tau(\xi)\sqrt{(a+\xi)/(a-\xi)}\ d\xi \ ,$$

$$K_{II}^{-} = \frac{1}{\sqrt{\pi a}} \int_{-a}^{a} \tau(\xi)\sqrt{(a-\xi)/(a+\xi)}\ d\xi \qquad (2.27)$$

In the case of constant stress distribution, $\tau(\xi) = \tau_0 = $ const, eqs (2.27) yield

$$K_{II}^{+} = K_{II}^{-} = \tau_0\sqrt{\pi a} \qquad (2.28)$$

If a pair of forces $\pm Q$ acts at points $(b,0^+)$ and $(b,0^-)$ respectively, the stress intensity factors are

$$K_{II}^{+} = \frac{Q}{\sqrt{\pi a}}\sqrt{(a+b)/(a-b)} \ , \quad K_{II}^{-} = \frac{Q}{\sqrt{\pi a}}\sqrt{(a-b)/(a+b)} \qquad (2.29)$$

For constant stresses τ_0, applied near the crack tip regions, $b \leq |\xi| \leq a$ (as in Dugdale's model), one can find

$$K_{II}^{\pm} = \frac{2}{\pi}\tau_0\sqrt{\pi a}\left(\frac{\pi}{2} - \sin^{-1}\frac{b}{a}\right) \qquad (2.30)$$

(2) Periodic array of parallel cracks in an infinite plate (Fig.6.2).

Cracks of length $2a$ with a distance d between cracks are considered. The K_{II}-solution for uniform stress distribution, τ_0 , on crack surfaces (or uniform remote stresses τ_0) has been derived by Savruk (1988):

$$K_{II} = \frac{4\tau_0}{\pi} K(th\frac{3\pi\lambda}{4}) \sqrt{(a/3\lambda)\, th(\frac{3\pi\lambda}{4})} \qquad (2.31)$$

with $\lambda = 2a/d$, and K is the complete elliptical integral of the first kind. The solution for an arbitrary distribution of shear stresses is rather complicated and may be found in Savruk's (1988) book.

(3) Semi-infinite crack in an infinite plate (Fig.6.3).

Stress intensity factor for an arbitrary stress distribution is determined as follows (Panasyuk et al., 1976):

$$K_{II} = \sqrt{\frac{2}{\pi}} \int_0^\infty \frac{\tau(\xi)}{\sqrt{\xi}} d\xi \qquad (2.32)$$

The function $\tau(\xi)$ is assumed in such a way that the integral in eq.(2.32) takes a finite value. If the region near crack tip, $0 \leq \xi \leq a$, is subjected to constant shear stresses τ_0, eq.(2.32) yields

$$K_{II} = \frac{2\sqrt{2}}{\pi} \tau_0 \sqrt{\pi a} \qquad (2.33)$$

In the case of a pair of shear forces $\pm Q$ acting at points $(b,0^+)$ and $(b,0^-)$ one can find

$$K_{II} = Q \sqrt{\frac{2}{\pi b}} \qquad (2.34)$$

(4) Periodic array of semi-infinite cracks in an infinite plate (Fig.6.4).

An approximate solution of this problem has been derived in a closed form by special approximation of a kernel of the singular integral equation (Savruk, 1988)

$$K_{II} = \sqrt{\frac{6}{d}} \int_0^\infty \frac{\tau(\xi)}{\sqrt{1 - \exp(-3\pi\xi/d)}} d\xi \qquad (2.35)$$

(5) Edge crack of finite length a in a half-plane (Fig.6.5).

Several approximate solutions of this problem have been derived in the literature. According to Panasyuk *et al.* (1976), the stress intensity factor for an arbitrary stress distribution is of the form

$$K_{II} = \sqrt{\frac{2\alpha a^{\alpha-1}}{\pi}} \int_0^\infty \frac{\tau(\xi)\, d\xi}{\sqrt{a^\alpha - \xi^\alpha}} \qquad (2.36)$$

with $\alpha = 2\pi^2/(\pi^2-4)$. For the stress distribution of polynomial type, $\tau(\xi) = \tau_0 (\xi/a)^n$, eq.(2.36) is reduced to

$$K_{II} = \tau_0 \sqrt{\frac{2a}{\alpha}} \frac{\Gamma((n+1)/2)}{\Gamma(n/2+1)} \qquad (2.37)$$

Making use of the alternating technique, Hartranft and Sih (1973) have found Green's function which is the value of the stress intensity factor due to a pair of shear forces $\pm Q$ acting at points $(c,0^+)$ and $(c,0^-)$ of crack surfaces respectively

$$k_{II} = \frac{2Q}{\sqrt{\pi a}} [\, 1 + (1 - \varepsilon^2)(0.2945 - 0.3912\varepsilon^2 + 0.7685\varepsilon^4$$

$$- 0.9942\varepsilon^6 + 0.5094\varepsilon^8)\,] / \sqrt{1 - \varepsilon^2} \qquad (2.38)$$

with $\varepsilon = c/a$. The stress intensity factor of an arbitrarily loaded edge crack in a half-plane can be calculated by integrating Green's function (2.38) over the crack length. For example, for constant shear stresses one can get

$$K_{II} = 1.1215\, \tau_0 \sqrt{\pi a} \qquad (2.39)$$

At $\varepsilon = 0$, eq.(2.38) yields

$$K_{II} = 1.2945\, \frac{2Q}{\sqrt{\pi a}} \qquad (2.40)$$

which is the solution of the problem when two opposite shear forces Q are applied at the crack mouth ($\xi=0$, $\eta=\pm 0$).

If a tensile load P parallel to the ξ-axis is applied to a half-plane boundary in the point $(0,b)$ (Fig.6.5), the corresponding value of the stress intensity factor was derived by integrating (2.38) (Rooke and Jones, 1979)

$$K_{II} = -\frac{1-\zeta^2}{\sqrt{\pi a}} P\; (1.294 - 1.184\zeta + 5.442\zeta^2 - 28.14\zeta^3 + 41.80\zeta^4$$

$$- 22.38\zeta^5 + 3.162\zeta^6) \qquad (2.41)$$

with $\zeta = b/(b+a)$.

Freund (1978) has solved the problem with prescribed displacements of a half-plane boundary

$$u_\xi = \delta = \text{const} \quad \text{for } \xi=0,\ \eta>0\ ,$$

$$u_\xi = -\delta = \text{const} \quad \text{for } \xi=0,\ \eta<0\ ;$$

the result is

$$K_{II} = \frac{8\mu\delta}{(1+\kappa)\sqrt{\pi a}} \qquad (2.42)$$

where μ is the shear modulus, $\kappa=3-4\nu$ for plane strain and $\kappa=(3-\nu)/(1+\nu)$ for plane stress conditions.

(6) <u>Edge crack in a half-plane with a stiffened edge under uniform tension (Fig.6.6).</u>

Let a rigid stamp of length b be joined with a half-plane edge as shown in Fig.6.6. The force P parallel to the crack line acts on the half-plane through the stamp. This problem has been solved by Hasebe (1979, 1981) by conformal mapping technique. Two types of boundary conditions were studied: (a) loading with no stamp rotation and (b) loading with stamp rotation at an angle φ; corresponding results are presented in the table below (K_I -values are given over the lines, K_{II} - values are given below the lines).

a/b	$K_{I,II}/(P\sqrt{\pi/a})$					$K_{I,II}/(\mu\varphi\sqrt{\pi a})$				
	κ					κ				
	3.0	2.5	2.0	5/3	1.0	3.0	2.5	2.0	5/3	1.0
0.002	0.020	0.019	0.017	0.015	0.007					
	0.004	0.005	0.006	0.006	0.006					
0.001						0.681	0.709	0.715	0.692	0.454
						0.178	0.231	0.294	0.341	0.413
0.1	0.089	0.084	0.077	0.071	0.053	0.238	0.258	0.285	0.308	0.379
	0.049	0.050	0.049	0 049	0.044	0.228	0.253	0.285	0.313	0.392
0.4	0.153	0.150	0.146	0.143	0.134	0.097	0.110	0.128	0.145	0.202
	0.115	0.114	0.113	0.111	0.105	0.158	0.178	0.205	0.229	0.307
0.8	0.207	0.206	0.205	0.205	0.203	0.038	0.043	0.050	0.057	0.080
	0.184	0.184	0.183	0.183	0.181	0.100	0.113	0.131	0.147	0.200
1.0	0.224	0.224	0.223	0.223	0.223	0.024	0.027	0.032	0.036	0.051
	0.212	0.213	0.213	0.213	0.212	0.080	0.090	0.105	0.118	0.161
5/3	0.251	0.251	0.251	0.251	0.252	0.005	0.006	0.006	0.007	0.010
	0.279	0.280	0.281	0.282	0.284	0.033	0.037	0.043	0.048	0.065
2.5	0.260	0.260	0.260	0.260	0.261	0.001	0.001	0.001	0.001	0.002
	0.323	0.324	0.325	0.325	0.327	0.015	0.016	0.019	0.021	0.029
10.	0.263	0.263	0.263	0.263	0.263	0.	0.	0.	0.	0.
	0.390	0.390	0.391	0.391	0.392	0.001	0.001	0.001	0.001	0.002

In both cases the mixed Mode I-II crack tip deformation takes place. When the stamp and the crack are of equal length, $a/b=1$, in case (a) the absolute values of K_I and K_{II} are close, while in case (b) the ratio $|K_{II}/K_I|$ is of the value about 3.

(7) Periodic array of parallel edge cracks in a half-plane (Fig.6.7).

Numerical results of solving this problem by the method of singular integral equations (Panasyuk *et al.*, 1976) are summarized below for the case of constant shear stresses τ_0 applied to crack surfaces:

a/d	0.	0.2	0.4	0.6	0.8	1.0	2.0	3.0
$K_{II}/(\tau_0 \sqrt{\pi a})$	1.1214	1.1320	1.2072	1.3291	1.4575	1.5797	2.0941	2.5075

(8) Layer of finite length bounded to a half-space (Fig.6.8).

This problem has been solved by the method of singular integral equations (Chantaramungkorn and Keer, 1975). Both the layer and half-space are assumed to be of identical material. Constant pressure, p, acts parallel to the crack plane. Numerical K_I and K_{II} values are presented in the table below for two crack tips (A and B):

$\dfrac{c}{h}$	$\dfrac{d}{c}$	$\dfrac{K_{II}(A)}{p\sqrt{\pi c}}$	$\dfrac{K_{II}(B)}{p\sqrt{\pi c}}$	$\dfrac{K_I(A)}{p\sqrt{\pi c}}$	$\dfrac{K_I(B)}{p\sqrt{\pi c}}$
0.5	1.25	0.648	0.458	1.349	-1.309
1.0	1.25	0.367	0.188	0.398	-0.325
	1.50	0.385	0.198	0.390	-0.321
	2.00	0.387	0.200	0.390	-0.320
	3.00	$\mathcal{C}'$	0.200	0.390	-0.320
2.0	1.25	0	0.066	0.188	-0.076
3.0	1.25	0.185	0.033	0.145	-0.033

Note that practically for all values of geometrical parameters studied, the condition $|K_{II}/K_I| < 1$ holds.

(9) Edge crack in a strip (Fig.6.9).

Approximate formula for the stress intensity factor at constant shear stresses, τ_0, applied to crack surfaces is given by Tada et al. (1973):

$$K_{II} = \tau_0 \sqrt{\pi a} \, f_0(\frac{a}{W}) \ ,$$

$$f_0(\frac{a}{W}) = [\ 1.122 - 0.561(\frac{a}{W}) + 0.085(\frac{a}{W})^2 + 0.180(\frac{a}{W})^3] / \sqrt{1 - \frac{a}{W}} \qquad (2.43)$$

which is said to be accurate within 2% for $0 \le \frac{a}{W} \le 1$. In the case of a pair of shear forces Q acting at the crack edge (see Fig.6.9) an expression for K_{II} is of the form (Tada et al., 1973)

$$K_{II} = \frac{2Q}{\sqrt{\pi a}} [\ 1.30 - 0.65(\frac{a}{W}) + 0.37(\frac{a}{W})^2 + 0.28(\frac{a}{W})^3] / \sqrt{1 - \frac{a}{W}} \qquad (2.44)$$

which is accurate within 1% for $0 \le \frac{a}{W} \le 1$.

Making use of an asymptotic interpolation technique, Cheng and Finnie (1990) have derived the stress intensity factor for an arbitrary stress distribution, $\tau(\xi) = \tau_0 \bar{\tau}(\xi)$, as follows:

$$K_{II} = \tau_0 \sqrt{\pi a} \, f_0(\frac{a}{W}) \, f(\frac{a}{W}) \ , \qquad (2.45)$$

with $f_0(\frac{a}{W})$ to be determined from eq.(2.43), and

$$f(\frac{a}{W}) = \int_0^{a/W} \frac{\partial}{\partial \xi} \left[1 - (1-\xi) \, \frac{2}{\pi} \cos^{-1} \left(\frac{\xi(1-a/W)}{(1-\xi)a/W} \right) H(\xi, \frac{a}{W}) \right] \bar{\tau}(\xi) \, d\xi \ ,$$

$$\qquad (2.46)$$

$$H(\xi, \frac{a}{W}) = 1 - \frac{0.12}{1.12} \xi(1 - 2.5\frac{a}{W})(1 - \frac{a}{W}) / (\frac{a}{W})$$

(10) Edge crack in a three-point bend specimen (Fig.6.10).

Mixed-mode stress intensity factors, K_I and K_{II}, for an asymmetrically located edge crack in a three-point bend specimen have been calculated by the boundary collocation method (Ke et al., 1978). Dimensionless functions $F_I = K_I / [M/(t W^{3/2})]$ and $F_{II} = K_{II} / [Q/(t W^{1/2})]$ are summarized in the table below with F_I being above the line and F_{II} being below the line (M and Q are the bending moment and shear force in a cracked section; t and W are the specimen thickness and width):

$\dfrac{a}{W}$	2B/L						
	0	1/6	2/6	3/6	4/6	5/6	11/12
0.40	7.71	8.50	8.55	8.36	8.33	8.50	8.50
	0	1.032	1.400	1.350	1.298	1.376	1.644
0.45	8.86	9.67	9.72	9.38	9.48	9.55	...
	0	1.142	1.562	1.488	1.466	1.464	...
0.50	10.27	11.48	11.50	11.60	11.15	11.59	11.53
	0	1.410	1.864	1.840	1.664	1.660	1.760
0.55	12.11	13.30	13.60	13.03	12.90	13.46	...
	0	1.588	1.980	2.050	1.976	2.100	...
0.60	14.47	14.25	14.65	14.91	14.88	14.74	14.50
	0	2.348	2.248	2.276	2.320	2.294	2.090

The value of K_I is found to be much higher than K_{II} .

(11) Edge crack in a four-point bend specimen (Fig.6.11).

Pure Mode II crack tip deformation is expected in the loading scheme presented in Fig.6.11. This specimen has been employed by Tohgo and Ishii (1992) for measurements of the fracture toughness, J_{IIC} . The stress intensity factor has been found from finite-element calculations:

$$K_{II} = 1.37 \frac{F}{Wt} \sqrt{\pi a} \ . \quad F = \frac{5}{8} P \tag{2.47}$$

where W and t are the specimen width and thickness, respectively. Note that varying distances in the loading frame, combined Mode I-II conditions can be obtained with various mixity factor (Tohgo and Ishii, 1992).

(12) Edge crack in a cantilever beam (Fig.6.12).

Stress intensity factors, K_I and K_{II} , have been found by the body force method (Murakami, 1980). Dimensionless functions

$$F_I = K_I / [(6TL/W^2)\sqrt{\pi a}] \ , \quad F_{II} = K_{II} / [(T/W)\sqrt{\pi a}]$$

($T = \tau_0 W$) are presented below for different values of the crack depth:

a/W	0.1	0.2	0.3	0.4	0.5
F_I	0.94	1.00	1.12	1.25	1.36
F_{II}	0.43	0.68	0.94	1.17	1.36

Since $L/W>1$, then

$$\frac{K_I}{K_{II}} = \frac{F_I}{F_{II}}\left(\frac{6L}{W}\right) \gg 1,$$

i.e. Mode I deformation is predominant for this specimen.

(13) Edge crack in a double cantilever beam (Fig.6.13).

A double cantilever beam is considered with different cross sections, $A_1 = th_1$ and $A_2 = th_2$, where t is the beam thickness (Fig.6.13). A pair of forces, P, is applied to the beam edges. The stress intensity factor is determined as follows (Tada, 1974):

$$K_{II} = C\frac{P}{\sqrt{2tA}} \tag{2.48}$$

with

$$A = \frac{A_1 A_2}{A_1 + A_2},$$

$C = 1$ for plane stress,

$C = \dfrac{1}{\sqrt{1-v^2}}$ for plane strain.

If $A_1 = A_2$ and a horizontal displacement δ of the beam is given, eq.(2.48) is reduced to the following:

$$K_{II} = C\frac{E\delta}{a}\sqrt{\frac{2A}{t}} \tag{2.48a}$$

(14) End-notched flexure specimen in three-point bending (Fig.6.14).

This type of specimen has been employed by Mall and Mol (1991) in Mode II fracture toughness testing of ceramic composites. In preparation phase, the specimen is notched on one end and subjected to Mode I loading to create a sharp crack of length a which is shown in Fig.6.14. The fracture toughness is expressed in terms of the critical energy release rate as follows:

$$G_{\mathrm{IIC}} = \frac{P_C^2}{2t} \frac{\mathrm{d}C}{\mathrm{d}a} \qquad (2.49)$$

where P_C is a critical force, t is the specimen thickness. C is the specimen compliance. An approximate formula for evaluation of the C value is given by Russel and Street (1982):

$$C = \frac{1+1.5(2a/L)^3}{4Et(h/L)^3} \qquad (2.50)$$

However, Mall and Mol (1991) demonstrated that the real comliance function differs essentially from that determined by eq.(2.50), and thus C-calibration curves are to be found experimentally for certain specimen geometry and test conditions (temperature etc.).

(15) Compact specimen in shearing (Fig.6.15).

The stress analysis of this specimen has been performed by the finite-element method (Hoyniak and Conway, 1979). Two types of boundary conditions (with and without restrictions on horizontal displacements of the applied load) and two different directions of the applied load have been considered; these are refered to as Cases 1 to 4 in Fig.6.15. In general, mixed mode type of the crack tip deformation is observed for this specimen. Figure 7a shows variation of the stress intensity factor K_{II} for the Case 2 of loading found by the finite-element method (Hoyniak and Conway, 1979) and the boundary collocation method (Jones and Chisholm, 1975), for three values of the characteristic size of the specimen: H = 0.5, 1.0 and 1.5 in. In Fig.7b, both the Mode II stress intensity factor, K_{II}, and the mixity factor, $S = |K_{\mathrm{II}}| / \sqrt{K_{\mathrm{I}}^2 + K_{\mathrm{II}}^2}$, are presented for different schemes of loading (after Savruk, 1988). One can conclude that nearly pure Mode II crack tip deformation is found for the Case 3.

(16) Punch-through shear specimen (Fig.6.16).

This specimen (cubic in shape) has been applied for fracture toughness (K_{IIC}) measurements of concrete. i.e. extremely brittle material (Davis et al., 1985). The calibration of the stress intensity factor has been performed by the finite-element method. The specimen dimensions in that analysis were: W = 100 mm, b = 10 mm. H = 30, 40 and 50 mm. Numerical results by Davis et al. (1985) on the dimensionless stress intensity factor

$$Y_{\mathrm{II}} = \frac{2W(W-a-b)}{P} \frac{K_{\mathrm{II}}}{\sqrt{\pi a}}$$

for a larger crack (of length a) are presented in the table below.

a/W	Y_{II} for H=50 mm	Y_{II} for H=40 mm	Y_{II} for H=30 mm
0.25	4.833	4.151	3.589
0.30	4.802	4.109	3.573
0.35	4.769	4.088	3.550
0.40	4.743	4.071	3.521
0.45	4.690	4.067	3.510
0.50	4.394	3.809	3.335
0.55	4.438	3.863	3.405
0.60	4.544	3.978	3.484

For prescribed specimen dimensions the opening mode stress intensity factor was found to be of the order lower than the value of K_{II}.

(17) Compact Mode II fracture specimen (Fig.6.17).

This specimen has been designed and employed for fracture toughness (K_{IIC} and J_{IIC}) measurements of perspex (extremely brittle material) (Banks-Sills and Arcan, 1986) and Al 7075-T7351 (typically ductile material) (Banks-Sills and Sherman, 1991). The specimen geometry is presented in Fig.6.17. The load is applied through a special frame so that no bending moment acts at a cracked section (this is shown schematically in Fig.6.17). The finite element method has been used for elastic and elastic-plastic analysis of the specimen. An approximate formula for the stress-intensity factor was derived by Banks-Sills and Arcan (1986). Also calibration curves for evaluation of the J_{II}-value are presented by Banks-Sills and Sherman (1991).

It should be noted in conclusion of this brief review on Mode II stress intensity factors, that application of cracked geometries shown in Figs 6.11, 6.14, 6.15 (Case 3), 6.16 and 6.17 allows for pure Mode II crack tip deformation. For the other geometries mixed Mode I-II conditions take place with different ratio of K_I to K_{II} (depending on a geometry and scheme of loading). It is important to note than at $K_i < 0$ compressive stresses act along a crack line inducing contact and friction between crack surfaces; this results in reducing an actual in-shear mode stress intensity factor and leads to necessity to reformulate boundary conditions. Also, in the presence of the crack surfaces interaction, the proof of the J-integral path-independence becomes invalid and application of the J-integral to ductile fracture analysis is questionable.

2.7. Some Results on Mode II Fracture Toughness Measurement

Some results on determination of fracture toughness in Mode II available from the literature are summarized in Table 2.1. For comparison purposes, values of Mode I fracture toughness, K_{IIC}/K_{IC} ratio and crack initiation angle θ_i (with respect to the original crack line) are listed.

Table 2.1

Reference	Material	K_{IC} MPa$\sqrt{m}$	K_{IIC} MPa$\sqrt{m}$	$\dfrac{K_{IIC}}{K_{IC}}$	θ_i (deg)	Specimen
Banks-Sills and Arcan (1986)	perspex			0.89	63-70	Fig. 6.17
Banks-Sills and Sherman (1991)	Al 7075-T7351	29.2	54.1	1.85	0	Fig. 6.17
Jones and Chisholm (1979)	Al 2024-T4	37.4	44.0	1.18	≈ 0	Fig. 6.15
Hoyniak and Conway (1979)	Al 2024-T4	37.4	55.8	1.49	≈ 0	Fig. 6.15
Tohgo et al. (1990)	steel SM41A	500[†]	205[†]	0.64	0	Fig. 6.11
Tohgo and Ishii (1992)	Al 6061-T651	15.3[†]	45.2[†]	1.72	0	Fig. 6.11
Davies et al. (1985)	soil cement		0.42		≈ 0	Fig.6.16
Awaji and Sato (1978)	graphite 7474 graphite SM1-24	0.94 0.81	1.09 0.89	1.16 1.09	67 67	Center-cracked disc
Mall and Mol (1991)	alumosilicate ceramic composite		0.297[‡]		0	Fig. 6.14
Suresh et al. (1990)	Al$_2$O$_3$ ceramic	3.32[‡]	3.2[‡]	0.96		Fig.6.11

Notes: [†] The J-integral value, kN/m.
[‡] The G_{IIC} value, kN/m.

3. Plastic Stress and Strain Fields near a Crack Tip in Mode II

In previous chapter, analyses of the crack tip plastic zone size and shape are based upon the linear-elastic solution for the stress field. The only plasticity parameter involved in those analyses is the yield stress, τ_Y. In reality, there exists material strain hardening which affects significantly material behavior in yielding and leads to redistribution of stress and strain fields.

The dominant singularity at a crack tip in a power strain hardening material has been investigated by Hutchinson (1968a) and Rice and Rosengren (1968) (HRR-solution). In those papers, Mode I stress-strain fields in plane stress and plane strain have been derived for material of the Ramberg-Osgood type, as well as for perfectly plastic one. Further studies were devoted to the elastic-plastic analysis of the crack tip fields in pure Mode II plane strain (Hutchinson, 1968b; Shih, 1974) and pure Mode III (Rice, 1968b), as well as combined Mode I-II (Shih, 1974; Nemat-Nasser and Obata, 1984), I-III (Pan and Shih, 1989) and II-III (Pan and Shih, 1990).

Note that finite-element analyses of mixed-mode crack tip fields led to some important conclusions: (1) the dominant HRR-singularity derived originally within deformation plasticity is valid when incremental plasticity is employed to describe material behavior; (2) in mixed-mode conditions, there is only slight deviation of the dominant stress field singularity order from that in the HRR-solution (Pan and Shih, 1990). Thus, the HRR-solution appeares to be a good approximation of real stress and strain fields near a crack tip in metallic materials.

In what follows, a brief review of the HRR-solution for pure Mode I and Mode II is presented. In addition, variation of the dominant stress and strain fields at a crack tip in Mode II versus strain hardening exponent is analysed both for plane strain and plane stress.

3.1. Dominant Singularity of the Crack Tip Fields

A plane crack is considered in an elastic-plastic material obeying the J_2-flow theory. The stress-strain curve in shearing is approximated by the Ramberg-Osgood equation

$$\frac{\gamma}{\gamma_Y} = \frac{\tau}{\tau_Y} + \alpha \left(\frac{\tau}{\tau_Y}\right)^N \tag{3.1}$$

where τ_Y and $\gamma_Y = \tau_Y/\mu$ are the yield stress and strain respectively, μ is the shear modulus, N is the strain hardening exponent (N >1), α is the material constant. The plastic deformation is assumed to be incompressible, independent of the hydrostatic stress component, $\sigma_{kk}/3$, and, thus, be a function of the deviatoric stress components, s_{ij}, i.e.

$$\varepsilon_{ij} = \varepsilon_{ij}^e + \varepsilon_{ij}^P , \qquad (3.2)$$

where

$$\varepsilon_{ij}^e = \frac{1+\nu}{E} s_{ij} + \frac{1-2\nu}{3E} \sigma_{kk}\delta_{ij} ,$$

$$(3.3)$$

$$\varepsilon_{ij}^P = \frac{3}{2} \frac{\varepsilon_e^P}{\sigma_e} s_{ij} ,$$

with

$$s_{ij} = \sigma_{ij} - \frac{1}{3} \sigma_{kk}\delta_{ij} \qquad (3.4)$$

The effective stress, σ_e , and plastic strain, ε_e^P , corresponding to the J_2-flow theory are

$$\sigma_e = \sqrt{3J_2}$$

or

$$\sigma_e = \sqrt{\frac{3}{2} s_{ij} s_{ij}}$$

or, in explicit form,

$$\sigma_e = \left\{ \frac{1}{2}[(\sigma_{xx}-\sigma_{yy})^2+(\sigma_{yy}-\sigma_{zz})^2+(\sigma_{zz}-\sigma_{xx})^2] + 3(\tau_{xy}^2+\tau_{yz}^2+\tau_{zx}^2) \right\}^{1/2} , \quad (3.5a)$$

$$\varepsilon_e^P = \sqrt{\frac{2}{3} \varepsilon_{ij}^P \varepsilon_{ij}^P}$$

or

$$\varepsilon_e^P = \sqrt{\frac{2}{3}} \left[(\varepsilon_{xx}^P)^2 + (\varepsilon_{yy}^P)^2 + (\varepsilon_{zz}^P)^2 + 2(\varepsilon_{xy}^P)^2 + 2(\varepsilon_{yz}^P)^2 + 2(\varepsilon_{zx}^P)^2 \right]^{1/2} \quad (3.5b)$$

Making use of eqs (3.1)-(3.3),(3.5) the following relation is obtained between the effective stress and plastic strain:

$$\varepsilon_e^P = \alpha\varepsilon_Y \left(\frac{\sigma_e}{\sigma_Y}\right)^N \qquad (3.6)$$

with $\varepsilon_Y=\gamma_Y/\sqrt{3}$, $\sigma_Y=\sqrt{3} \tau_Y$. Since the near crack tip fields with a high level of plastic deformations are considered, the stress-strain relation may be approximated by

$$\varepsilon_{ij} \cong \varepsilon_{ij}^P = \frac{3}{2} \alpha\varepsilon_Y \left(\frac{\sigma_e}{\sigma_Y}\right)^{N-1} \frac{s_{ij}}{\sigma_Y} \qquad (3.7)$$

where eqs (3.3) and (3.6) are taken into account.

The order of the dominant stress and strain fields singularity can be obtained directly from the analysis of the path-independent J-integral

(Rice, 1968a). Thus, for a circular contour of radius r enclosing the crack tip the J-integral (2.5) is expressed as (Rice and Rosengren, 1968)

$$J = r \int_{-\pi}^{\pi} (W \cos\theta - \sigma_{ij}n_j \frac{\partial u_i}{\partial x}) \, d\theta \tag{3.8}$$

Since the value of J-integral is independent on r, both terms in brackets of eq.(3.8) have to reveal the singularity of the form

$$W \sim r^{-1} \, , \qquad \sigma_{ij}n_j \frac{\partial u_i}{\partial x} \sim r^{-1} \tag{3.9}$$

The strain energy density for a power-law material is expressed as (Kanninen and Popelar, 1985)

$$W = \frac{N}{N+1} \alpha \sigma_Y \varepsilon_Y \left(\frac{\sigma_e}{\sigma_Y}\right)^{N+1} \tag{3.10}$$

Equations (3.9) and (3.10) lead to the following general representation of stress, strain and displacement fields near the crack tip (Rice and Rosengren, 1968):

$$\sigma_{ij}(r,\theta;\alpha,N) = \sigma_Y K(\alpha,N) \, r^{-1/(N+1)} \, \Sigma_{ij}(\theta;N)$$

$$\sigma_e(r,\theta;\alpha,N) = \sigma_Y K(\alpha,N) \, r^{-1/(N+1)} \, \Sigma_e(\theta;N)$$

$$\tag{3.11}$$

$$\varepsilon_{ij}(r,\theta;\alpha,N) = \alpha\varepsilon_Y K^N(\alpha,N) \, r^{-N/(N+1)} \, E_{ij}(\theta;N)$$

$$u_i(r,\theta;\alpha,N) = \alpha\varepsilon_Y K^N(\alpha,N) \, r^{1/(N+1)} \, U_{ij}(\theta;N)$$

where the coordinate functions, $\Sigma_{ij}, \Sigma_e, E_{ij}, U_i$, and the amplitude of the dominant singularity, K, are to be determined by solving a boundary value problem. Note that the same result on the dominant field singularity was obtained by Hutchinson (1968a) when analysing the first eigenvalue of corresponding differential equation for the Airy function.

3.2. Formulation of the Boundary Value Problem

For further stress and strain analysis, the Airy stress function Ψ is introduced as follows (Hutchinson, 1968a; Rice and Rosengren, 1968)

$$\Psi(r,\theta) = Kr^s \sigma_Y \phi(\theta) \tag{3.12}$$

The stress components which satisfy the equilibrium equations are

$$\sigma_{\theta\theta} = \frac{\partial^2\Psi}{\partial r^2} \, , \quad \sigma_{rr} = \frac{1}{r}\frac{\partial\Psi}{\partial r} + \frac{1}{r^2}\frac{\partial^2\Psi}{\partial\theta^2} \, , \quad \tau_{r\theta} = -\frac{\partial}{\partial r}\left(\frac{1}{r}\frac{\partial\Psi}{\partial\theta}\right)$$

or, using eqs (3.11) and (3.12),

$$\Sigma_{\theta\theta} = s(s-1)\phi \, , \quad \Sigma_{rr} = s\phi + \phi'' \, , \quad \Sigma_{r\theta} = (1-s)\phi' \tag{3.13}$$

with $s = (2N+1)/(N+1)$.

   Substituting stress components (3.13) into the compatibility equation

$$r^{-1} \frac{\partial^2}{\partial r^2}(r\varepsilon_{\theta\theta}) + r^{-2} \frac{\partial^2 \varepsilon_{rr}}{\partial \theta^2} - r^{-1} \frac{\partial \varepsilon_{rr}}{\partial \varepsilon_r} - 2r^{-2} \left(r\frac{\partial \varepsilon_{r\theta}}{\partial \theta}\right) = 0 \ .$$

one can find

$$\left(\frac{d^2}{d\theta^2} + \frac{N}{N+1}\right)(\Sigma_e^{N-1} S_{rr}) - \frac{N}{(N+1)^2} \Sigma_e^{N-1} S_{\theta\theta} - \frac{2}{N+1} \frac{d}{d\theta}(\Sigma_e^{N-1} S_{r\theta}) = 0, \quad (3.14)$$

where S_{ij} are dimensionless deviatoric stress components,

$$S_{ij} = \Sigma_{ij} - \frac{1}{3}\Sigma_{kk}\delta_{ij}$$

Note that expressions for Σ_e and S_{ij} are different for plane strain and plane stress. After certain algebraic rearrangements, one can find for the case of plane strain

$$\Sigma_e = \left[\frac{3}{4}(\Sigma_{rr} - \Sigma_{\theta\theta})^2 + 3\Sigma_{r\theta}^2\right]^{1/2} \ ,$$

$$\Sigma_e = \left[\frac{3}{4}\left(\phi'' + \frac{2N+1}{(N+1)^2}\phi\right)^2 + \frac{3N^2}{(N+1)^2}(\phi')^2\right]^{1/2} \ , \quad (3.15)$$

and

$$\left[\frac{d^2}{d\theta^2} + \frac{N(N+2)}{(N+1)^2}\right]\left[\Sigma_e^{N-1}\left(\phi'' + \frac{2N+1}{(N+1)^2}\phi\right)\right] + \frac{4N}{(N+1)^2}\frac{d}{d\theta}\left(\Sigma_e^{N-1}\phi'\right) = 0 \quad (3.16)$$

Calculations for the case of plane stress yield

$$\Sigma_e = (\Sigma_{rr}^2 + \Sigma_{\theta\theta}^2 - \Sigma_{rr}\Sigma_{\theta\theta} + 3\Sigma_{r\theta}^2)^{1/2} \ ,$$

$$(3.17)$$

$$\Sigma_e = \left[\left(\phi'' + \frac{2N+1}{N+1}\right)^2 + \frac{N^2(2N+1)^2}{(N+1)^4}\phi^2 - \frac{N(2N+1)}{(N+1)^2}\phi\left(\phi'' + \frac{2N+1}{N+1}\right) + \frac{3N^2}{(N+1)^2}(\phi')^2\right]^{1/2}$$

and

$$\left(\frac{d^2}{d\theta^2} + \frac{N}{N+1}\right)\left[\Sigma_e^{N-1}\left(2\phi'' + \frac{(N+2)(2N+1)}{(N+1)^2}\phi\right)\right] + \frac{N}{(N+1)^2}\Sigma_e^{N-1}\left[\phi'' - \frac{(N-1)(2N+1)}{(N+1)^2}\phi\right]$$

$$+ \frac{6N}{(N+1)^2}\frac{d}{d\theta}\left(\Sigma_e^{N-1}\phi'\right) = 0 \quad (3.18)$$

Equations (3.16) and (3.18) are forth-order differential equations for the ϕ function resolved for the fourth-order derivative, $d^4\phi/d\theta^4$.

The boundary conditions for the stress function can be formulated from the following considerations. Since the crack surfaces are traction-free, $\sigma_{\theta\theta}(\pm\pi)=\tau_{r\theta}(\pm\pi)=0$, or making use of eqs (3.13), we get in terms of the stress function

$$\phi(\pm\pi) = \phi'(\pm\pi) = 0 \tag{3.19}$$

It is evident that the stress function is to be an even function of θ for Mode I crack problem and an odd function of θ for Mode II crack problem. Thus the boundary conditions are

$$\phi'(0) = \phi'''(0) = \phi(\pi) = \phi'(\pi) = 0 \tag{3.20}$$

for Mode I, and

$$\phi(0) = \phi''(0) = \phi(\pi) = \phi'(\pi) = 0 \tag{3.21}$$

for Mode II.

3.3. Calculation of the Amplitude of the HRR-Fields

Since the boundary value problem formulated in the previous section is solved, the amplitude K of the dominant singular fields (3.11) is the only unknown parameter. It was shown by Hutchinson (1968a) that the K-value is expressed via the J-integral, the stress function and its derivatives, as well as parameters of the Ramberg-Osgood equation. Substituting eqs (3.10) and (3.11) into eq.(3.8) one can find

$$J = \alpha\sigma_Y\varepsilon_Y I(N)K^{N+1}, \quad \text{or} \quad K = \left[\frac{J}{\alpha\sigma_Y\varepsilon_Y I(N)}\right]^{1/(N+1)} \tag{3.22}$$

with

$$I(N) = \int_{-\pi}^{\pi} \left\{ \frac{N}{N+1}\Sigma_e^{N+1}\cos\theta - \frac{1}{N+1}(U_r\Sigma_{rr} + U_\theta\Sigma_{r\theta})\cos\theta \right.$$
$$\left. - [\Sigma_{rr}(U_\theta - U'_r) - \Sigma_{r\theta}(U_r + U'_\theta)]\sin\theta \right\} d\theta \tag{3.23}$$

The I-value depends on the strain hardening exponent N, as well as on the deformation mode and plane strain/plane stress conditions. The displacement functions and their derivatives obtained from Cauchy's equations are

$$U_r = \frac{3}{4}(N+1)\Sigma_e^{N-1}\left[\phi'' + \frac{2N+1}{(N+1)^2}\phi\right],$$

$$U'_r = \frac{3}{4}(N+1)\frac{d}{d\theta}(\Sigma_e^{N-1})\left[\phi'' + \frac{2N+1}{(N+1)^2}\phi\right]$$
$$+ \frac{3}{4}(N+1)\Sigma_e^{N-1}\left[\phi''' + \frac{2N+1}{(N+1)^2}\phi'\right], \tag{3.24}$$

$$U_\theta = \frac{N+1}{N}U'_r + 3\Sigma_e^{N-1}\phi', \quad U'_\theta = -\frac{N+2}{N+1}U_r$$

for plane strain, and

$$U_r = (N+1) \Sigma_e^{N-1} \left[\phi'' + \frac{(N+2)(2N+1)}{2(N+1)^2} \phi \right] ,$$

$$U'_r = (N+1) \frac{d}{d\theta} (\Sigma_e^{N-1}) \left[\phi'' + \frac{(N+2)(2N+1)}{2(N+1)^2} \phi \right]$$

$$+ (N+1) \Sigma_e^{N-1} \left[\phi''' + \frac{(N+2)(2N+1)}{2(N+1)^2} \phi' \right] \qquad (3.25)$$

$$U_\theta = \frac{N+1}{N} U'_r + 3\Sigma_e^{N-1} \phi' ,$$

$$U'_\theta = \frac{1}{2} \Sigma_e^{N-1} \left[\frac{(N-1)(2N+1)}{(N+1)^2} \phi - \phi'' \right] - U_r$$

for plane stress.

3.4. Numerical Solution of the Boundary Value Problem

As it follows from the previous analysis, derivation of the dominant singular terms of elastic-plastic crack tip fields is reduced to determination of the stress function which is to satisfy the fourth-order differential equation (3.16) or (3.18) and boundary conditions (3.20) or (3.21) (depending upon the mode of deformation and plane strain/plane stress conditions). Thus, the two-point boundary value problem is to be solved. For this purpose, the fourth-order Runge-Kutta integration scheme and the shooting method are employed. The latter allows for reducing the two-point boundary value problem to Cauchy's problem.

For Mode II crack the boundary conditions (3.21) can be reformulated into the initial conditions as follows

$$\phi(0) = 0; \quad \phi'(0) = \varphi_1; \quad \phi''(0) = 0; \quad \phi'''(0) = \varphi_2 \qquad (3.26)$$

where φ_1 and φ_2 are determined through an iteration process to satisfy the boundary conditions at $\theta = \pi$:

$$\phi(\pi) = \phi'(\pi) = 0 \qquad (3.19a)$$

Here two notions are to be remarked:

(1) Only φ_1 to φ_2 ratio affects the solution of the boundary value problem. Indeed, it follows from eqs (3.7),(3.11),(3.13),(3.15),(3.17),(3.22)-(3.25) that

$$\Sigma_{ij} \sim \varphi_1, \quad \Sigma_e \sim \varphi_1, \quad E_{ij} \sim \varphi_1, \quad U_i \sim \varphi_1^N, \quad I(N) \sim \varphi_1^{N+1}, \quad K \sim \varphi_1^{-1} ,$$

and no absolute values of stress, strain and displacement components depend on φ_1. Thus, an arbitrary value of φ_1 (or φ_2) may be choosen. In the present analysis, by analogy with Hutchinson (1968a,b) and Shih (1974), the φ_1-value is put to satisfy the normalization condition

$$\Sigma_{e,\max} = 1 ,$$

while the φ_2-value is found by the shooting method to satisfy the boundary conditions (3.19a).

(2) Both boundary conditions (3.19a) are satisfied simultaneously. The proof of this fact is given by Rice and Rosengren (1968) and is based on the proof of the J-integral path-independence (Rice, 1968a). Since the crack surfaces are traction-free, the following relation is valid at $\theta=\pi$ and for any r-value:

$$-\sigma_{\theta\theta}\frac{\partial u_\theta}{\partial r} + \tau_{r\theta}\frac{\partial u_r}{\partial r} = 0 \,,$$

and "the vanishing of $\tau_{r\theta}$ on the crack surface implies the vanishing of $\sigma_{\theta\theta}$" (Rice and Rosengren, 1968).

In solving the boundary value problem, no convergence was found for certain initial values of φ_2 with the derivative ϕ''' tending to infinity. Thus, an appropriate first approximation function $\varphi_2=\varphi_2(N)$, both for plane strain and plane stress, has been derived in numerical experiment and employed after in the iterative process. The iterative process is stopped when the following condition is satisfied

$$\max \{|\phi(\pi)| \,;\, |\phi'(\pi)|\} < \delta \,,$$

with $\delta=10^{-4}$. A step size of 0.45° is found to be the best choise in the Runge-Kutta integration procedure. Further diminishing of the step size does not affect accuracy of the solution. Under above conditions, the convergence of numerical procedure is obtained in two to nine iterations within the range of the strain hardening exponent $1<N\leq80$, both for plane strain and plane stress.

The variation of stress and strain fields, Σ_{ij} and E_{ij}, at a crack tip in Mode II for plane strain and plane stress conditions are presented in Fig.8 and Fig.9 respectively (in those figures the index "t" corresponds to "θ"); computations were performed for the range of the strain hardening exponent from $N=1.01$ to $N=80$, and the limiting cases may be refered respectively as to purely elastic and perfectly plastic solutions.

4. Rate Sensitivity of Material Properties

Three materials with different rate sensitivity of their plasticity properties have been analysed, and the constants in the Ramberg-Osgood equation (τ_Y, α, N) change accordingly as functions of strain rate:

(1) *mild steel*; the basic data on the rate sensitivity of the yield stress are available from the work of Campbell and Ferguson (1970) where steel of the following chemical composition was studied: 0.12%C, 0.10%Si, 0.62%Mn, 0.029%S, <0.004%Pb. Also data of Klepaczko (1969) on technically pure iron (0.05%C) and Tanaka and Kinoshita (1967) (0.03%C) were used to study strain rate effect on parameters describing stress-strain relation;

(2) *fully annealed titanium alloy* Ti6Al4V; the data on behavior of stress-strain curves at different strain rates are available from the paper by Maiden and Green (1966);

(3) *aluminum alloy* Al 6061-T6 (1%Mg, 0.6%Si, 0.25%Cu, 0.25%Cr); the strain rate effect on the yield stress and stress-strain curves for this alloy was studied by Maiden and Green (1966), some additional results can be found in the work of Jiang and Chen (1974).

The behavior of those materials has been analysed for the case of room temperature and strain rates from 10^{-4} to 10^3 s^{-1}.

Figure 11 shows stress-strain curves for technically pure iron obtained in pure shear at the strain rate range $\dot{\gamma} = 1.31 \times 10^{-4}...55$ s^{-1} (Klepaczko, 1969). For this material, the lower (τ_{YL}) and upper (τ_{Y0}) yield stresses, as well as the slope of stress-strain curve, are changed significantly with increasing strain rate. The experimental data of

Klepaczko (1969) on variation of τ_{YL} versus log $\dot{\gamma}$ are shown in Fig.12a, corresponding results of Campbell and Ferguson (1970) and Tanaka and Kinoshita (1967) are also presented. Note that original results of the latter authors obtained in compression are transformed here to the stress-strain diagram in shear according to

$$\tau_{YL} = \sigma_{YL}/\sqrt{3}, \quad \gamma = \sqrt{3}\,\varepsilon \qquad (4.1)$$

An averaged τ_{YL} versus log $\dot{\gamma}$ curve is fitted to the experimental data in Fig.12a within the strain rate range from 10^{-4} to 10^5 s^{-1}.

Based on results of Klepaczko (1969), Fig.11, the Ramberg-Osgood constants N and α in eq.(3.1), have been found and they are shown versus strain rate in Fig.12b. It was observed in many studies on mild steel (see, e.g., Klepaczko, 1969) that with increasing strain rate the slope of the strain hardening part of the stress-strain curve diminishes. Above certain level of strain rate $(\dot{\gamma} > 10^2 s^{-1})$ when adiabatic heating is of importance, this part of the stress-strain diagram shows a negative slope. Since it is impossible in the present analysis to model "negative" strain hardening, it is assumed that the value of N tends to infinity at high strain rates $(\dot{\gamma} > 10^2 s^{-1})$. This

case corresponds to the model of elastic-perfectly-plastic material. With this assumption taken into account, the N versus log $\dot{\gamma}$ curve in Fig.12b is extrapolated to $\dot{\gamma}=10^3$ s^{-1}. An appropriate extrapolation of the constant α versus log $\dot{\gamma}$ is also shown. Based on results presented in Fig.12a,b, one can conclude that there is strong effect of strain rate on the Ramberg-Osgood parameters for mild steel. Both the lower yield stress, τ_Y, and strain hardening exponent, N, are rapidly increasing with log $\dot{\gamma}$, while the value of α is slightly decreasing.

Figure 13 shows test data of Maiden and Green (1966) obtained in compression for titanium alloy Ti6Al4V in the range of strain rate $\dot{\varepsilon} = 4\times10^{-3}...20$ s^{-1}, or after transformation according to (4.1), $\dot{\gamma} = 6.9\times10^{-3}...34.6$ s^{-1}. The strain rate dependence of the yield stress, τ_Y, for this alloy is shown in Fig.14a. Here the yield stress in shear is found as $\tau_Y = \sigma_{0.2}/\sqrt{3}$.

The τ_Y versus log $\dot{\gamma}$ curve is extrapolated to two extreme limits $\dot{\gamma}=10^{-4}$ s^{-1} and $\dot{\gamma}=10^3$ s^{-1}. Variation of the constants in the Ramberg-Osgood equation is presented in Fig.14b. One can conclude that no much effect of strain rate on α and N is observed. Both the N versus log $\dot{\gamma}$ and α versus log $\dot{\gamma}$ curves are approximated by straight lines and, thus, extrapolated within the whole range of the strain rate considered (Fig.14b).

Test data on Al 6061-T6 (Maiden and Green, 1966) in compression at the range of strain rate $\dot{\varepsilon}=9\times10^{-3}...910$ s^{-1} or, equivalently, $\dot{\gamma}=1.56\times10^{-2}...1.58\times10^3$ s^{-1} (Fig.15), reveal no strain rate effect on the stress-strain curve. The curve is approximated by the Ramberg-Osgood equation (3.1) with $\tau_Y=175$ MPa, N=4.3 and $\alpha=1.54$. Similar results but with a small rate sensitivity of the yield stress, σ_Y, have been reported for the same material by Jiang and Chen (1974), within the range of strain rate $\dot{\varepsilon}=1.6\times10^{-3}...210$ s^1, or $\dot{\gamma}=2.8\times10^{-3}...360$ s^{-1}. Their data are presented in Fig.16 as τ_Y versus log $\dot{\gamma}$ and show a linear dependence of the yield stress versus logarithm of strain rate.

It is important to note that in Fig.15 the engineering stress-strain curves which are presented with no account for adiabatic heating at high strain rates. In fact, if the effect of adiabatic heating is considered, an aluminum alloy reveals strain rate sensitivity of its mechanical properties.

Note also that at high strain rates ($\dot{\gamma} >10^3$ s^{-1}), the 0.2% proof stress of aluminum alloy becomes rate sensitive and its behavior is similar to that of yield stress observed for steels.

5. Strain Rate Effect on Evolution of the Crack Tip Plastic Zone for Structural Materials Via SSY Approximation

In the previous chapters rate sensitivity of mechanical properties of mild steel. titanium and aluminum alloys in the strain rate range $\dot{\gamma}=10^{-4}...10^3$ s^{-1} has been discussed, as well as the two-parameter model of the plastic zone near a crack tip in Mode II has been analyzed within the SSY approximation. In that model both size and shape of the plastic zone depend strongly on the ratio of the applied shear stress to the yield stress, τ_{appl}/τ_Y, as well as on the crack geometry specified by the value of the stress intensity factor, K_{II}. In the next part the analysis of evolution of the plastic zone near the crack tip in Mode II with parametric variation of the strain rate is performed for different materials.

The crack geometries. which are of practical interest, are: (1) semi-infinite crack in an infinite plate and (2) finite length edge crack in a strip. The first geometry represents the limiting case of a very large crack which is typical for problems arising in geomechanics, pipeline safety assessment etc. The second one corresponds to specimen geometries used in fracture toughness tests in Mode II (Banks-Sills and Arcan. 1986; Banks-Sills and Sherman, 1991; Davies et al., 1985; Kalthoff and Winkler, 1987; Maccagno and Knott, 1992; Mason et al., 1992; Nishioka et al., 1991; Tohgo et al., 1989; Tohgo and Ishii, 1992). The geometry used by Kalthoff and Winkler (1987) and Nishioka et al. (1991) with crack length $a = 50$ mm and specimen width $W = 100$ mm is studied in the present work.

Analysis of the evolution of plastic zone with strain rate is carried out for constant value of applied stress. i.e. $\tau_{appl}(\dot{\gamma})=$const, while the yield stress as a function of the strain rate is involved. Thus, the load level is characterized by the ratio of τ_{appl} to the yield stress τ_{YS} in test with $\dot{\gamma}=10^{-4}$ s^{-1}, which is refered to as quasi-static case. Two different stress levels are analysed: $\tau_{appl}/\tau_{YS}=0.2$ and 0.5.

To characterize the evolution of plastic zone, three parameters are introduced:

(1) plastic zone size ahead of the crack tip, $r_p(\theta=0)$, which is normally the maximum size;

(2) half the plastic zone hight, h_{max} (since the plastic zone is symmetric with respect to the crack line, its total maximum hight equals to $2h_{max}$);

(3) the ratio of the plastic zone size behind the crack tip to that ahead of the crack tip, $r_p(\theta=\pi)/r_p(\theta=0)$; this parameter characterizes asymmetry of the shape of plastic zone.

In the case of a semi-infinite crack the values of $r_p(0)$ and h_{max} are normalized by the crack length, a. Analyses are carried out for plane strain conditions with Poisson's ratio $v=0.33$.

Estimations of the strain rate effect on the evolution of plastic zone near the tip of a semi-infinite and an edge crack in mild steel are presented in Fig.17 and Fig.18. One can find significant reduction of the size of plastic zone with increasing strain rate from 10^{-4} to 10^3 s^{-1}. For the stress level $\tau_{appl}/\tau_{YS}=0.2$ (Figs 17a and 18a), reduction of $r_p(0)$ and h_{max},

within the range of $\dot{\gamma}$ considered, reaches value of five times for the two crack geometries studied, while the ratio $r_p(\pi)/r_p(0)$ is kept nearly constant and equal 1, i.e. the plastic zone is nearly symmetric with respect to the y-axis ($\theta=\pi/2$). For the stress level $\tau_{appl}/\tau_{YS}=0.5$ (Figs 17b and 18b), there is stronger rate effect both on the plastic zone size and shape. If the strain rate is increased from 10^{-4} to 10^3 s^{-1}, the values of $r_p(0)$ and h_{max} for a semi-infinite crack are diminished respectively 7.4 and 6.0 times. For an edge crack this reduction reaches 5.6 and 5.2 times. One can see also from Figs 17b and 18b a significant change in the shape of plastic zone which is asymmetrical in quasi-static loading and nearly symmetrical at high strain rate. The asymmetry of the plastic zone for quasi-static loading is characterized by factor $r_p(\pi)/r_p(0)=0.47$ for a semi-infinite crack and 0.76 for an edge crack.

Significant strain rate effect on the size and shape of plastic zone found for mild steel is a consequence of strong rate sensitivity of the lower

yield stress. The latter is increased 2.2 times with increasing $\dot{\gamma}$ from 10^{-4} to 10^3 s^{-1}. For titanium alloy corresponding increase of the yield stress reaches 1.4 which results in a lower reduction of the plastic zone in comparison to steel. At $\tau_{appl}/\tau_Y=0.2$, the size of plastic zone is diminished twice for both crack configurations (Figs 19a and 20a). At $\tau_{appl}/\tau_Y=0.5$, the value of $r_p(0)$ is decreased respectively 2.6 and 2.2 times for a semi-infinite and an edge crack, while the value of h_{max} is diminished twice for both crack configurations (Figs 19b and 20b). The change in the factor $r_p(\pi)/r_p(0)$ is similar to that observed for mild steel with the shape of plastic zone being more asymmetric at higher strain rates and $\tau_{appl}/\tau_Y=0.5$.

As it is mentioned in Chapter 4, no rate sensitivity of the yield stress for aluminum alloy is found at $\dot{\gamma}=10^{-4}...10^3$ s^{-1}. Thus, one can expect no strain rate effect on the size and shape of plastic zone within this range of $\dot{\gamma}$. The predicted values of the parameters of the plastic zone geometry are listed below:

		$\tau_{appl}/\tau_Y=0.2$	$\tau_{appl}/\tau_Y=0.5$
Semi-infinite crack	$r_p(0)/a$	0.017	0.168
	h_{max}/a	0.008	0.045
	$r_p(\pi)/r_p(0)$	0.929	0.470
Edge crack	$r_p(0)$, mm	1.605	11.39
	h_{max}, mm	0.730	4.64
	$r_p(\pi)/r_p(0)$	0.994	0.79

Note that the present approach to estimate the size and shape of plastic zone takes no account of stress redistribution due to plasticity. If Irwin's correction is applied, the value of r_p ahead of the crack tip is twice larger then predicted by Figs 17 to 20, while the $r_p(\pi)$ and h_{max} values may remain unchanged. Thus, more significant plastic zone asymmetry can be expected with the plastic zone being predominantly concentrated ahead of the crack tip. For instance, with Irwin's correction, the $r_p(\pi)/r_p(0)$ factor for an edge crack in mild steel at $\tau_{appl}/\tau_{YS}=0.5$ reaches value 0.38. This result is in qualitative agreement with the finite-element solution of Banks-Sills and Sherman (1990). (Since a specimen with stress concentrator is analyzed by those authors, quantitative comparison of results is not available.)

It seems reasonable to say, by analogy with Mode I crack, eqs (1.4) and (1.5), that certain relations between the maximum size of plastic zone ($r_{p,max}$), material fracture toughness (K_{IIC}) and minimum specimen thickness (B) must exist. If it is the case and the ratio $r_p(0)/B$ is considered as a measure of plasticity effects at the crack tip, the results on variation of r_p with strain rate can be used in predicting the minimum thickness (or

width) of specimen versus $\dot{\gamma}$. For example, at the stress level $\tau_{appl}/\tau_{YS}=0.5$ (which is normal in Mode II fracture toughness tests; see Banks-Sills and Sherman, 1991), our results for an edge crack in mild steel (Fig.18b) predict the specimen thickness at high strain rate ($\dot{\gamma}=10^3$ s^{-1}) 5.6 times smaller than in quasi-static test ($\dot{\gamma}=10^{-4}$ s^{-1}). For titanium alloy at the same conditions (Fig.20b), reduction of the specimen size is 2.2 times.

6. Strain Rate Effect on Behavior of the Crack Tip
Fields in Mode II Via the HRR-Solution

The results on evolution of the plastic zone with strain rate as a parameter presented in Chapter 5 are based exclusively on the rate sensitivity of the yield stress. Some additional information on the behavior of crack tip fields at different strain rates can be obtained from analysis of the HRR-solution, eqs (3.11), which incorporate parameters of the stress-strain curve. However, it is important to note that the HRR-solution cannot be directly employed to evaluate the size of the plastic zone near crack tip. Indeed, the plastic zone boundary is interpreted as a line of the constant equivalent stress, i.e. $\sigma_e = \sigma_Y$ with $\sigma_e^P = 0$. Since the elastic stress and strain components have been neglected when deriving the HRR-field (see eq.(3.7)), the latter seems to be valid only at high stress and strain levels,

$$\sigma_e > \sigma_Y \quad \text{and} \quad \varepsilon_e^P >> \varepsilon_Y ,$$

or, equivalently, in a small vicinity of the crack tip with a radius being much smaller the plastic zone size, i.e. $r_{HRR} << r_p$. Moreover, eqs (3.11) yield only the dominant components of the crack tip field. The range of dominance of the HRR-solution is often determined as (e.g., Du et al., 1991)

$$r_{HRR} \cong \beta \frac{J}{\sigma_Y} \tag{6.1}$$

with β ranging from about 2 to 5. In the case of numerical example presented in Fig.18b (Mode II crack of finite length in mild steel) one can find from eq.(6.1) $r_{HRR} = 0.05...0.1$ mm.

Rice and Rosengren (1968) calculated boundaries $r_\sigma(\theta)$ of the equal equivalent stress versus the strain hardening exponent in Mode I. Their results on the r_σ-evolution are in qualitative agreement with direct computations of the size and shape of plastic zone near the crack tip (Shih, 1974). Thus, a qualitative analysis of the behavior of plastic zone near the crack tip at different strain rates can be performed employing the HRR-solution. However, it seems to be more rational in such analysis to characterize the evolution of crack tip fields via the equivalent plastic strain which simplifies identification of a corresponding point of stress-strain curves obtained at different strain rates.

6.1. Evolution of the Strain Field near a Crack Tip in Mode II
for Mild Steel and Titanium Alloy

Numerical examples of the strain field near a crack tip are given for the case of a finite length edge crack in a strip with $a = 50$ mm and $W = 100$ mm. Corresponding assessments of evolution of the plastic zone founded on the SSY-approximation are presented in Figs 18 and 20 for mild steel and titanium alloy respectively.

Making use of eqs (3.6),(3.11),(3.22) and (2.7), one can find the radius of a boundary of the equal equivalent plastic strain $\varepsilon_e^P = \beta_\varepsilon \gamma_Y$ (with β_ε=const) as follows

$$r_\varepsilon = \frac{1 - v^2}{3\alpha I(N)} \left(\frac{\alpha}{\sqrt{3}\,\beta_\varepsilon}\right)^{(N+1)/N} \Sigma_e^{N+1} \left(\frac{K_{II}}{\tau_Y}\right)^2 \qquad (6.2)$$

Here the small scale yielding and plane strain conditions at the crack tip are assumed; also the Huber-Mises yield criterion is employed.

Figure 21 presents variation of r_ε-boundaries at the crack tip in mild steel at the strain rate range $\dot\gamma = 1.31\times10^{-4}...10^3$ s^{-1}. Two deformation levels are ana'ysed: $\varepsilon_e^P = 0.03$ and 0.06 which correspond approximately to points with $\gamma = 0.05$ and 0.1 on the stress-strain diagrams in Fig.11. The results in Fig.21 demonstrate more complicated and somewhat different behavior of the crack tip fields versus the strain rate than those presented in Fig.18a,b. With increasing strain rate the dimensionless radius

$$R_\varepsilon = r_\varepsilon \left(\frac{\tau_{YS}}{K_{II}}\right)^2$$

of the r_ε-boundaries ahead of the crack tip sligtly diminishes and after takes the maximum value at $\dot\gamma = 2.85\times10^{-2}$ s^{-1}. The values of $R_{\varepsilon,max}$ are 0.0072 and 0.003 for $\varepsilon_e^P = 0.03$ and 0.06 respectively. Further increase in the strain rate results in fast diminishing of the R_ε value ahead of the crack tip. This nonmonotonic variation of the $R_{\varepsilon,max}$ value is a consequance of a complex dependence of plasticity parameters (σ_Y, α, N) upon the strain rate (Fig.12). At lower strain rates (1.31×10^{-4} s^{-1} to 2.85×10^{-2} s^{-1}) the value of α is nearly constant, and increase of σ_Y and N with strain rate leads to $R_{\varepsilon,max}$ be almost unchanged. At higher strain rates the HRR-solution predicts substantial reduction in the value of $R_{\varepsilon,max}$ due to decreasing of α and increasing of σ_Y, which effect is much stronger than expansion of the R_ε-zone due to increase of the strain hardening exponent.

In contrast, the R_ε value behind the crack tip and the maximum hight of r_ε-boundaries decrease monotonically with increasing $\dot\gamma$. Another important feature of r_ε-boundaries behavior consists in fast diminishing of the $r_\varepsilon(\pi)/r_\varepsilon(0)$ ratio which changes from 0.24 at $\dot\gamma = 1.31\times10^{-4}$ s^{-1} to 0.05 at $\dot\gamma = 10^3$ s^{-1}. Thus, if a certain correlation between r_ε and r_p values exists, one can conclude that at high strain rates almost the whole plastic zone area is concentrated ahead of the crack tip; note that the SSY-approximation (Fig.18) predicts the plastic zone at high strain rates nearly symmetrical with respect to the y-axis.

Numerical results on evolution of r_ε-boundaries at the crack tip in titanium alloy Ti6Al4V are presented in Fig.22 for $\varepsilon_e^P = 0.02$. This deformation level corresponds to $\gamma^P = 0.035$ and total deformation $\varepsilon_e = 0.032...0.036$ in Fig.13. Comparing to mild steel, no significant rate sensitivity of r_ε-boundaries at the crack tip in titanium alloy is observed: with increasing strain rate from 10^{-4} s^{-1} to 10^3 s^{-1}, the maximum size and hight of the r_ε-boundary is diminished approximately 15%, while the size of the r_ε-boundary behind the crack tip is decreased twice. This is due to relatively weak rate sensitivity of the plasticity parameters for titanium alloy.

6.2. Comparison of Approximate Results on the Plastic Zone Analysis with Numerical Solutions

Only a few numerical solutions on the plastic zone near a crack tip in Mode II are known. Shih (1974) and Pan and Shih (1990) published results on variation of the plastic zone geometry versus the strain hardening exponent at constant α and σ_Y. Their finite-element solutions are constructed within the framework of the boundary layer formulation for small scale yielding and plane strain. Banks-Sills and Sherman (1990) obtained an elastic-plastic stress field for the specimen shown in Fig.6.17. Different levels of the applied load were analysed: $\tau_{appl}/\tau_Y = 0.35...0.52$, where τ_{appl} is a nominal stress defined as

$$\tau_{appl} = \frac{P}{t\,W} \, ,$$

t is the specimen thickness, W is the specimen width in a cracked section ($W = 30$ mm in Fig.6.17). The lower and upper load levels may be refered respectively to as a small scale yielding and fully plastic solutions.

Plastic zone boundaries versus N are shown in Fig.23, after Shih (1974) and Pan and Shih (1990). In both papers the constant α in the Ramberg-Osgood equation is equal 3/7. Variation of the plastic zone versus the load level is presented in Fig.24, after Banks-Sills and Sherman (1990). Their results are obtained for aluminum alloy Al 7075-T7351 with parameters of the Ramberg-Osgood equation found to be $\alpha=1.25$, N=14. Table 6.1 lists dimensionless parameters of the plastic zone geometry

$$R_{p,max} = r_p(0)\left(\frac{\tau_Y}{K_{II}}\right)^2 , \quad H_p = h_p\left(\frac{\tau_Y}{K_{II}}\right)^2 \quad \text{and} \quad r_p(\pi)/r_p(0)$$

found from the papers mentioned above, as well as results obtained in Chapter 2 founded on the two-parameter crack tip stress field representation (Fig.5b) and with Irwin's plasticity correction. One can conclude from analysis of numerical solutions that both effects of the strain hardening exponent and load level on the plastic zone behavior are similar: increase of N or τ_{appl}/τ_Y yields substantial growth of the plastic zone size

Table 6.1

Parameters of the plastic zone geometry

Reference	τ_{appl}/τ_Y	α	N	$R_{p.max}$	H_p	$r_p(\pi)/r_p(0)$
Shih (1974)	-	3/7	1	0.16	0.067	1.0
	-		3	0.24	0.080	0.5
	-		13	0.29	0.076	0.21
Pan and Shih (1990)	-	3/7	3	0.17	0.064	0.76
	-		10	0.21	0.061	0.32
Banks-Sills and Sherman (1990)	0.35	1.25	14	0.48	0.11	0.24
	0.45			0.69	0.12	0.15
	0.48			0.54	0.13	0.13
	0.52			0.43	0.10	0.15
Present study, 2-parametrical elastic stress field representation	0.2	-	-	0.34	0.071	0.46
	0.3			0.37	0.074	0.39
	0.5			0.53	0.085	0.23
Present study, r_σ-boundaries according to eq.(6.3)	-	3/7	3	0.26	0.075	0.28
	-		13	0.30	0.067	0.07
Present study, r_ε-boundaries at $\varepsilon_e^P/\varepsilon_Y = 1$	-	3/7	3	0.24	0.072	0.29
			13	0.38	0.091	0.06

ahead of the crack tip and diminishing of the $r_p(\pi)/r_p(0)$ ratio. At the same time only slight change in the H_p is observed.

One can find certain disagreement in reviewed numerical results. The data of Shih (1974) and Pan and Shih (1990) for identical conditions ($\alpha=3/7$, N=3) differ up to 50% when analysis is made for the $R_{p,max}$ value and $r_p(\pi)/r_p(0)$ ratio. Comparison of the plastic zone solution of Banks-Sills and Sherman (1990) with results cf Shih (1974) and Pan and Shih (1990) is not available because of the difference in values of α used in those analyses. Nevertheless, the asymmetry factor, $r_p(\pi)/r_p(0)$, in the SSY analysis ($\tau_{appl}/\tau_Y=0.35$) of Banks-Sills and Sherman (1990) is very close to that in Shih's (1974) solution with N=13.

It should be noted befor discussing results of the present study on the plastic zone behavior versus the load level, that the approach employed in

Chapter 2 together with Irwin's plasticity correction is equivalent to the use of the elastic-perfectly-plastic model ($N=\infty$). This is close to the case considered by Banks-Sills and Sherman (1990), and comparison of our results with the finite-element solution of Banks-Sills and Sherman (1990) seems to be resonable. One can find from the data presented in Table 6.1 that values of $R_{p,max}$ determined in the present study are within 20% of the numerical results, while the error in estimation of H_p and $r_p(\pi)/r_p(0)$ is higher (20...50%). Thus, for materials with high values of the strain hardening exponent the two-parameter crack tip field characterization together with Irwin's plasticity correction yield realistic assessments of the plastic zone size ahead of the crack tip in Mode II.

6.3. Correlation of r_σ and r_ε-Boundaries with the Plastic Zone Geometry

It is interesting to compare boundaries of equal equivalent stress and plastic strain with plastic zone configurations. Figure 25 shows variation of r_σ-boundaries versus the level of σ_e . Calculations were carried out for $\alpha=3/7$ and two values of the strain hardening exponent: $N=3$ and 13. After comparing of those results with data of Shih (1974) (see Fig.23a and Table 6.1), one can conclude coincidence of r_σ and r_p values ahead of the crack tip at $\sigma_e = 1.3\sigma_Y$ for $N=3$ and at $\sigma_e = 1.08\sigma_Y$ for $N=13$. It is evident that at $N\rightarrow\infty$ the condition $r_\sigma = r_p$ holds at $\sigma_e = \sigma_Y$; thus for $N\geq3$ the following relationship

$$\sigma_e = \sigma_Y (1 + 0.9/N) \tag{6.3}$$

seems to be valid to estimate the $r_p(0)$ value from the HRR-field. The numerical results on configuration of r_σ-boundaries for the stress level determined by eq.(6.3) are presented in Table 6.1. Note that not only values of $r_\sigma(0)$ but also the maximum hight of the r_σ-boundaries are in good agreement with r_p-solution of Shih (1974). At the same time the value of $r_\sigma(\pi)$ is underestimated. This is a consequance of the fact that the HRR-solution involves only dominant singular terms of the stress field. One could expect that the use of nonsingular terms in eqs (3.11) would lead to a more realistic assessments of r_σ as well as r_p-boundaries.

For the same conditions ($\alpha=3/7$, $N=3$ and 13), Fig.26 shows variation of r_ε-boundaries versus the level of ε_e^p . One can see a good agreement between r_ε-values ahead of the crack tip and r_p-solution of Shih (1974) at $\varepsilon_e^p = (1 ... 1.5) \varepsilon_Y$ (Table 6.1). Since the condition $r_\varepsilon(0) = r_p(0)$ is satisfied at nearly constant level of ε_e^p , the use of r_ε-boundaries to characterize the plastic zone behavior versus N seems to be preferable. However, this conclusion is valid only for materials which stress-strain curves can be approximated by the Ramberg-Osgood equation at low deformation levels, $\varepsilon_e^p \cong \varepsilon_Y$. It is not the case for mild steel which stress-strain diagram in low strain level is nonmonotonic (Fig.11).

7. Conclusions

In the present study an approximate parametric analysis of the strain rate effect on the crack tip fields in Mode II is carried out. Evolution of the plastic zone and crack tip stress and strain fields at different strain rates is modelled via corresponding quasi-static solutions which couple strain rate sensitivity with plasticity parameters (τ_Y, α, N). An attempt is made to predict the size and shape of the plastic zone within the SSY approximation based on the two-parameter characterization of the crack tip field, eq. (2.16). For materials with a high strain hardening, such approach together with Irwin's plasticity correction is found to provide an adequate evaluation of the plastic zone size ahead of the crack tip as well as the maximum hight of plastic zone. Our results on $r_{p,max}$-variation versus the load level are within 20% of the numerical solution by Banks-Sills and Sherman (1990), for τ_{appl}/τ_Y ranging from 0.35 to 0.52. By analogy with the case of Mode I (Larsson and Carlsson, 1973), the two-parameter characterization of the crack tip field can be employed in finite-element analysis through the boundary layer formulation. In this way more realistic plastic zone assessments can be obtained with minimum computational efforts.

Making use of the SSY approximation, evolution of the plastic zone near the crack tip is analysed at different strain rate for materials with different rate sensitivity of the yield stress. Significant decrease of the plastic zone size with increasing strain rate is found for mild steel. At the load level $\tau_{appl}/\tau_Y = 0.5$, which is typical for fracture toughness tests, increase of the strain rate from 10^{-4} s^{-1} to 10^{3} s^{-1} leads to 5.6... 7.4 times reduction in the maximum plastic zone size (depending upon a crack geometry). The rate sensitivity of the plastic zone size is stronger at higher load levels. For titanium alloy, the reduction factor of the plastic zone size is 2.2 at the same range of the strain rate. No rate sensitivity of the plastic zone is predicted for the aluminum alloy. Since the maximum size of the plastic zone can be considered as a measure of plasticity effects at the crack tip, one can expect reduction of the minimum specimen thickness for K_{IIC}-measurement at increased strain rates as proportional to the change of $r_{p,max}$.

When the HRR-solution is employed to characterize the crack tip fields, evolution of boundaries of equal equivalent stress and plastic strain can be derived. For mild steel, the maximum size of the r_ε-boundary changes in nonmonotonic way versus strain rate (Fig.21), with the maximum value at $\dot\gamma = 2.85 \times 10^{-2}$ s^{-1} for $\varepsilon_e^p = 0.03$ and at $\dot\gamma = 0.44$ s^{-1} for $\varepsilon_e^p = 0.06$. This maximum value found from Fig.21 is of the order $(10^{-2}... 10^{-3})a$, which is close to the process zone size. For deformation levels considered decrease of the r_ε-boundary for mild steel within the range of strain rate

from 10^{-4} s^{-1} to 10^3 s^{-1} constitutes 40...50%. In contrast, the size of r_ε-boundary for the titanium alloy is changed monotonically with strain rate, and the total reduction of the $r_{\varepsilon,max}$-value within the range of strain rate from 10^{-4} s^{-1} to 10^3 s^{-1} is 10%.

From the point of view of experimental investigation of crack initiation and fracture toughness measurement in Mode II, application of three types of specimens seems to be preferable: (a) specimen in asymmetric four-point bending (Fig.6.11); (b) compact specimen for three-point loading (Fig.6.15, Case 3); (c) compact specimen for two-point loading (Fig.6.17). These specimens provide pure Mode II at the crack tip. Some experimental data on determination of fracture toughness (Table 2.1) demonstrate that the K_{IIC}-values for metallic materials are normally higher than K_{IC}. However, the results of Tohgo et $al.$ (1990) show that it is not a common rule. For brittle materials (e.g., perspex, Al_2O_3 ceramics), the ratio K_{IIC}/K_{IC} is slightly less than unity. Note also that no unique fracture criterion can be employed to predict the crack initiation angle for brittle and ductile materials. The maximum tensile stress or minimum strain energy density criteria can be used in predicting a crack path in brittle materials, while the maximum shear stress criterion seems to control crack initiation in metals.

REFERENCES

Awaji, H. and Sato, S. (1978). Combined mode fracture toughness measurement by the disk test. *J. Engng Mater. Technol.* **100**, 175-182.

Banks-Sills, L. and Arcan, M. (1986). in *Fracture Mechanics: Seventeenth Volume*, ASTM STP 905, pp. 347-363.

Banks-Sills, L. and Sherman, D. (1990). Elasto-plastic analysis of a mode II fracture specimen. *Int. J. Fracture* **46**, 105-122.

Banks-Sills, L. and Sherman, D. (1991). J_{II} fracture testing of a plastically deforming material. *Int. J. Fracture* **50**, 15-26.

Betegòn, C. and Hancock, J.W. (1991). Two-parameter characterization of elastic-plastic crack-tip fields. *J. Appl. Mech.* **58**, 104-110.

Broek, D. (1987). *Elementary Engineering Fracture Mechanics* (Fourth revised edition). Martinus Nijhoff Publishers.

Bueckner, H.F. (1958). The propagation of cracks and the energy of elastic deformation. *Trans. ASME* **25**, No.5, 1225-1230.

Campbell, J.D and Ferguson, W.G. (1970). The temperature and strain-rate dependence of the shear strength of mild steel. *Phil. Mag.* **21**, 63-82.

Chantaramungkorn, K. and Keer, L.M. (1975). Stress analysis for a layer of finite length bonded to a half-space of identical material. *Int. J. Solids Structures* **11**, 1079-1096.

Cheng, W. and Finnie, I. (1990). K_{II} solutions for an edge-cracked strip. *Engng Fracture Mech.* **36**, 355-360.

Cherepanov, G.P. (1979). *Mechanics of Brittle Fracture*. New York: McGraw-Hill.

Davies, J., Morgan, T.G. and Yim, A.W. (1985). The finite element analysis of a punch-through shear specimen in mode II. *Int. J. Fracture* **28**, R3-R10.

Du, Z.Z., Betegòn,C. and Hancock, J.W. (1991). J dominance in mixed mode loading. *Int. J. Fracture* **52**, 191-206.

Duffy, A.R. et al. (1969). Fracture design practice for pressure piping. *Fracture*, Vol.1. Academic press, New York, pp. 159-232.

Dugdale, D.S. (1960). Yielding of steel sheets containing slits. *J. Mech. Phys. Solids* **8**, 100-108.

Freund, L.B. (1978). Stress intensity factor calculations based on a conservation integral. *Int. J. Solids Structures* **14**, 241-250.

Freund, L.B. (1990). *Dynamic Fracture Mechanics*. Cambridge University Press, U.S.A.

Hartranft, R.J. and Sih, G.C. (1973). Alternating method applied to edge and surface crack problems. *Methods of Analysis and Solutions of Crack Problems: Mechanics of Fracture*, Vol.1. Noordhoff, Leyden.

Hasebe, N. (1979). Uniform tension of a semi-infinite plate with crack at an end of a stiffened edge. *Ing.-Arch.* **48**, 129-141.

Hasebe, N. (1981). An edge crack in a semi-infinite plate welded to a rigid stiffener. *Proc. Japan Soc. Civil Engng* **314**, 149-157.

Holt, D.L., Babcock, S.G., Green, S.J. and Maiden, C.J. (1967). The strain-rate dependence of the flow stress in some aluminum alloys. *Trans. ASM* **60**, 152-159.

Hoyniak, D. and Conway, J.C. (1979). Finite element analysis of the compact shear specimen. *Engng Fracture Mech.* **12**, 301-306.

Hutchinson, J.W. (1968a). Singular behaviour at the end of a tensile crack in a hardening material. *J. Mech. Phys. Solids* **16**, 13-31.

Hutchinson, J.W. (1968b). Plastic stress and strain fields at a crack tip. *J. Mech. Phys. Solids* **16**, 337-347.

Irwin, G.R. (1957). Analysis of stresses and strains near the end of a crack traversing a plate. *J. Appl. Mech.* **24**, 361-364.

Irwin, G.R. (1960). Plastic zone near a crack and fracture toughness. *Proc. 7th Sagamore Conf.* pp. IV-63.

Jiang, C.W. and Chen, M.M. (1974). *Report No. AMMRC-CTR 74/23*. Watertown, MA.

Jones, D.L. and Chisholm, D.B. (1975). An investigation of the edge-sliding modes in fracture mechanics. *Engng Fracture Mech.* **7**, 261-270.

Kalthoff, J.F. and Winkler, S. (1987). Failure mode transition at high rates of shear loading. *Impact '87: International Conference on Impact*

Loading and Dynamic Behaviour of Materials, DGM Informationsgesellschaft, Verlag, Oberursel. **Vol.1,** pp. 185-195.

Kanninen, M.F. and Popelar, C.H. (1985). *Advanced Fracture Mechanics.* Oxford University Press, Oxford, U.K.

Ke, J.W., Chi, L.H. and Kao, H. (1978). Calculation of stress intensity factors for combined mode bend specimens. *Advances in Research of Strength and Fracture of Materials: Proc. 4th Int. Conf. Fracture (ICF4),* New York etc. **Vol.4,** pp. 123-133.

Klepaczko, J.R. (1969). The strain rate behavior of iron in pure shear. *Int. J. Solids Structures* **5,** 533-548.

Klepaczko, J.R. (1987). A practical stress-strain-strain rate-temperature constitutive relation of the power form. *J. Mechanical Working Technol.* **15,** 143-165.

Klepaczko, J.R. (1990). Dynamic crack initiation, some experimental methods and modelling. *Crack Dynamics in Metallic Materials,* Springer-Verlag, pp. 255-453.

Lee, Y.J. and Freund, L.B. (1990). Fracture initiation due to asymmetric impact loading of an edge cracked plate. *J. Appl. Mech.* **57,** 104-111.

Larsson, S.G. and Carlsson, A.J. (1973). Influence of non-singular stress terms and specimen geometry on small-scale yielding at crack tips in elastic-plastic materials. *J. Mech. Phys. Solids* **21,** 263-277.

Maccagno, T.M. and Knott, J.F. (1992). The mixed mode I/II fracture behaviour of lightly tempered HY130 steel at room temperature. *Engng Fracture Mech.* **41,** 805-820.

Maiden, C.J. and Green, S.J. (1966). Compressive strain-rate tests on six selected materials at strain rates from 10^{-3} to 10^{4} in/in/sec. *J. Appl. Mech.* **33,** 496-504.

Mall, S. and Mol, J.H. (1991). Mode II fracture toughness testing of a fiber-reinforced ceramic composite. *Engng Fracture Mech.* **38,** 55-69.

Mason, J.J., Lambros, J. and Rosakis, A.S. (1992). The use of a coherent gradient sensor in dynamic mixed-mode fracture mechanics experiments. *J. Mech. Phys. Solids* **40,** 641-661.

Murakami, Y. (1980). Analysis of mixed-mode stress intensity factors by body force method. *Numer. Meth. Fracture Mech.: Proc. 2nd Int. Conf.* (Swansea, 1980). pp. 145-159.

Nemat-Nasser, S. and Obata, M. (1984). On stress field near a stationary crack tip. *Mechanics of Materials* 3, 235-243.

Nishioka, T., Murakami, T., Takemoto, Y. and Sakakura, K. (1991). Mixed-mode impact fracture tests and their numerical simulation. *Mechanical Behaviour of Materials - VI: Proc. Sixth Int. Conf. (Kyoto, Japan).* Vol.1, pp. 457-462.

Pan, J. and Shih, C.F. (1990). Elastic-plastic analysis of combined mode II and III crack-tip fields under small-scale yielding conditions. *J. Appl. Mech.* 57, 259-267.

Panasyuk, V.V., Savruk, M.P. and Datsyshin, A.P. (1976). *Stress Distribution near Cracks in Plates and Shells.* Kiev. Naukova Dumka.

Rice, J.R. (1968a). A path independent integral and the approximate analysis of strain concentration by notches and cracks. *J. Appl. Mech.* 35, 379-386.

Rice, J.R. (1968b). Mathematical analysis in the mechanics of fracture. *Fracture,* Vol.2. Academic Press, New York, pp. 191-311.

Rice, J.R. (1974). Limitations to the small scale yielding approximation for crack tip plasticity. *J. Mech. Phys. Solids* 22, 17-26.

Rice, J.R. and Rosengren, G.F. (1968). Plane strain deformation near a crack tip in a power-law hardening material. *J. Mech. Phys. Solids* 16, 1-12.

Ritchie, R.O., Knott, J.F. and Rice, J.R. (1973). On the relationship between critical tensile stress and fracture toughness in mild steel. *J. Mech. Phys. Solids* 21, 395.

Rooke, D.P. and Jones, D.A. (1979). Stress intensity factors in fretting fatigue. *J. Strain Analysis* 14, 1-6.

Russell, A.L. and Street, K.N. (1982). Factors affecting the interlaminar fracture energy of graphite epoxy laminates. *Progress in Science and Engineering of Composites.* Japan Society of Composite Materials, Tokyo. pp. 279-289.

Savruk, M.P. (1988). *Stress Intensity Factors in Cracked Bodies: Handbook.* Kiev, Naukova Dumka.

Shih, C.F. (1974). Small-scale yielding analysis of mixed mode plane-strain crack problems. *Fracture Analysis,* ASTM STP 560, pp. 187-210.

Sih, G.C. (1973). Introductory chapter: A special theory of crack propagation. *Methods of Analysis and Solutions of Crack Problems: Mecanics of Fracture,* Vol.1. Noordhoff, Leyden.

Sih, G.C. (1974). Strain-energy density factor applied to mixed mode crack problems. *Int. J. Fracture* 10, 305-321.

Tada, H., Paris, P.C. and Irwin, G.R. (1973). *The Stress Analysis of Cracks: Handbook.* Hellertown, Del Research Corp.

Tada, H. (1974). Addition to Tada *et al.* (1973).

Takamatsu, T. and Ichikawa, M. (1991). Fracture criterion for initiation and stable crack growth under mode I-II mixed-mode loading conditions. *Mechanical Behaviour of Materials - VI: Proc. Sixth Int. Conf. (Kyoto, Japan).* Vol.4, pp. 257-262.

Tanaka, K. and Kinoshita, M. (1967). Compressive strength of mild steel at high strain rates at high temperature. *Bull. JSME* 10, 429.

Tohgo, K. and Ishii, H. (1992). Elastic-plastic fracture toughness test under mixed mode I-II loading. *Engng Fracture Mech.* 41, 529-540.

Tuba, I.S. (1966). A method of elastic-plastic plane stress and plane strain analysis. *J. Strain Analysis* 1, 115-122.

Figure Captions

Figure 1. Coordinate systems at a crack tip.

Figure 2. Schematic illustration of Irwin's correction for plasticity.

Figure 3. Plastic zone size ahead of the crack tip in Mode II based on the Dugdale model and Irwin's correction for plasticity.

Figure 4. Plastic zone shapes at the crack tip in Mode II based on the Huber-Mises and the Tresca yield criteria.

Figure 5. Plastic zone shapes at the crack tip in Mode II based on the two-parameter representation of the stress field and the Huber-Mises yield criterion.

Figure 6. Crack geometries in Mode II.

Figure 7. Calibration curves of the stress intensity factor for the compact shear specimen, Fig.6.15 ($\sigma=P/(tH)$, t is the specimen thickness). (a) K_{II} for the Case 2 of loading at different sizes of the specimen, after Hoyniak and Conway (1979). (b) K_{II} and S for different loading schemes, after Savruk (1988).

Figure 8. HRR stress and strain fields for Mode II crack in plane strain.
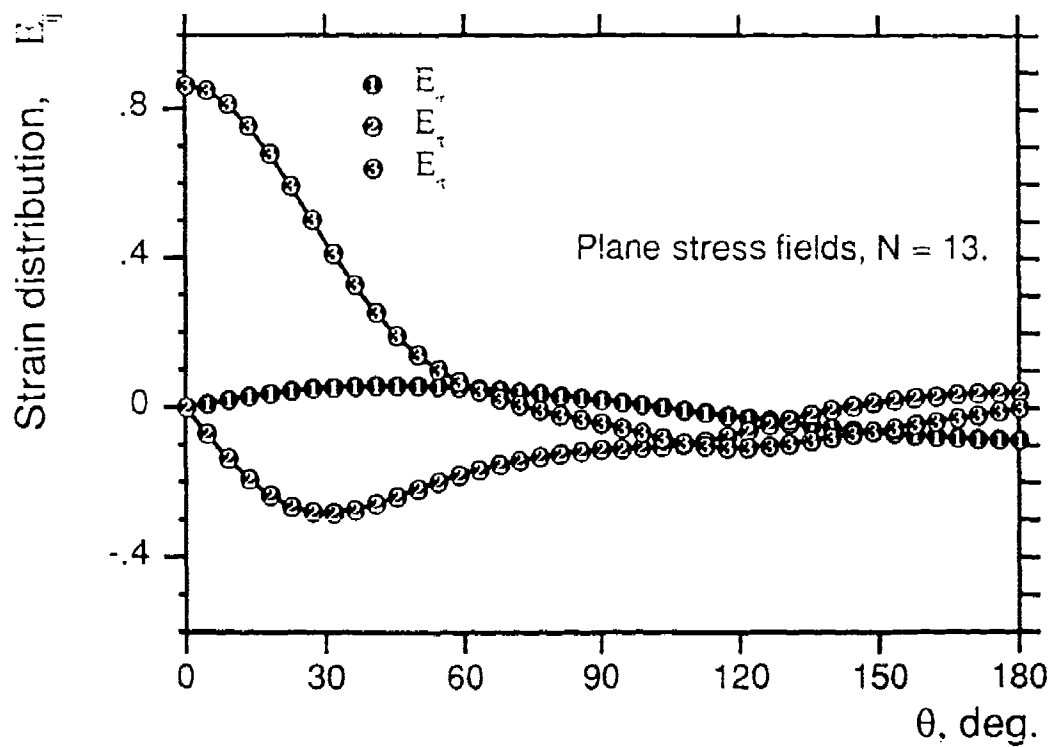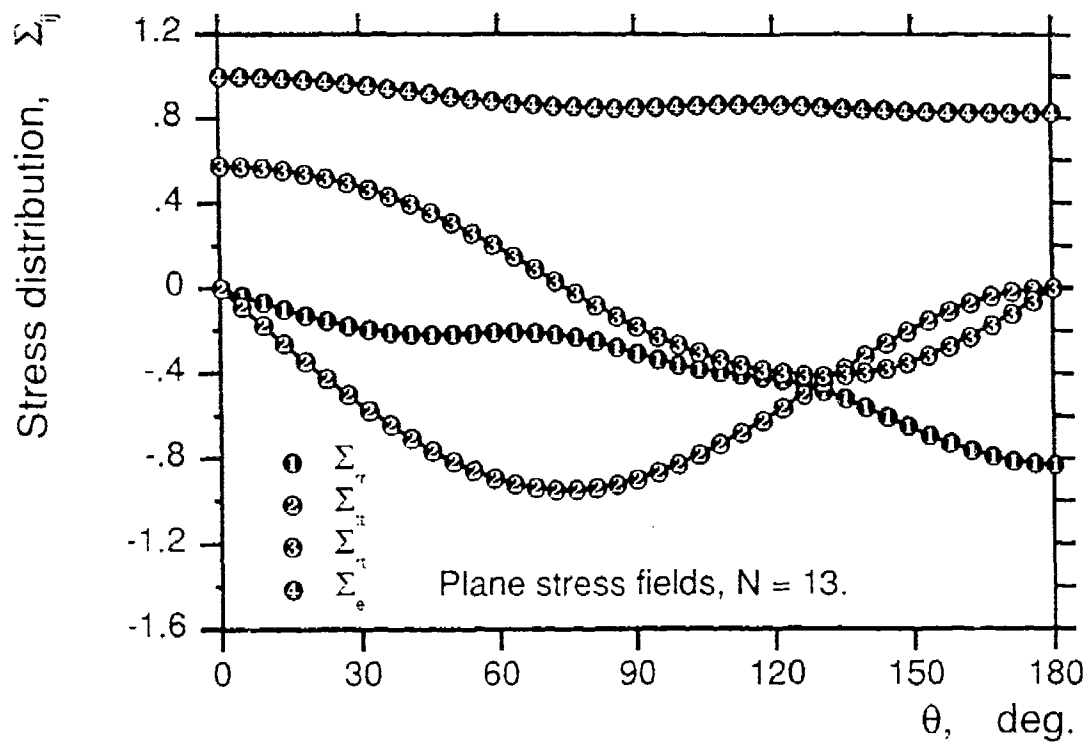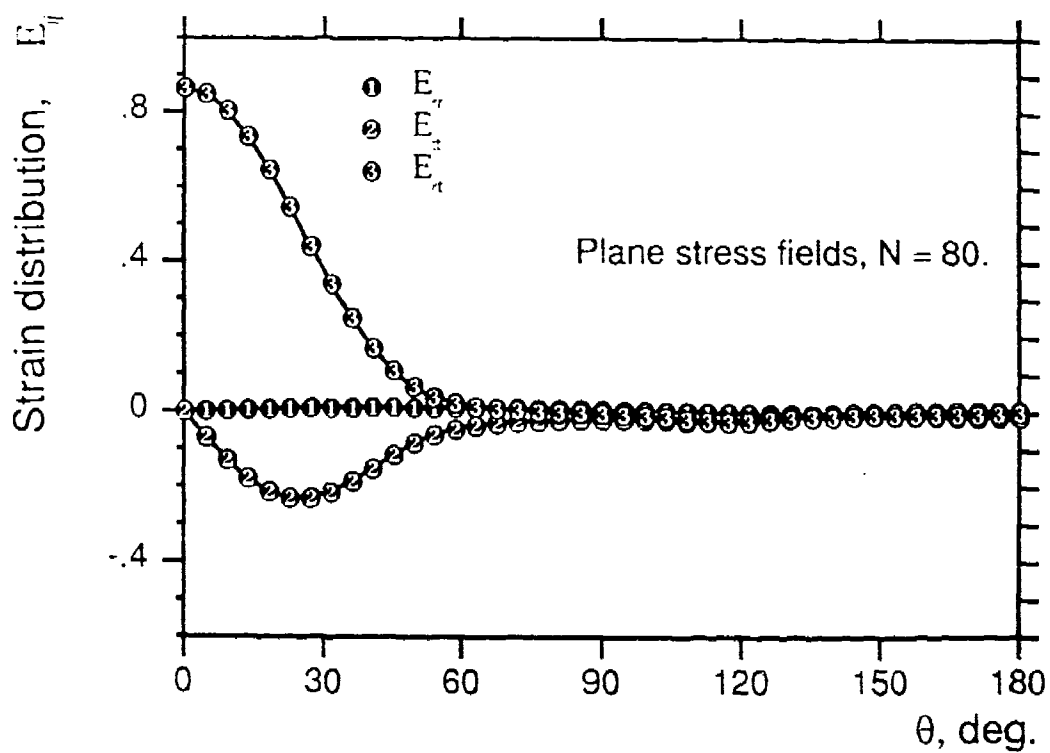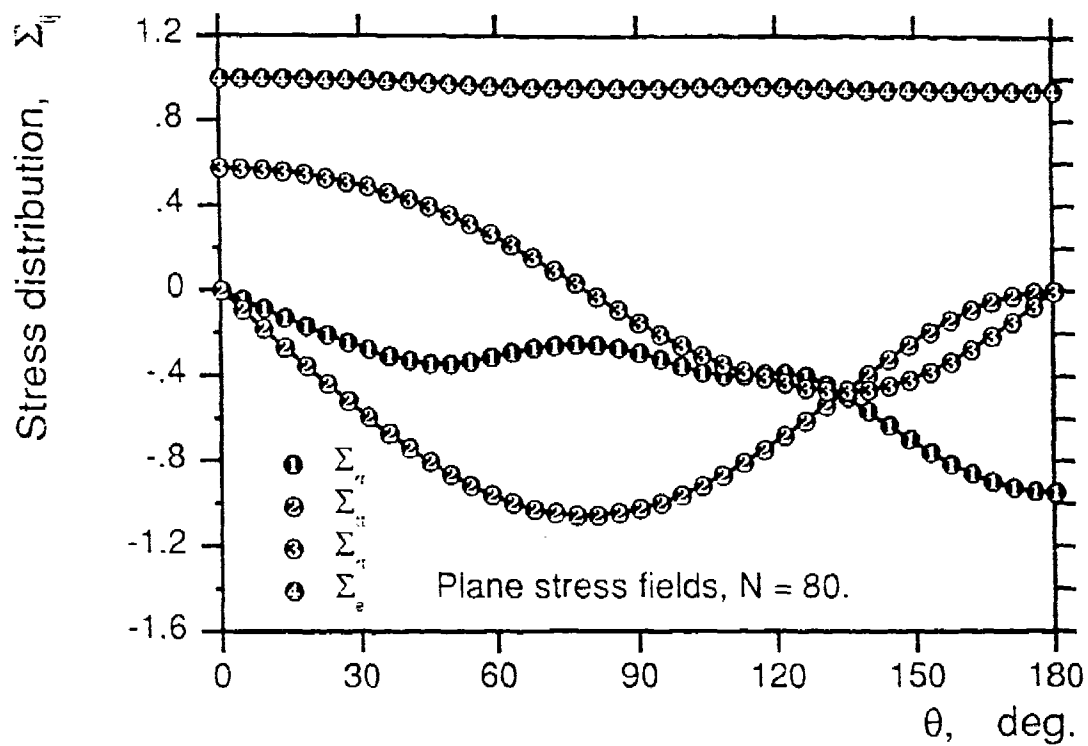
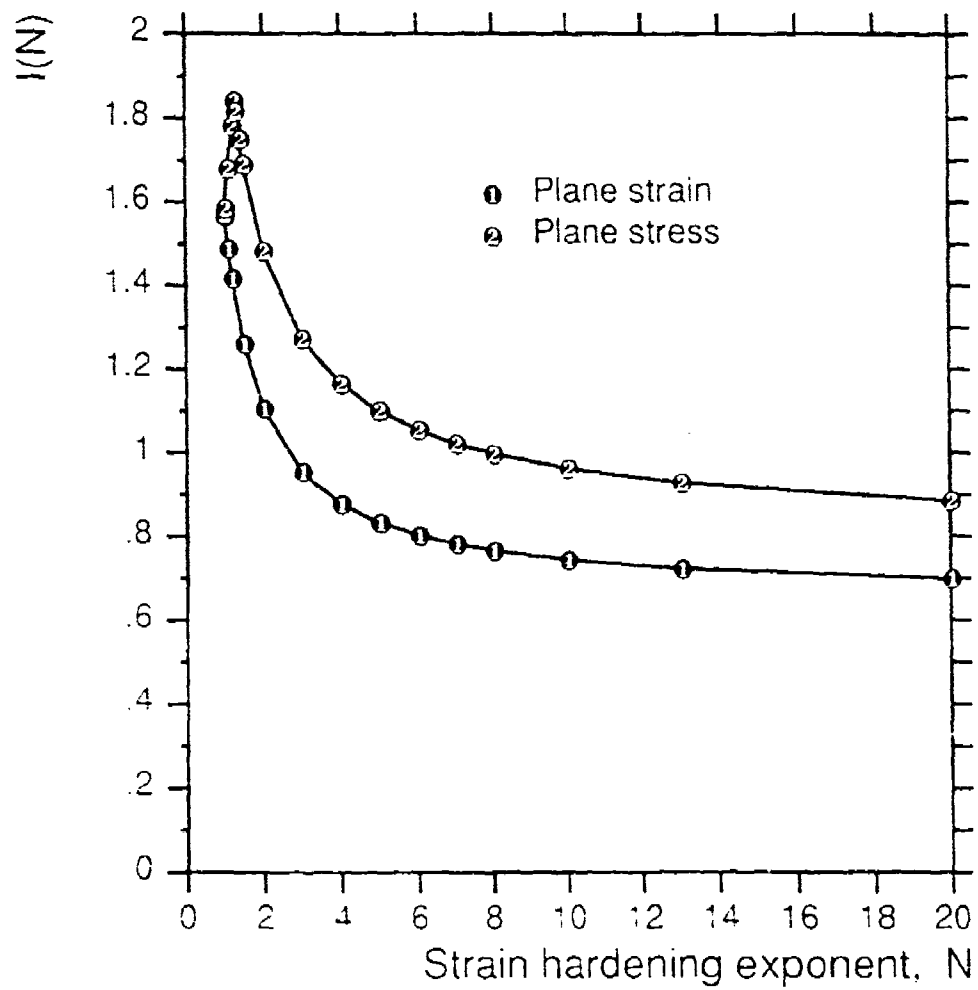Figure 9. HRR stress and strain fields for Mode II crack in plane stress.

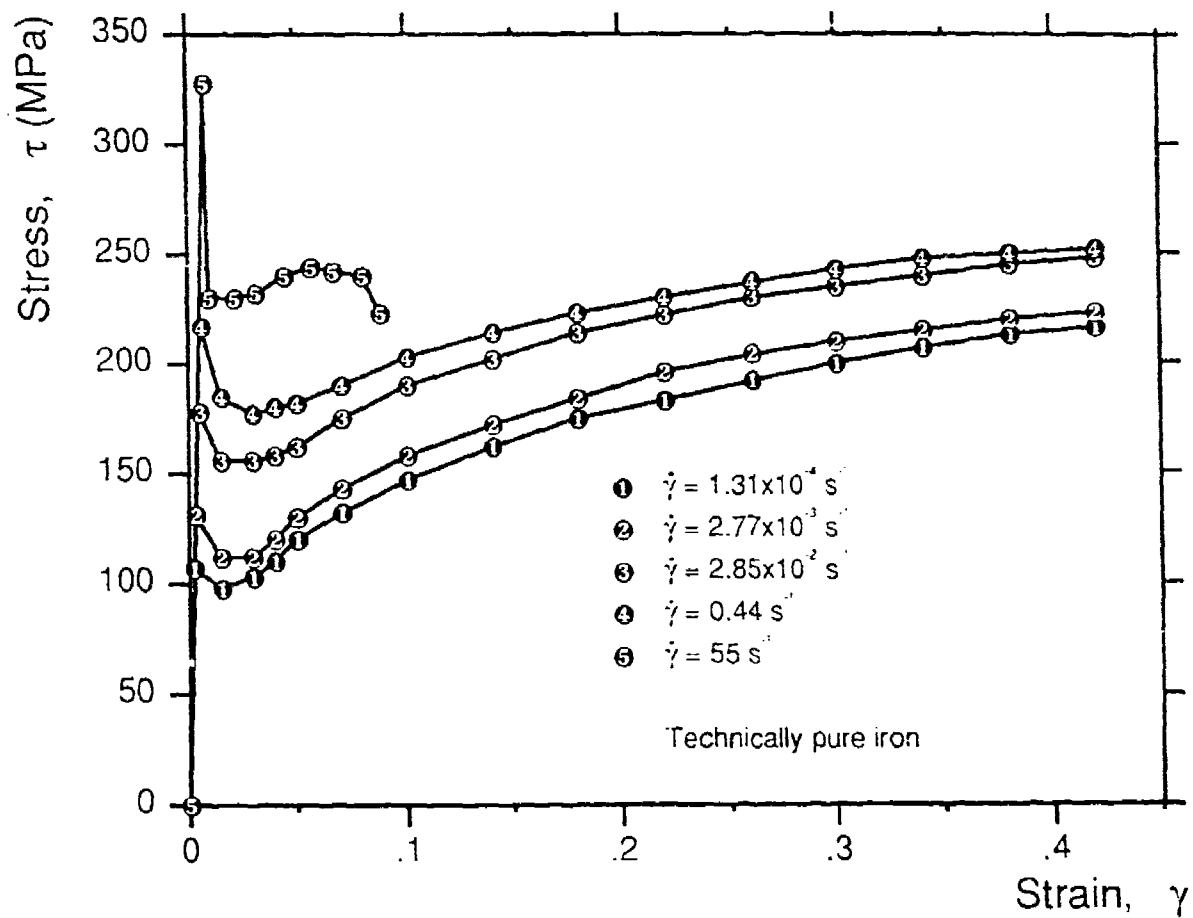Figure 10. Variation of the I(N)-factor versus N for plane strain and plane stress.

Figure 11. Stress-strain curves for technically pure iron in shear tests at different strain rates (data of Klepaczko,1969).
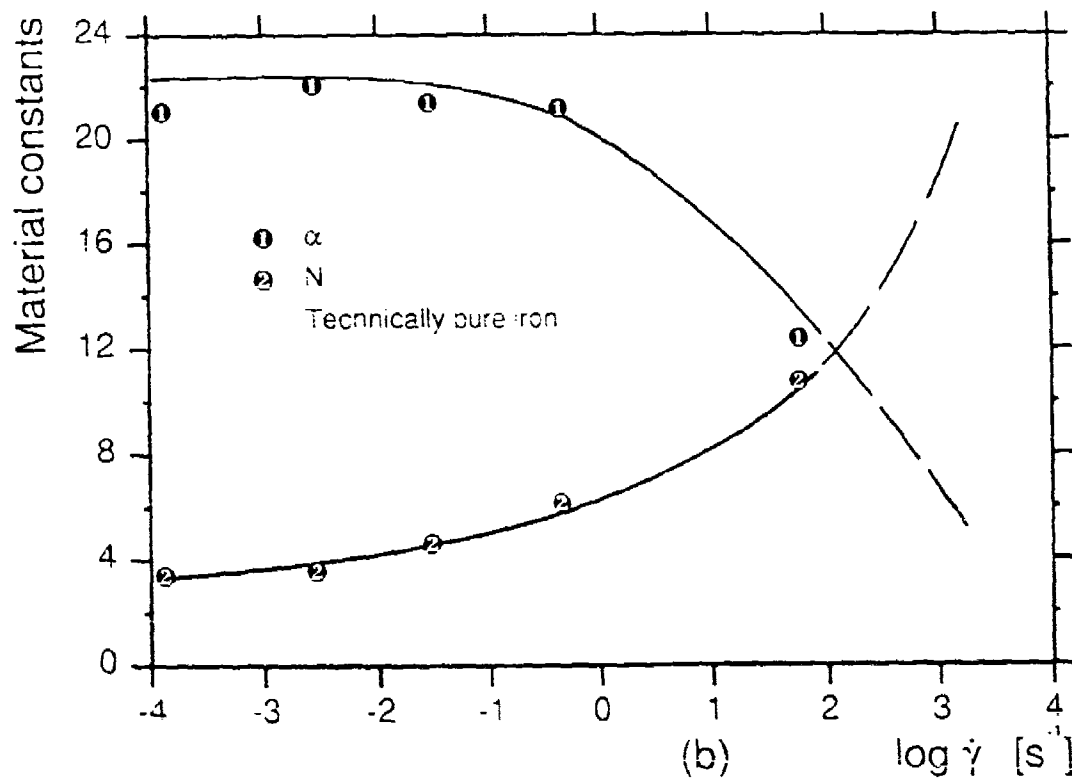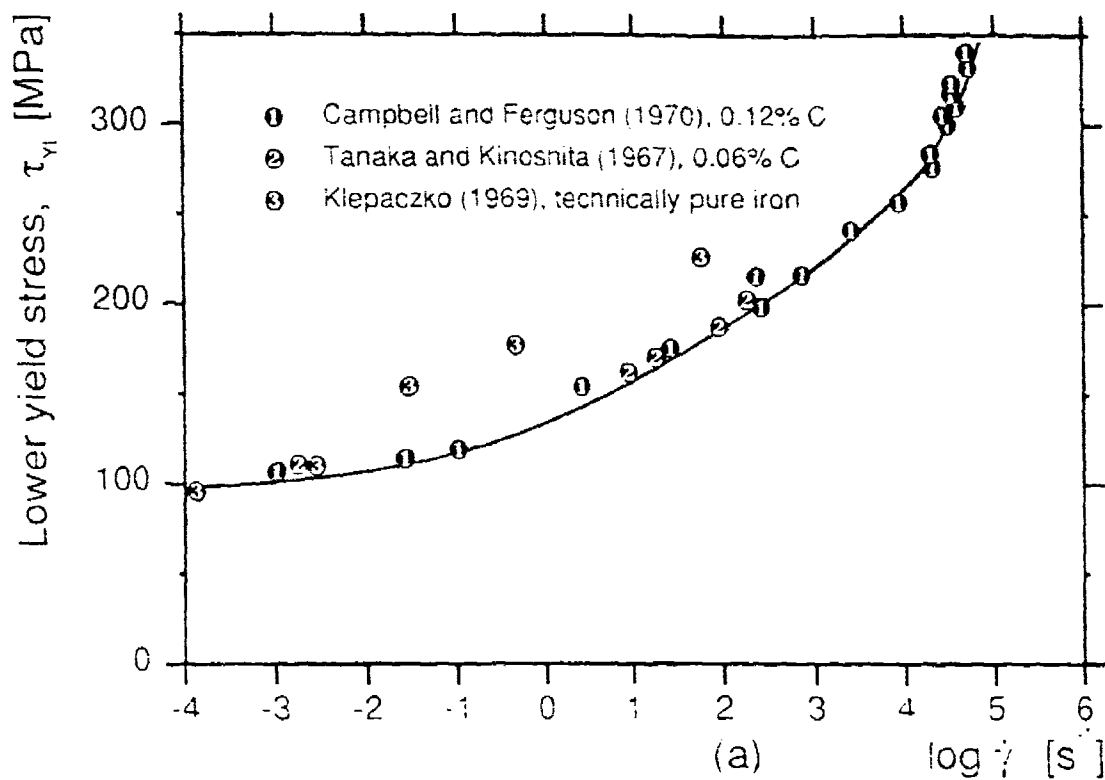
Figure 12. (a) Rate sensitivity of the lower yield stress in shear for mild steel and technically pure iron;
(b) Rate sensitivity of constants in the Ramberg-Osgood equation for technically pure iron.
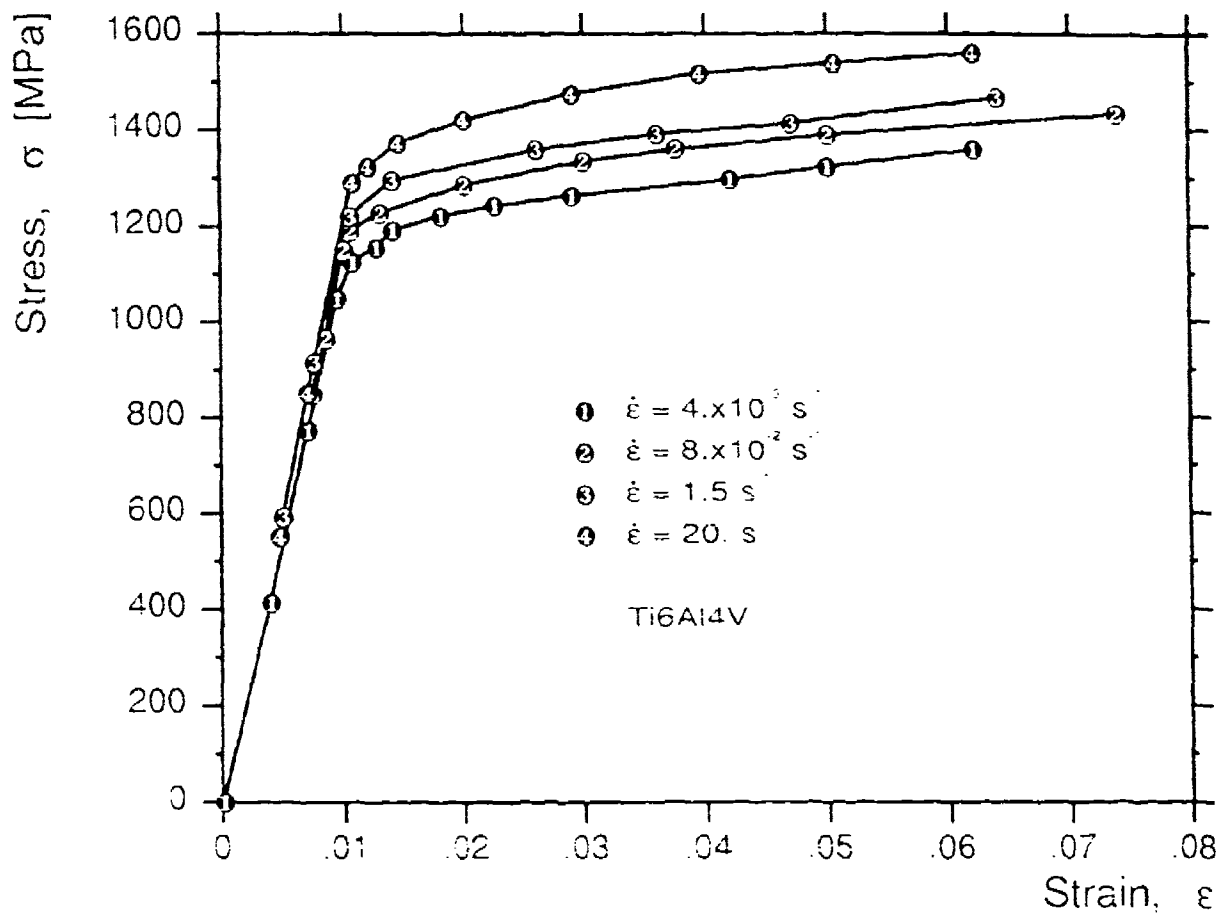
Figure 13. Stress-strain curves for titanium Ti6Al4V alloy from compression tests at different strain rates (data of Maiden and Green, 1966).
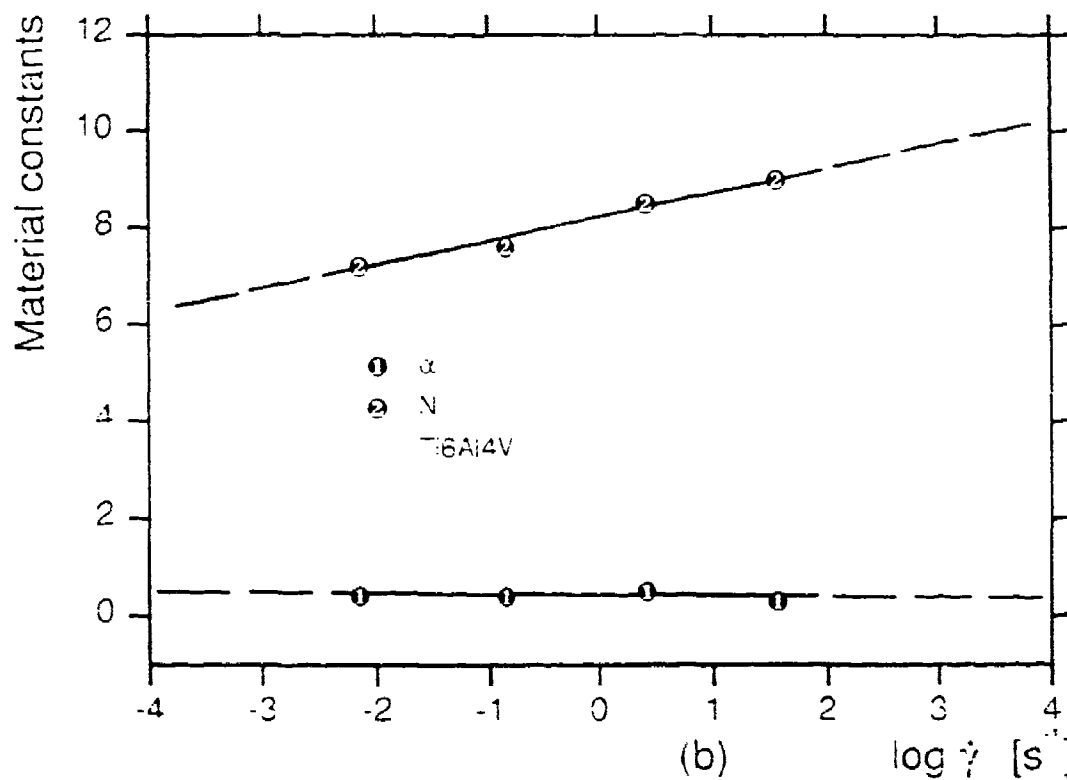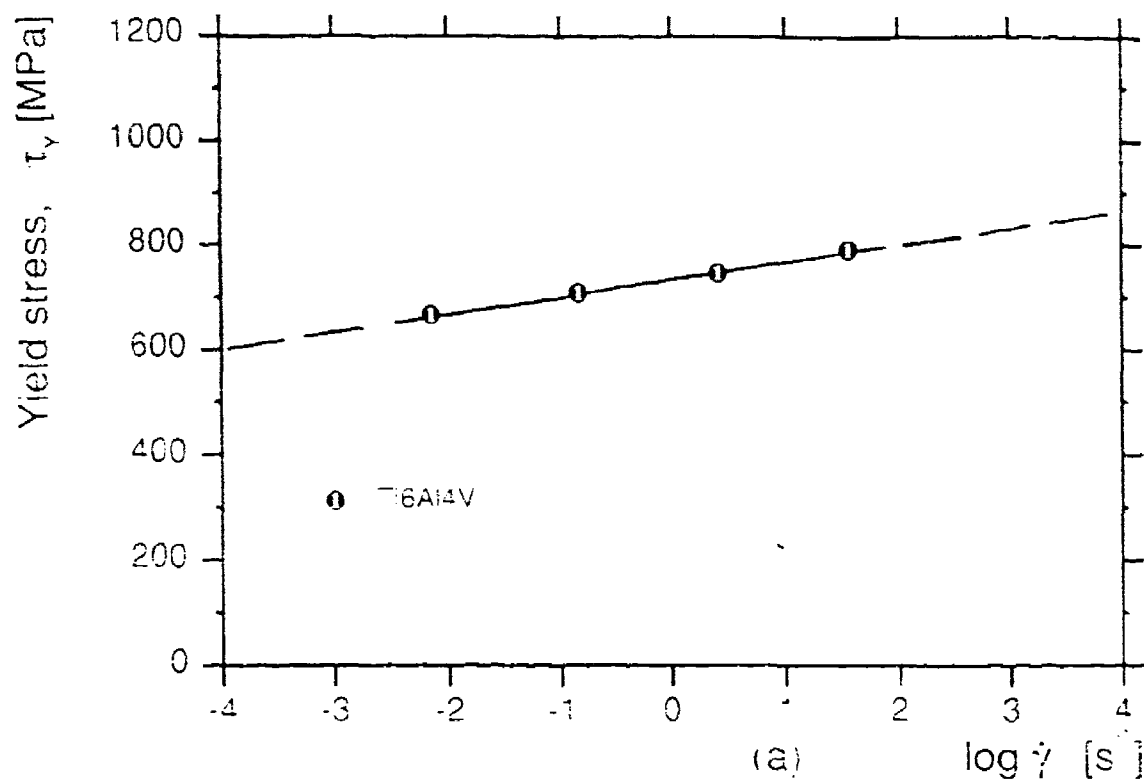
Figure 14. Rate sensitivity of the yield stress in shear and material constants in the Ramberg-Osgood equation for Ti6Al4V alloy.

Figure 15. Stress-strain curves for Al 6061-T6 alloy from compression tests at different strain rates (after Maiden and Green, 1966). Conversion factor for stress: 1 ksi = 6.895 MPa.

Figure 16. Rate sensitivity of the yield stress in shear for Al 6061-T6 alloy (data of Jiang and Chen, 1974).

Figure 17. Variation of parameters which characterize the geometry of plastic zone near the crack tip versus logarithm of strain rate for a semi-infinite crack in mild steel: (a) $\tau_{appl}/\tau_{YS}=0.2$; (b) $\tau_{appl}/\tau_{YS}=0.5$.

Figure 18. Variation of parameters which characterize the geometry of plastic zone near the crack tip versus logarithm of strain rate

Figure 1. Coordinate systems at a crack tip.

Figure 2. Schematic illustration of Irwin's correction
for plasticity.

Figure 3. Plastic zone size ahead of the crack tip in Mode II based on the Dugdale model and Irwin's correction for plasticity.

Figure 4. Plastic zone shapes at the crack tip in Mode II based on the Huber-Mises and the Tresca yield criteria.

Figure 5. Plastic zone shapes at the crack tip in Mode II based on the two-parameter representation of the stress field and the Huber-Mises yield criterion.

Figure 6.1

Figure 6.2
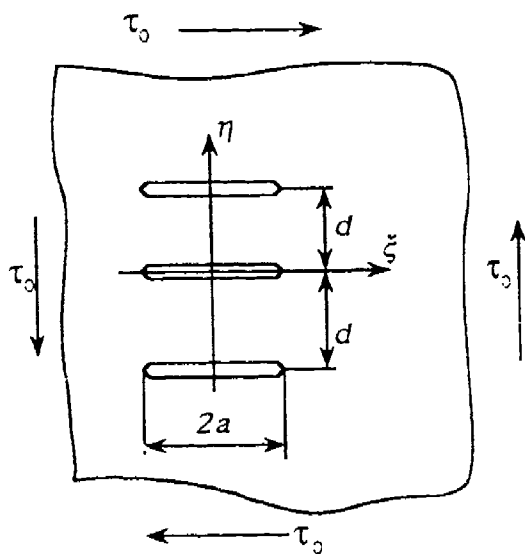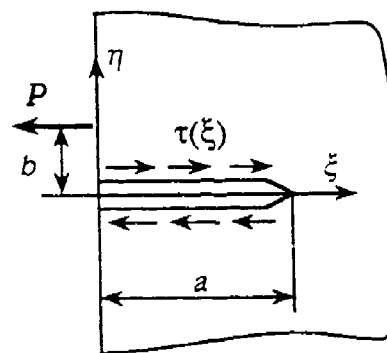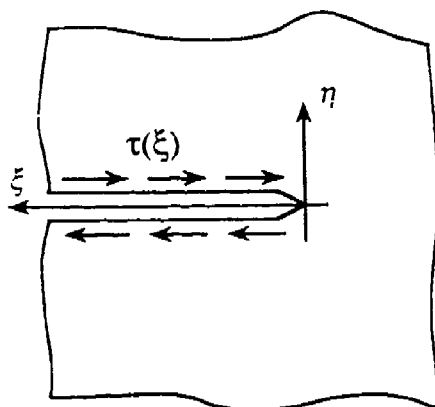
Figure 6.3
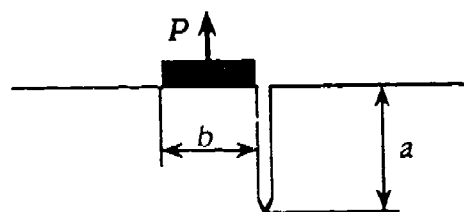
Figure 6.4
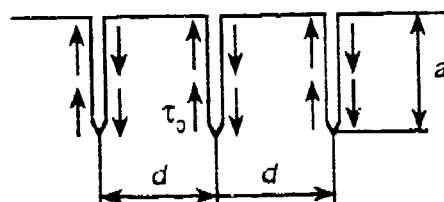
Figure 6.5

Figure 6.6

Figure 6.7
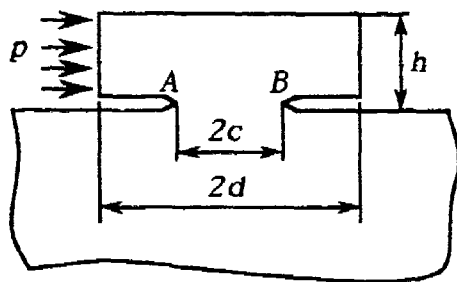
Figure 6.8
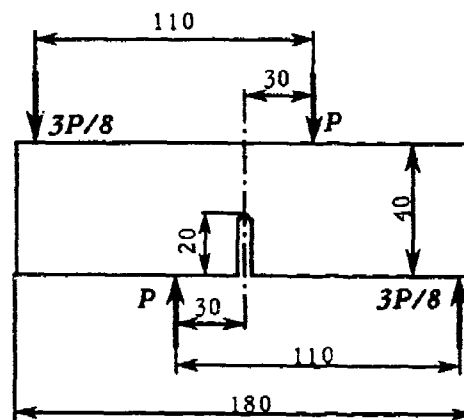
Figure 6.11
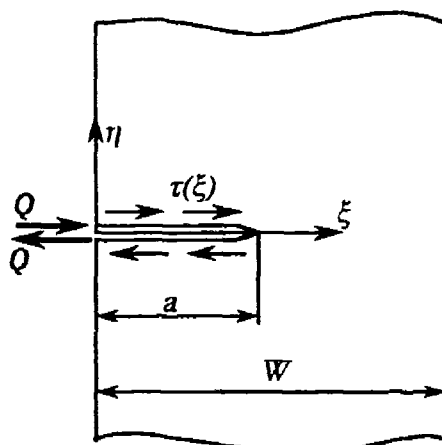
Figure 6.9
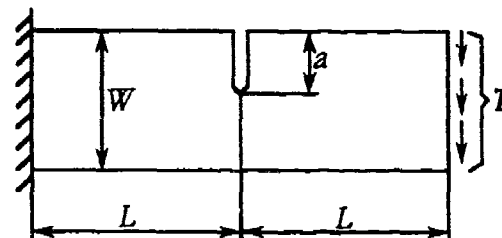
Figure 6.12
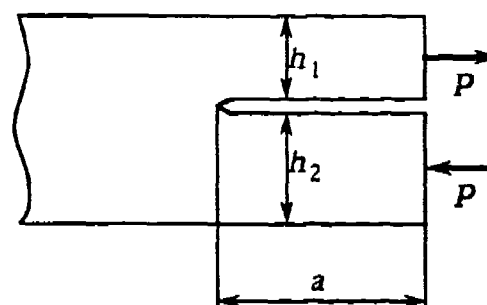
Figure 6.13
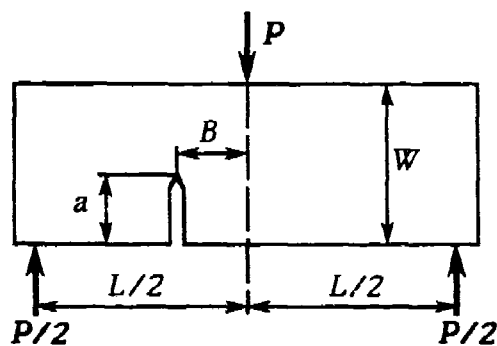
Figure 6.10
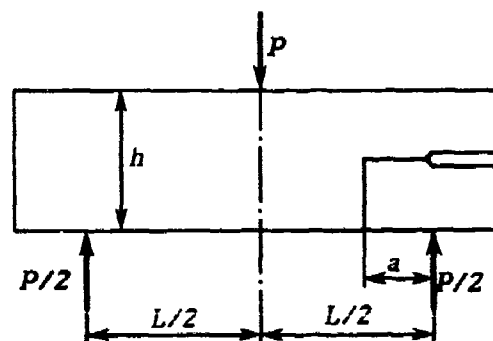
Figure 6.14
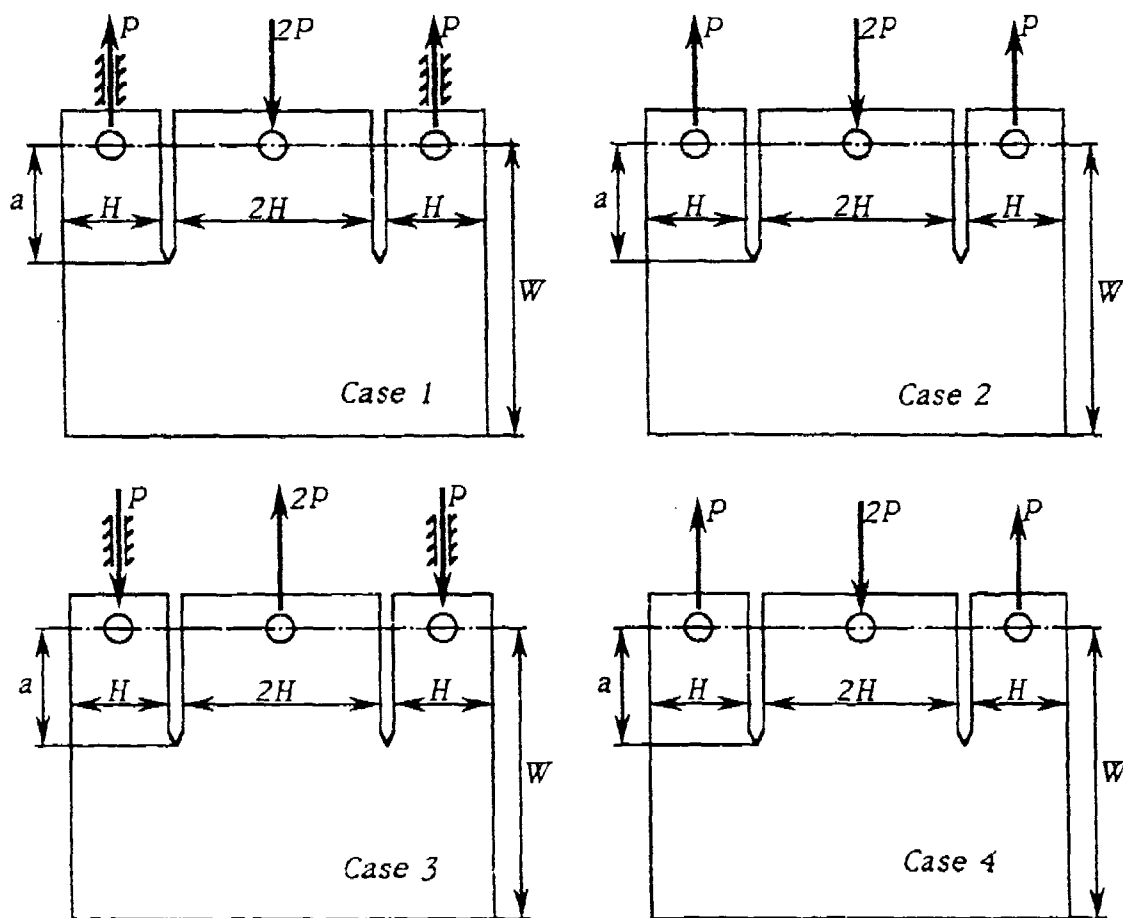
Figure 6.15
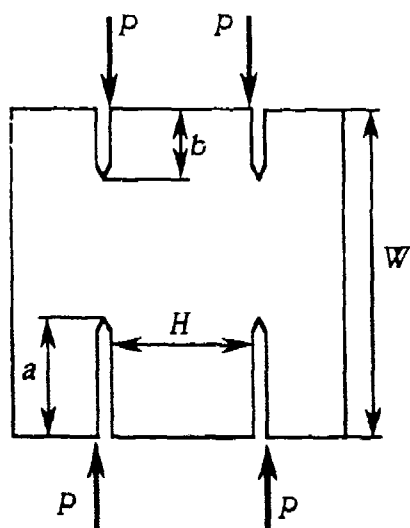
Figure 6.16
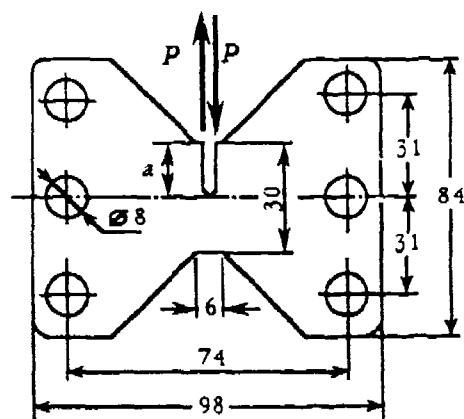
Figure 6.17

Figure 6. Crack geometries in Mode II.
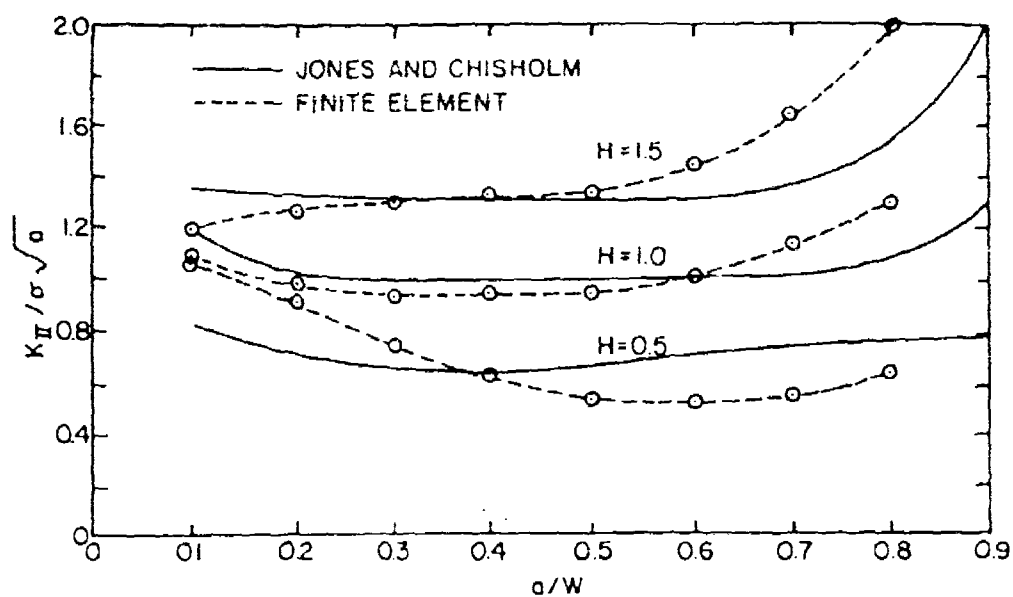
(a)
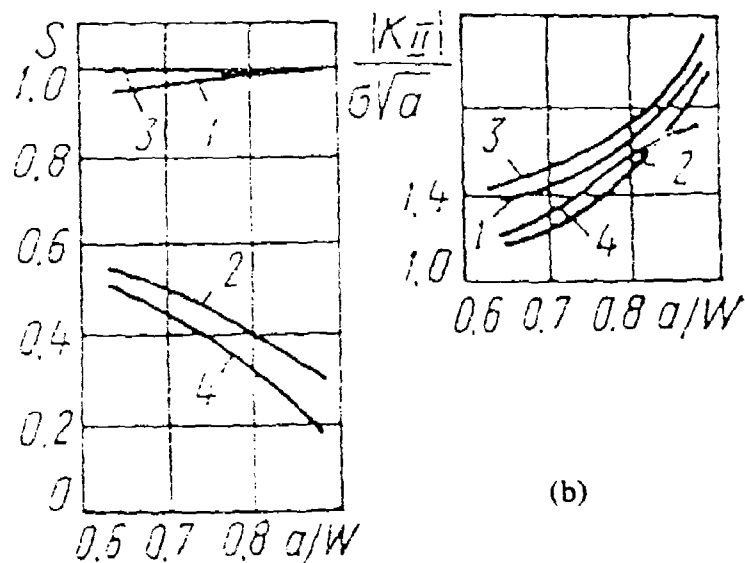
(b)

Figure 7. Calibration curves of the stress intensity factor for the compact shear specimen, Fig.6.15 ($\sigma = P/(tH)$, t is the specimen thickness). (a) K_{II} for the Case 2 of loading at different sizes of the specimen, after Hoyniak and Conway (1979). (b) K_{II} and S for different loading schemes, after Savruk (1988).
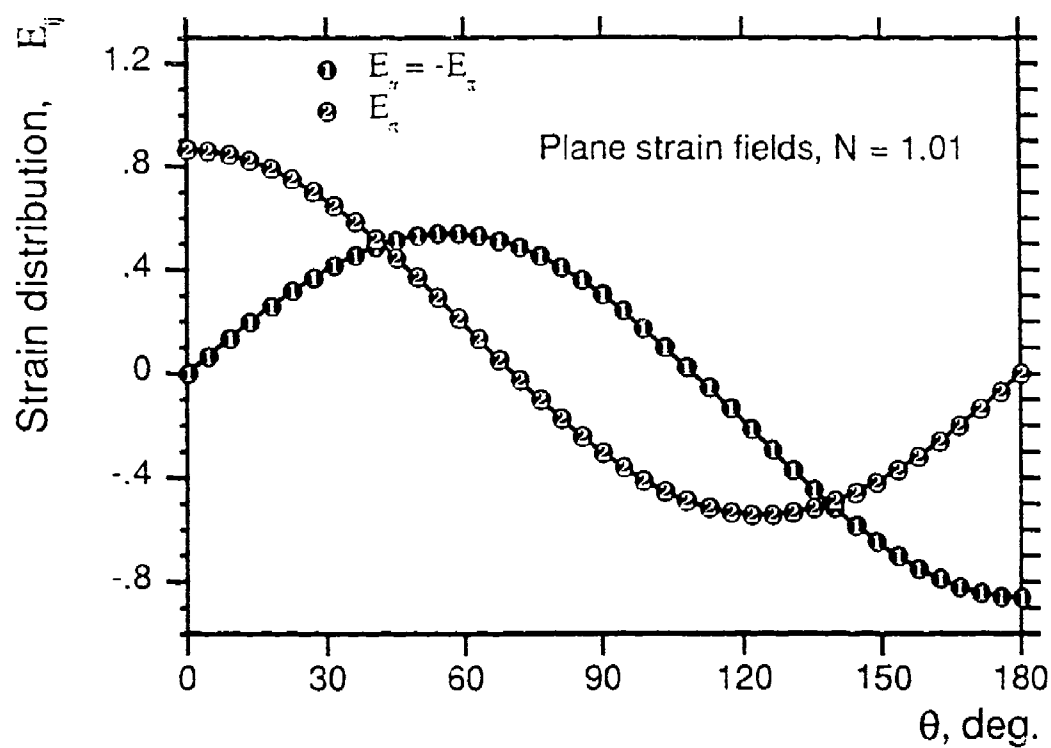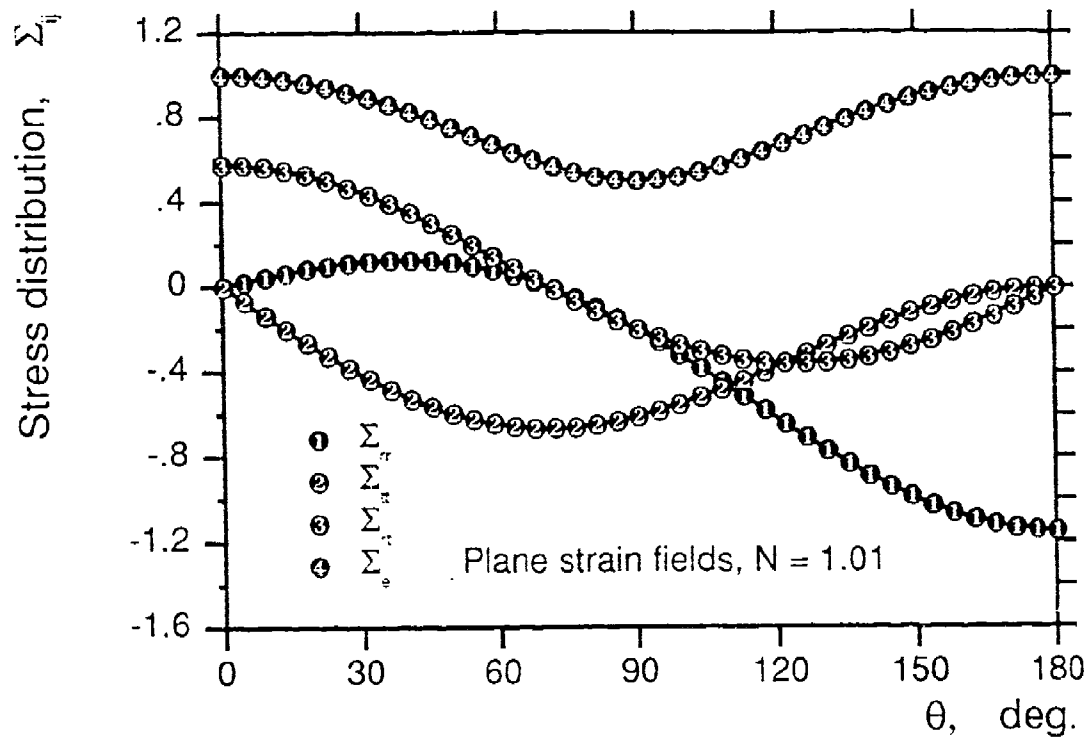
Figure 8a

Figure 8b

Figure 8c

Stress distribution, Σ_{ij}

- **1** Σ_{rr}
- **2** Σ_{rz}
- **3** Σ_{rz}
- **4** Σ_{z}

Plane strain fields, N = 7.

θ, deg.

Strain distribution, E_{ij}

- **1** $E_{rr} = -E_{z}$
- **2** E_{z}

Plane strain fields, N = 7.

θ, deg.

Figure 8d

Figure 8e

Stress distribution, Σ_{ij}

1.2

.8

.4

0

-.4

-.8

-1.2

-1.6

● Σ_{rr}
② $\Sigma_{\theta\theta}$
③ $\Sigma_{r\theta}$
④ Σ_e

Plane strain fields, N = 13.

0   30   60   90   120   150   180

θ, deg.

Strain distribution, E_{ij}

1.2

.8

.4

0

-.4

● $E_{rr} = -E_{\theta\theta}$
② $E_{r\theta}$

Plane strain fields, N = 13.

0   30   60   90   120   150   180

θ, deg.
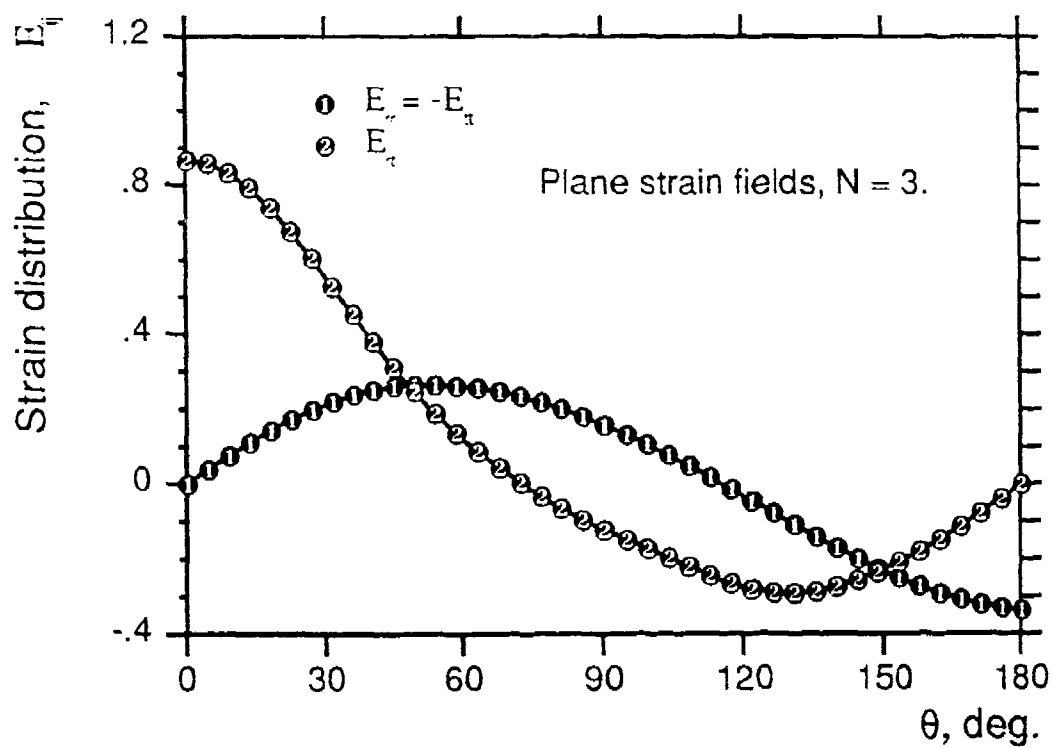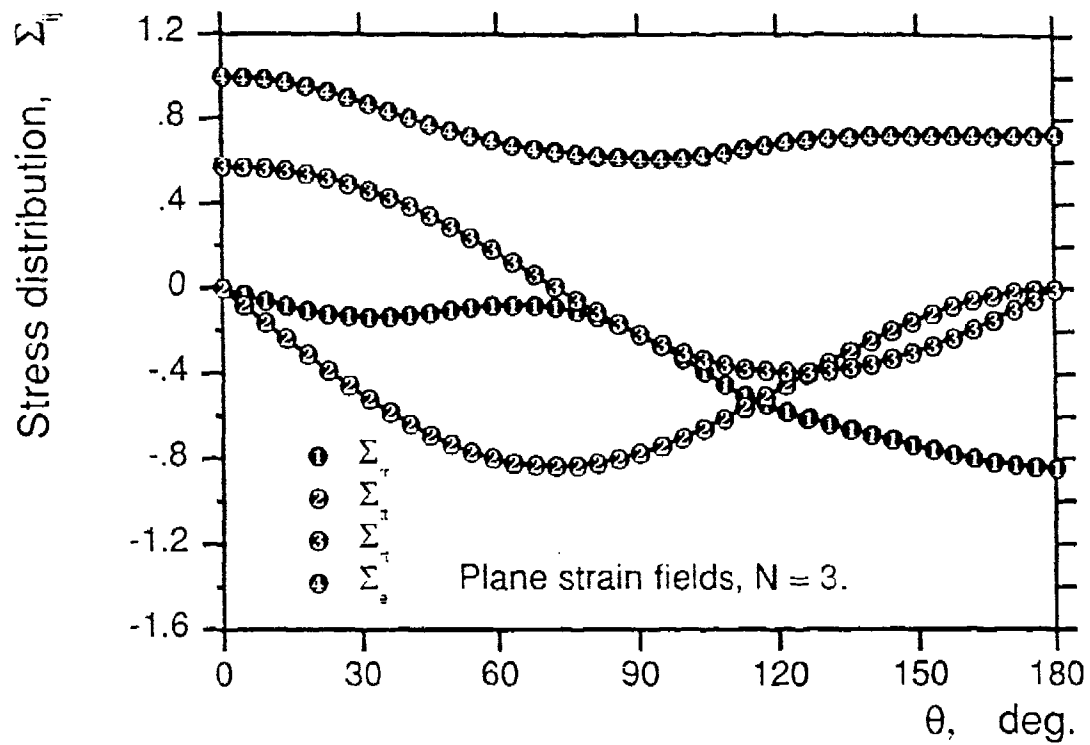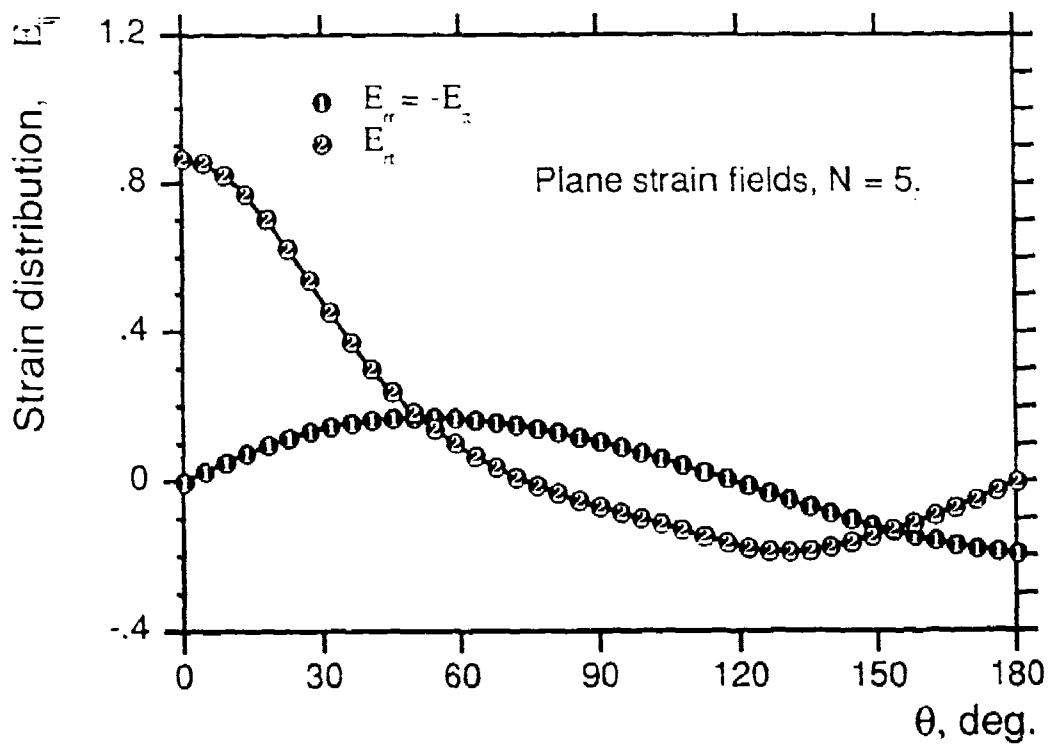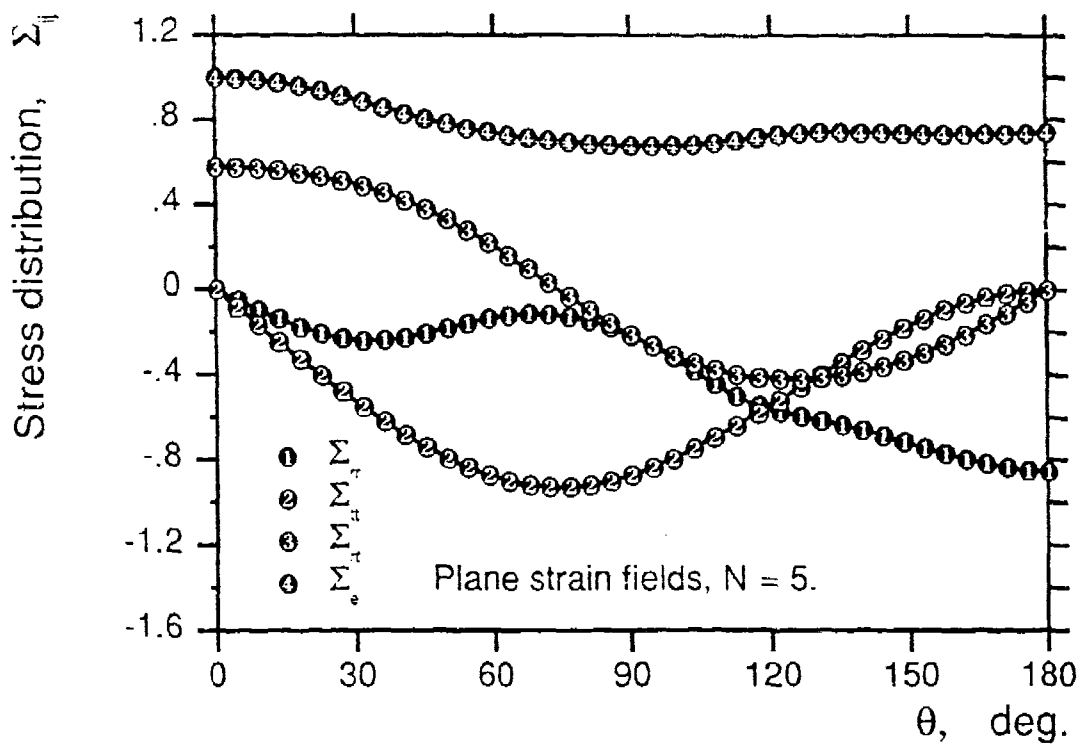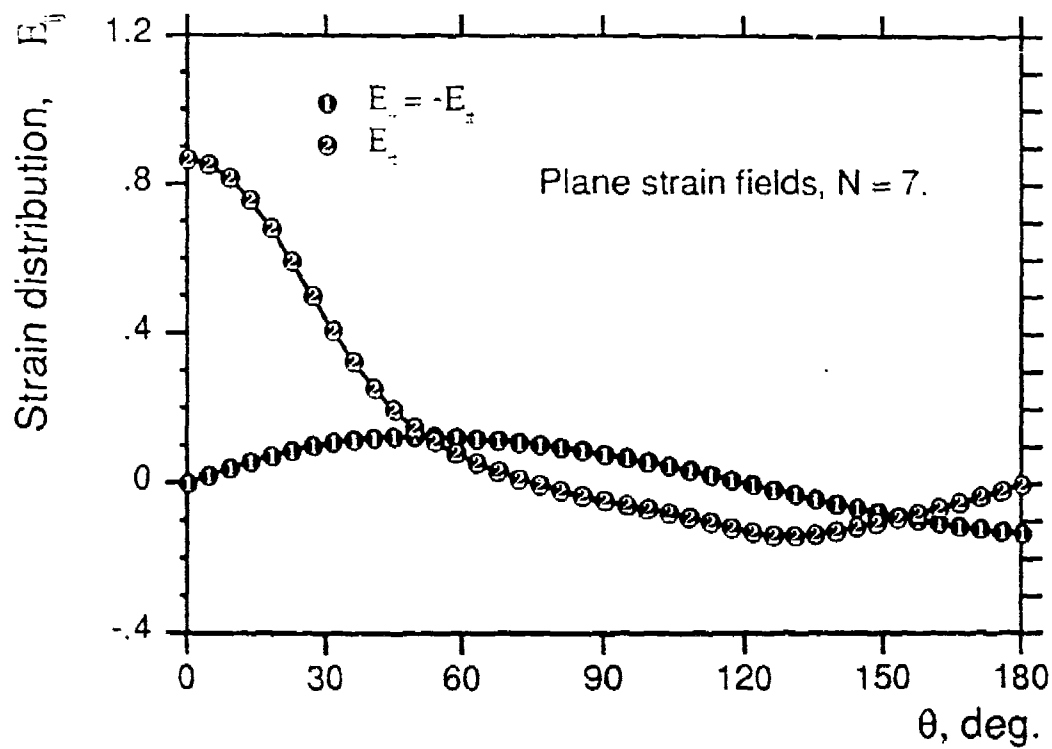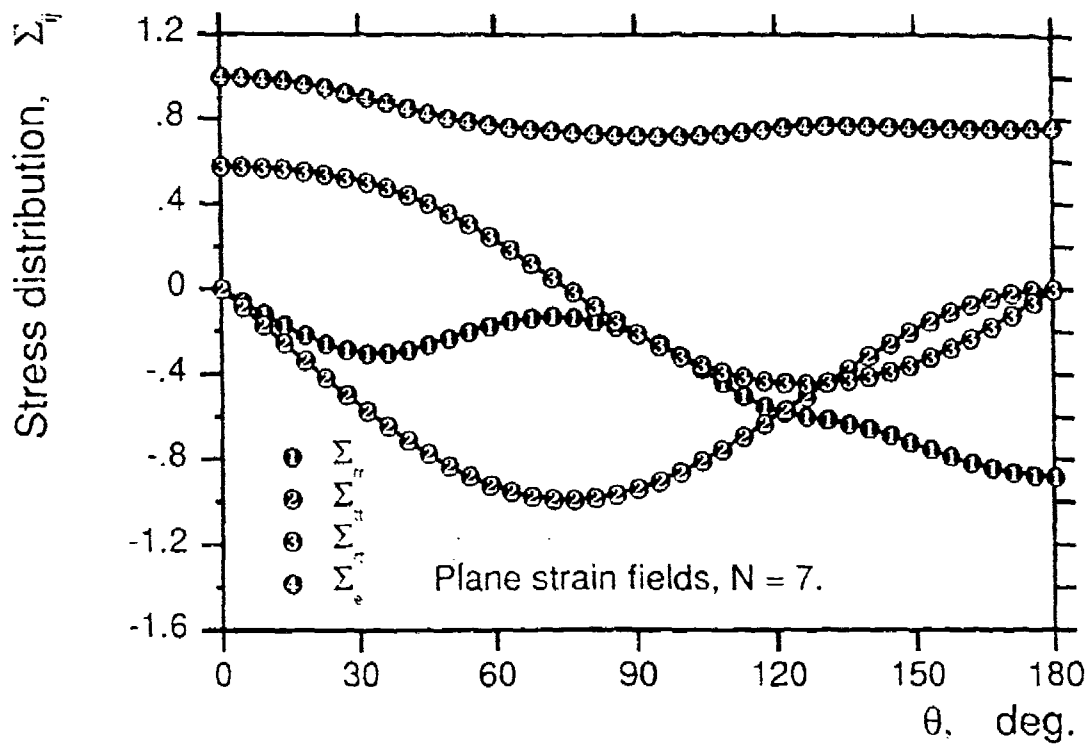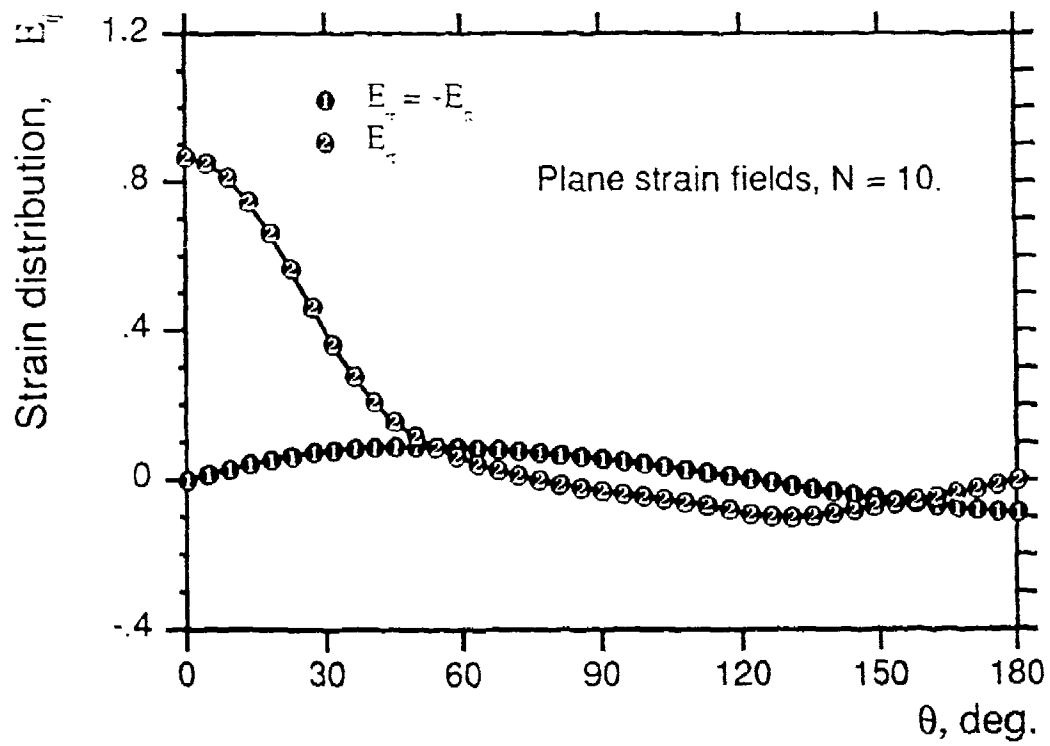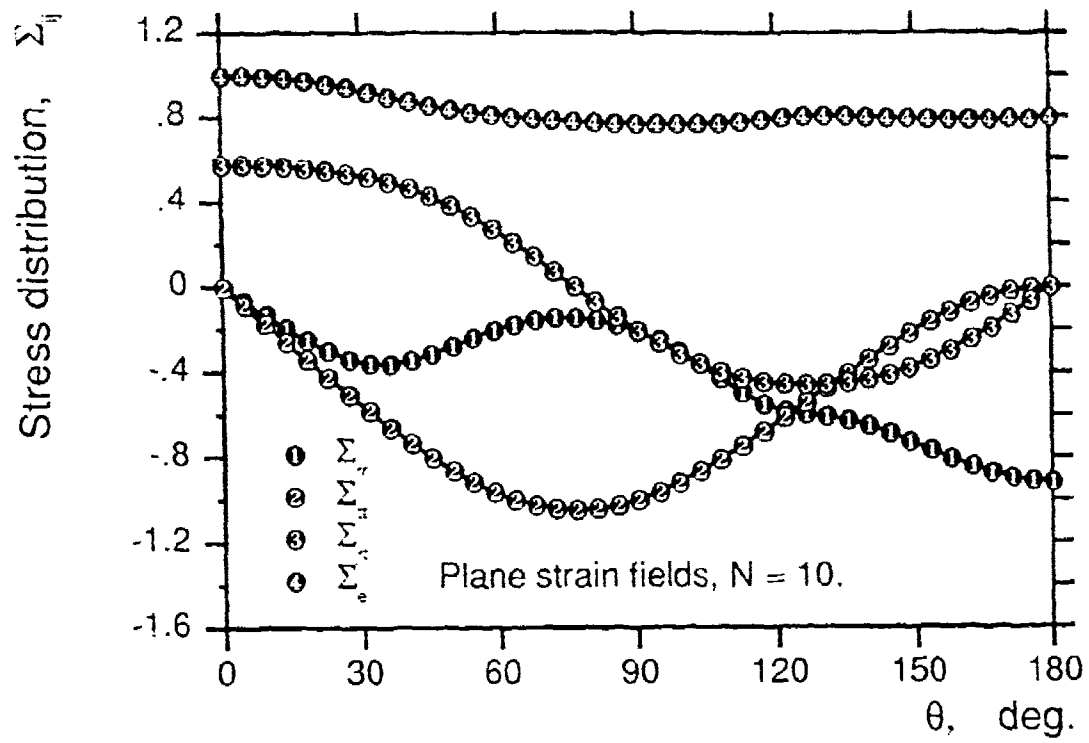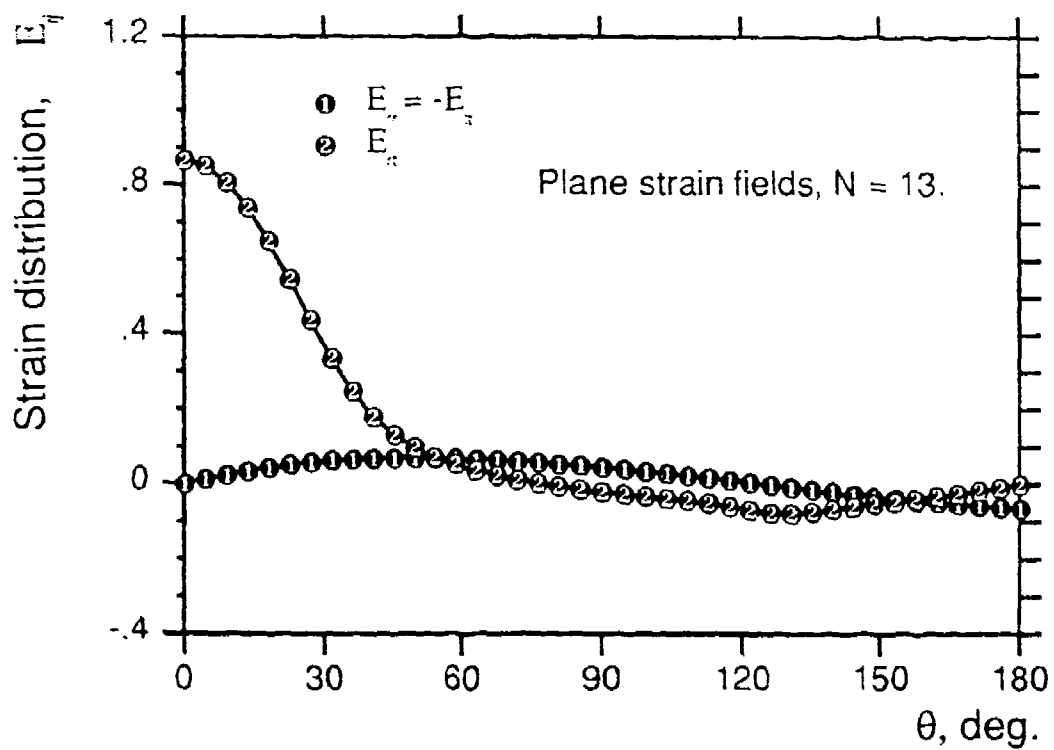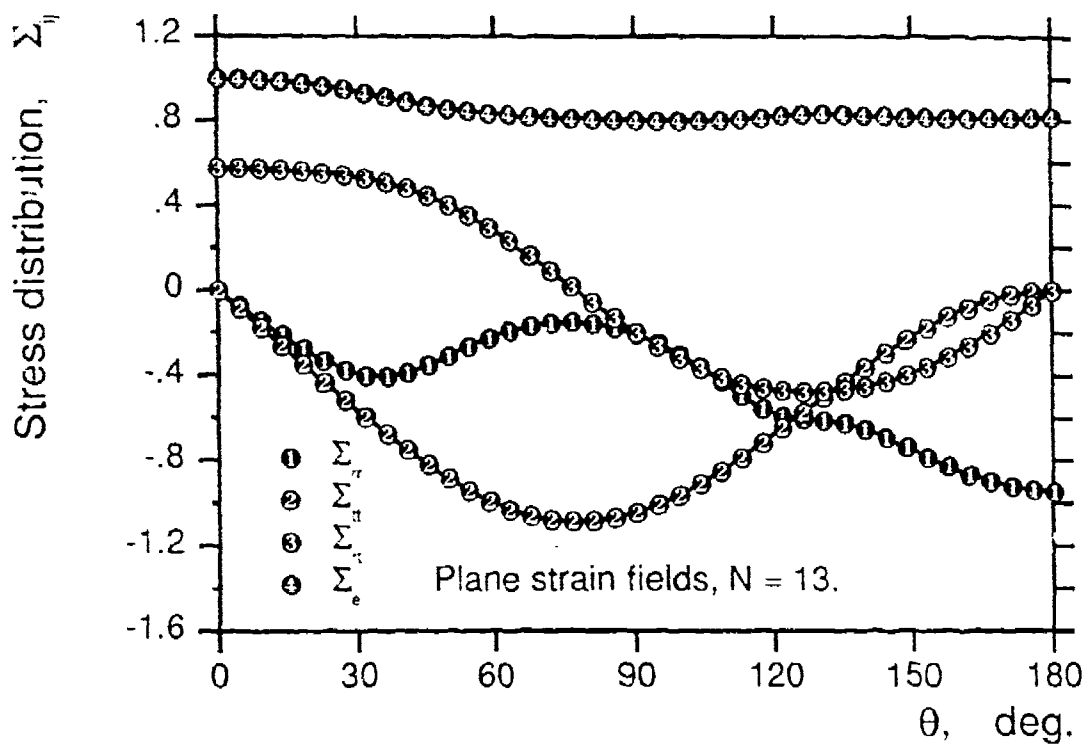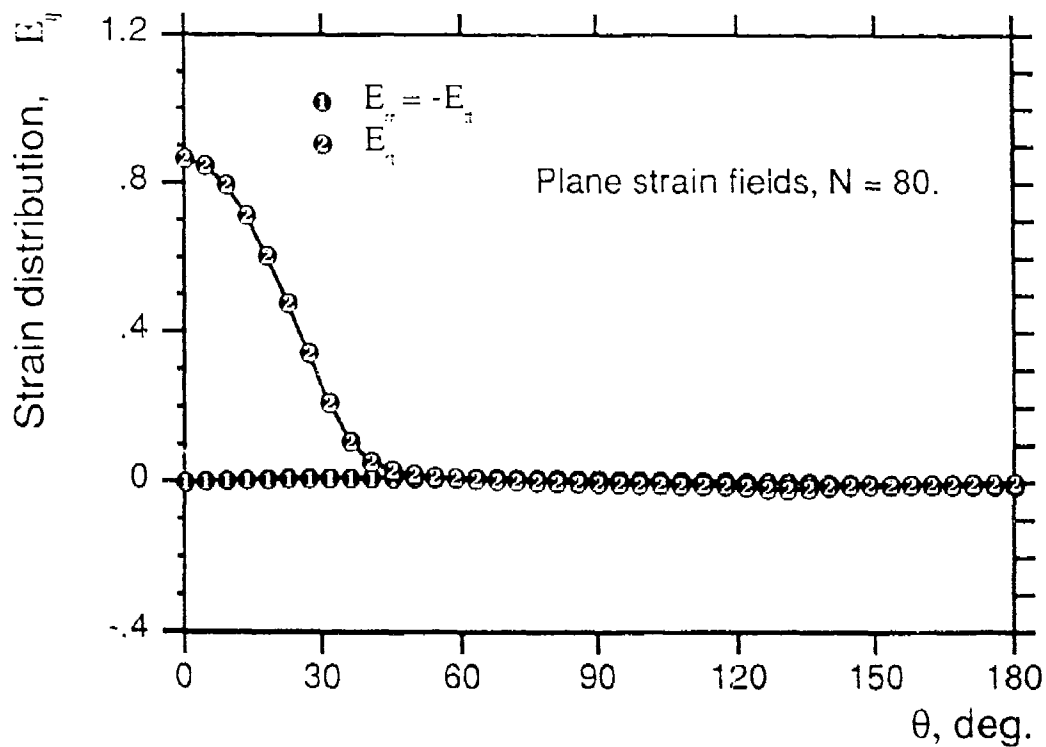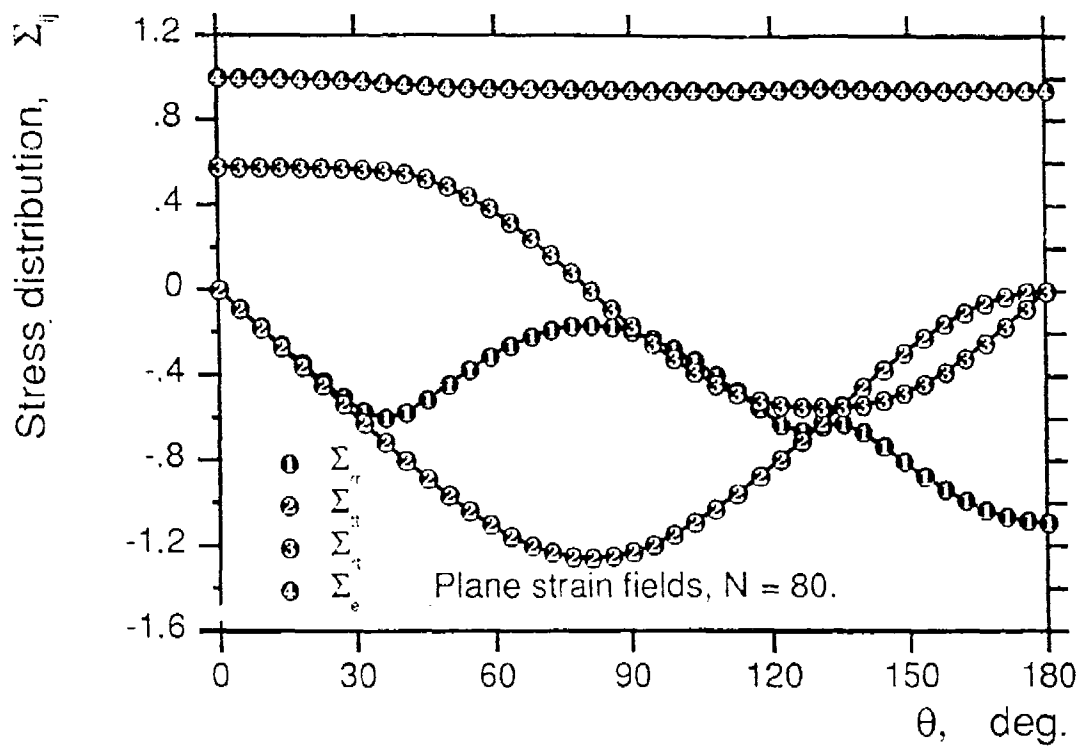
Figure 8f

Figure 8g

Figure 8. HRR stress and strain fields for Mode II crack in plane strain
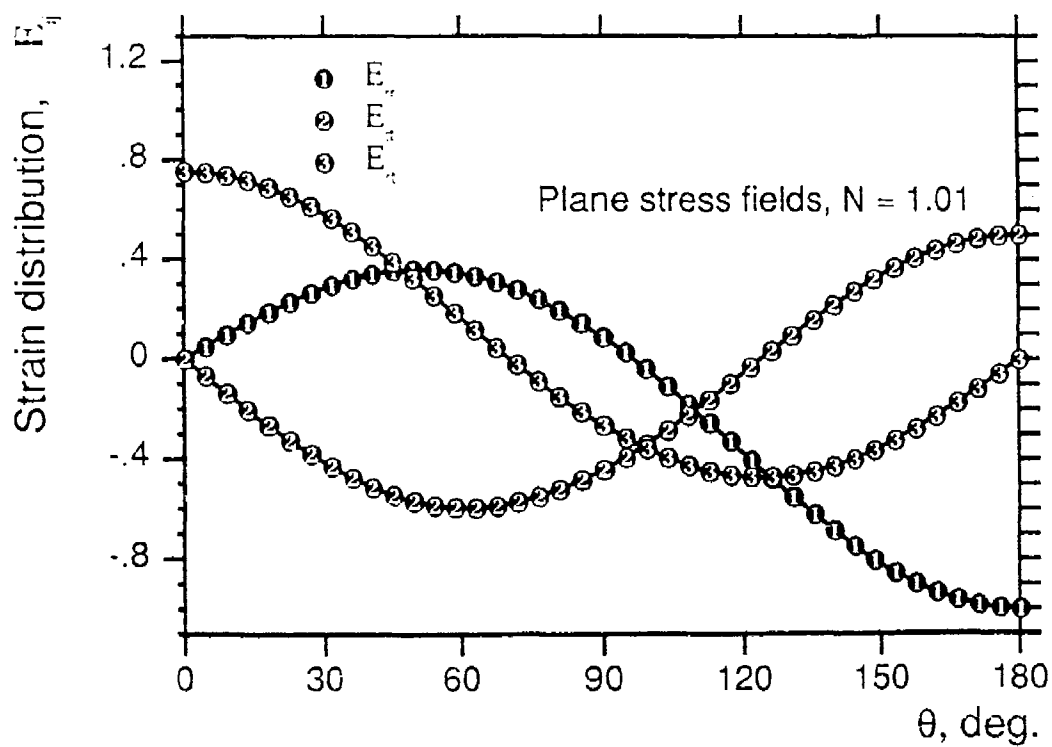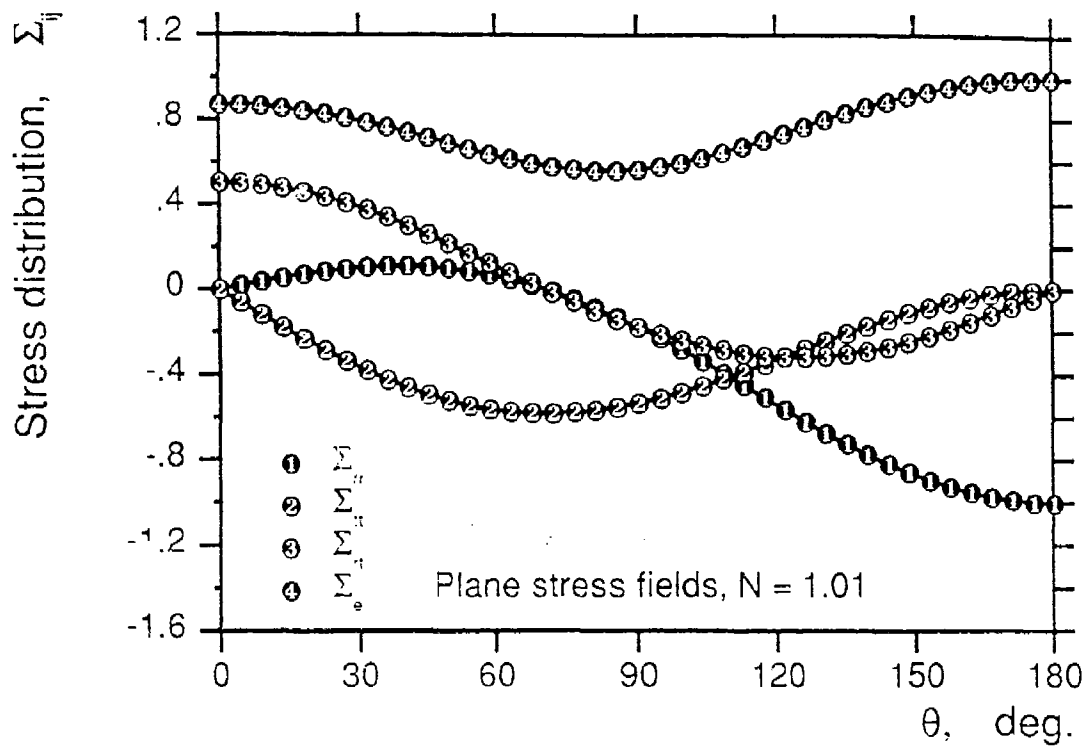
Figure 9a

Figure 9b

Figure 9c

Plane stress fields, N = 7.
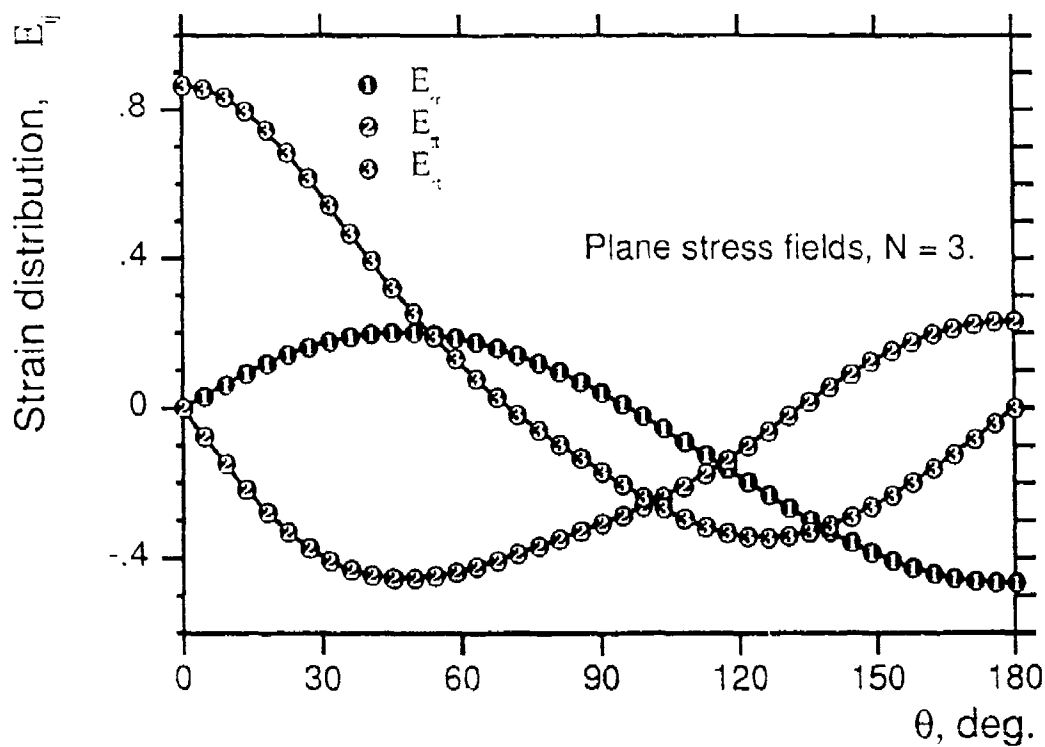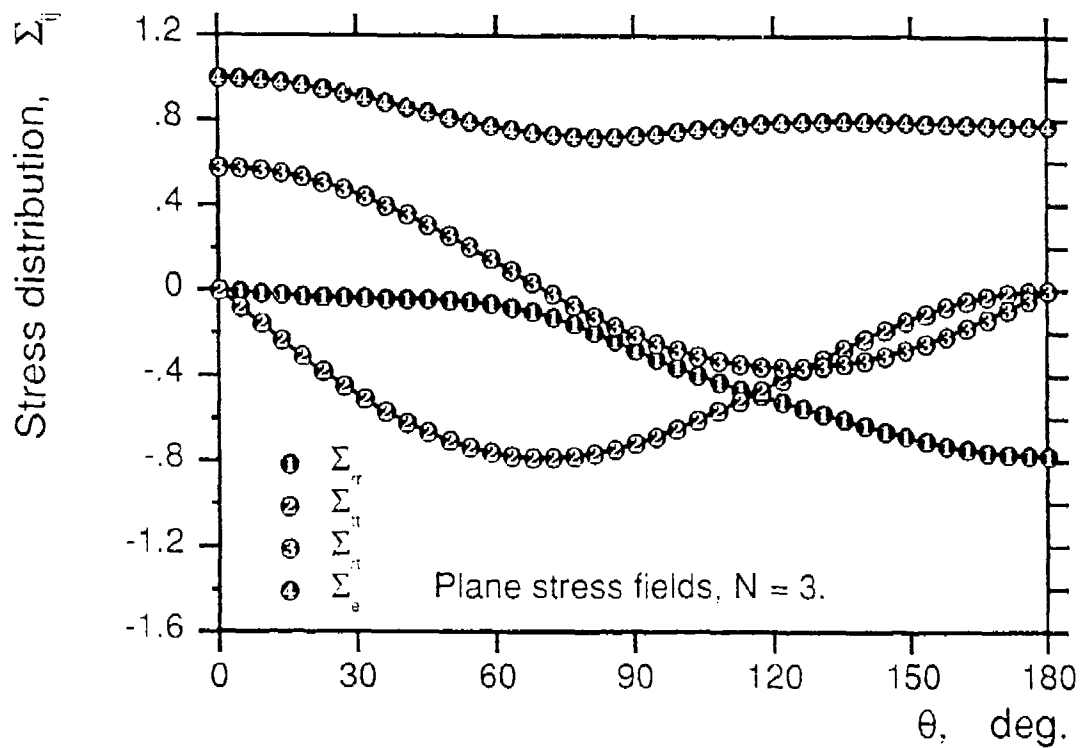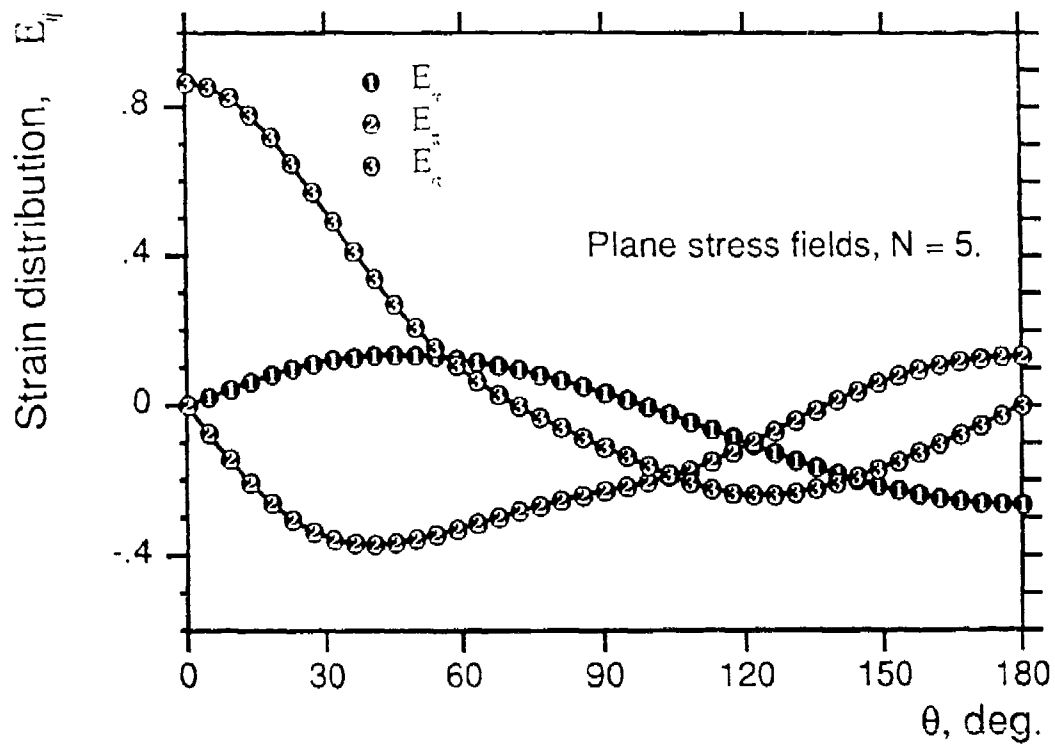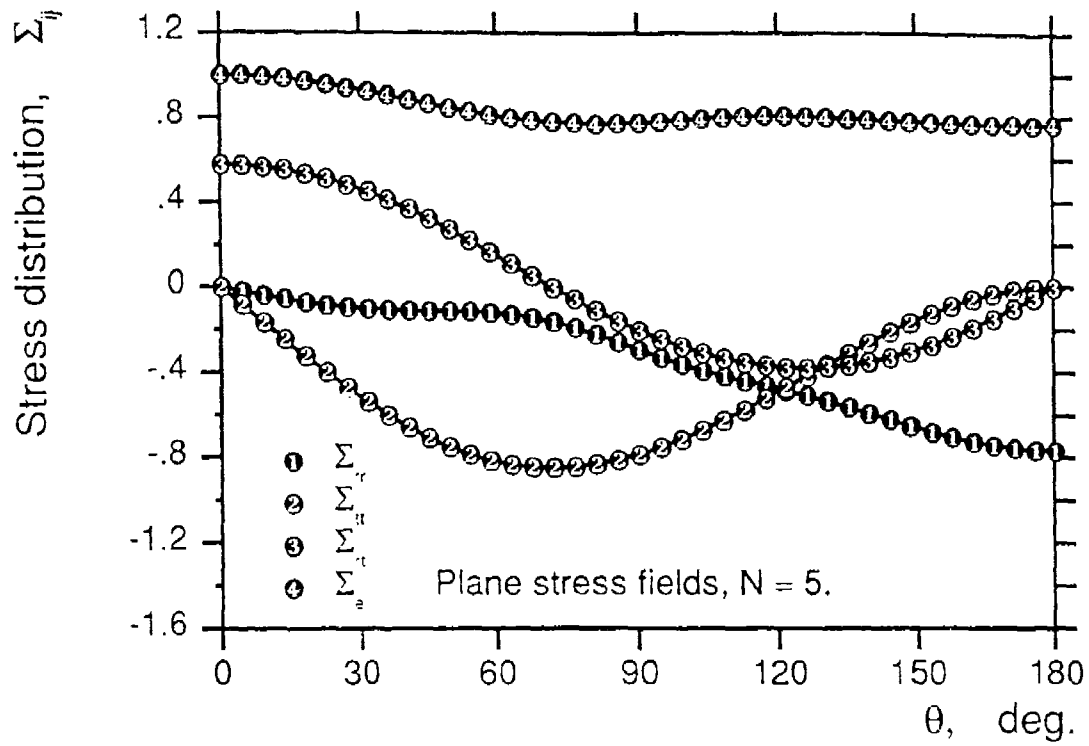
Plane stress fields, N = 7.
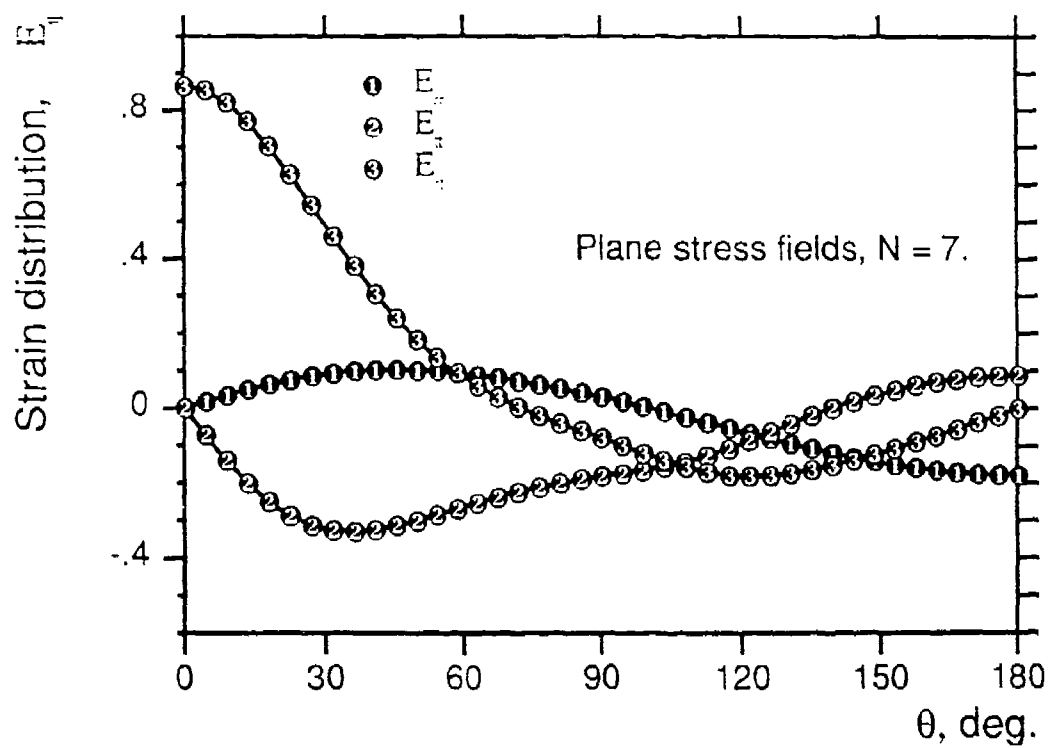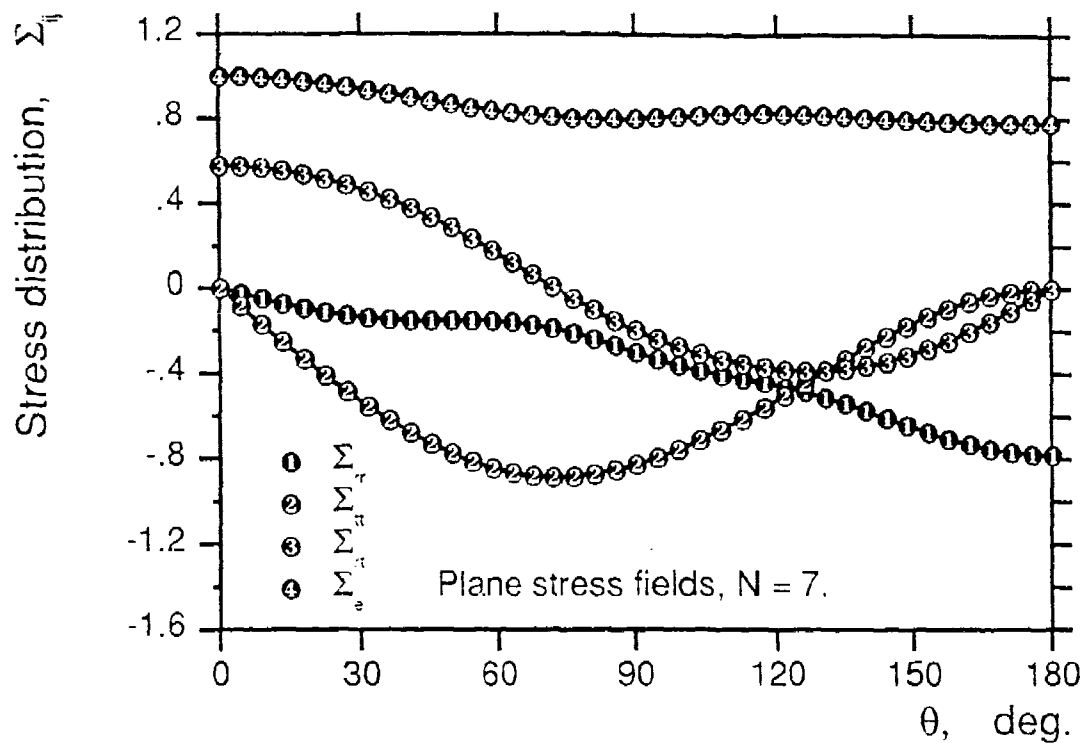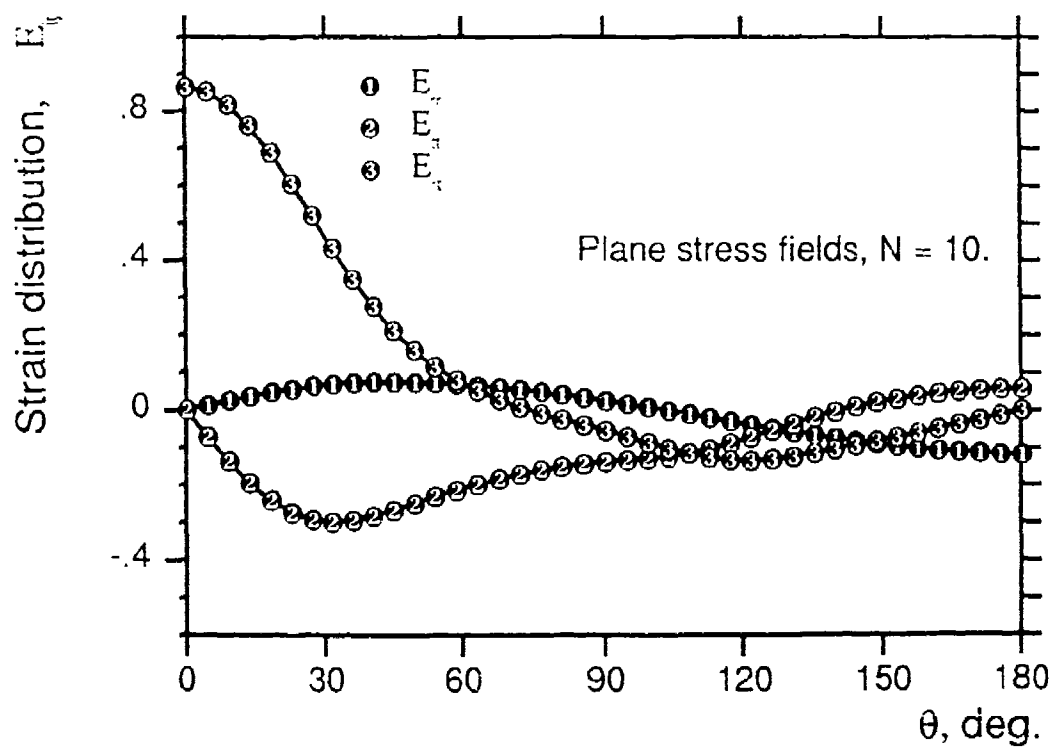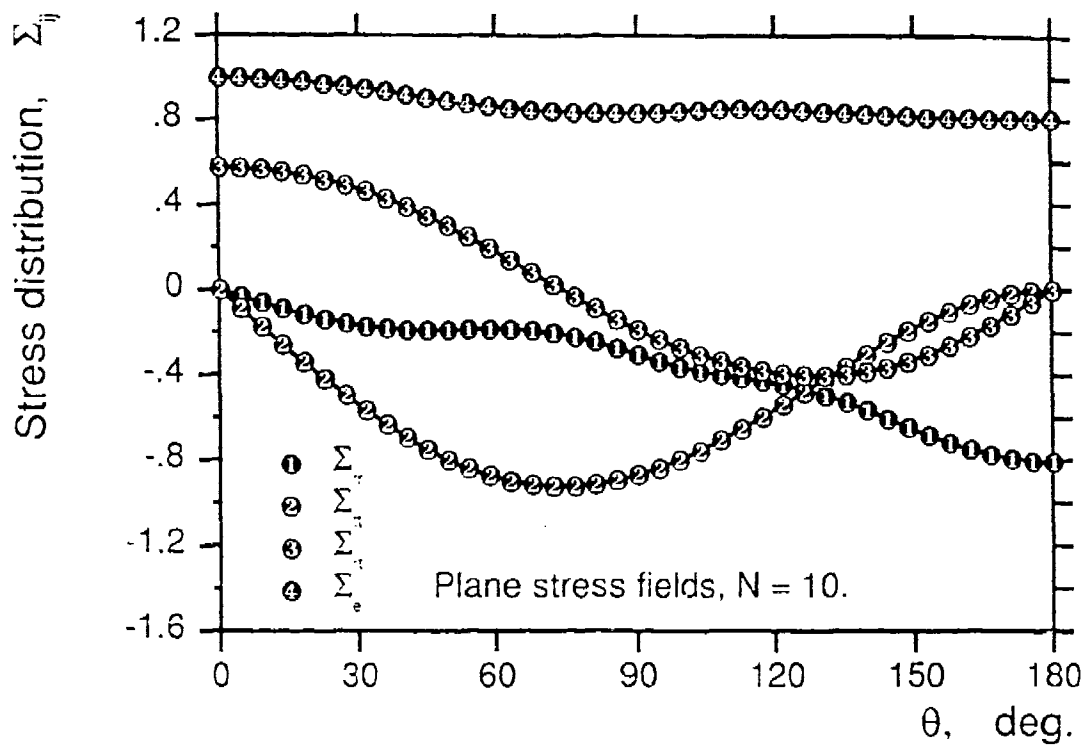
Figure 9d

Figure 9e

Figure 9f

Figure 9g

Figure 9. HRR stress and strain fields for Mode II crack in plane stress

Figure 10. Variation of the I(N)-factor versus N for plane strain and plane stress.

Figure 11. Stress-strain curves for technically pure iron in shear tests at different strain rates (data of Klepaczko, 1969).

Figure 12. (a) Rate sensitivity of the lower yield stress in shear for mild steel and technically pure iron;
(b) Rate sensitivity of constants in the Ramberg-Osgood equation for technically pure iron.

Stress, σ [MPa]

1600

1400

1200

1000

800

600

400

200

0

❶ ε̇ = 4.x10⁻¹ s
❷ ε̇ = 8.x10⁻² s
❸ ε̇ = 1.5 s
❹ ε̇ = 20. s

Ti6Al4V

0   .01   .02   .03   .04   .05   .06   .07   .08

Strain, ε

Figure 13. Stress-strain curves for titanium Ti6Al4V alloy from compression tests at different strain rates (data of Maiden and Green, 1966).

Figure 14. Rate sensitivity of the yield stress in shear and material constants in the Ramberg-Osgood equation for Ti6Al4V alloy.

Figure 15. Stress-strain curves for Al 6061-T6 alloy from compression tests at different strain rates (after Maiden and Green, 1966). Conversion factor for stress: 1 ksi = 6.895 MPa.

Figure 16. Rate sensitivity of the yield stress in shear for Al 6061-T6 alloy (data of Jiang and Chen, 1974).
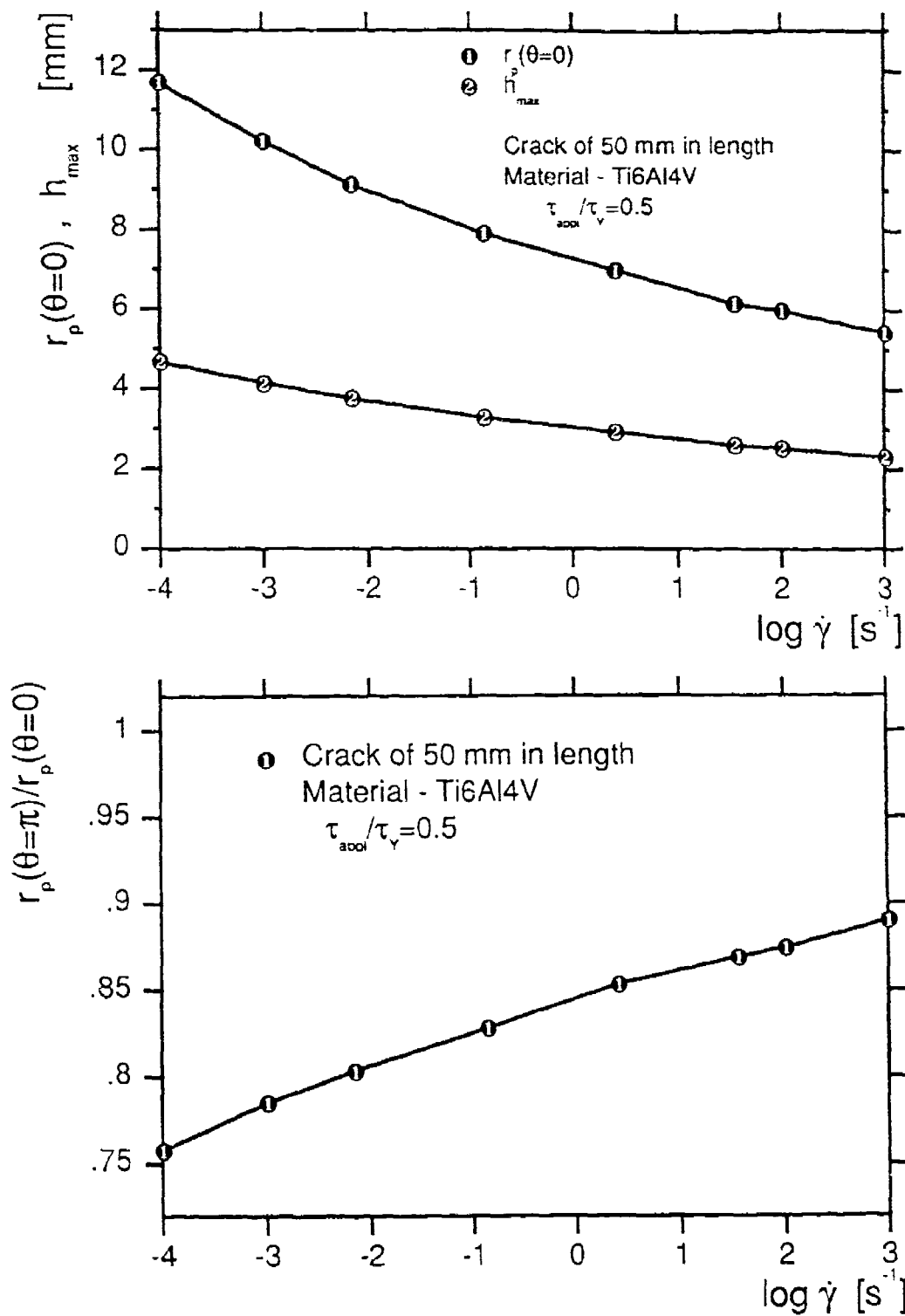
Figure 17a

Figure 17b

Figure 17. Variation of parameters which characterize the geometry of plastic zone near the crack tip versus logarithm of strain rate for a semi-infinite crack in mild steel: (a) $\tau_{appl}/\tau_{YS}=0.2$; (b) $\tau_{appl}/\tau_{YS}=0.5$.
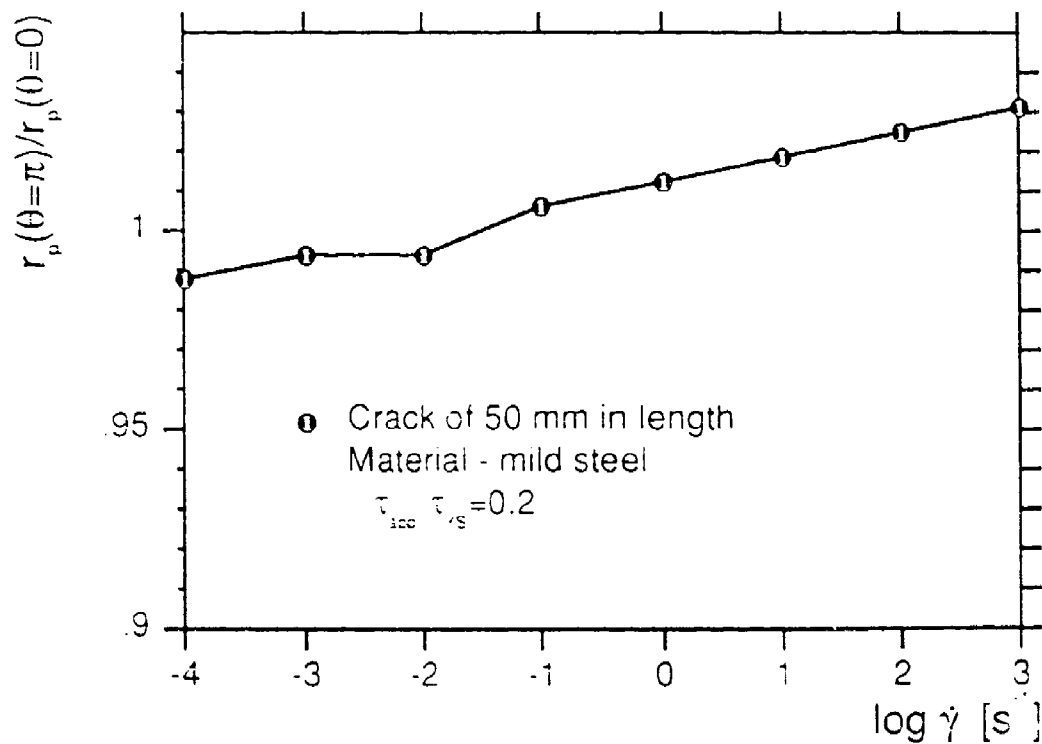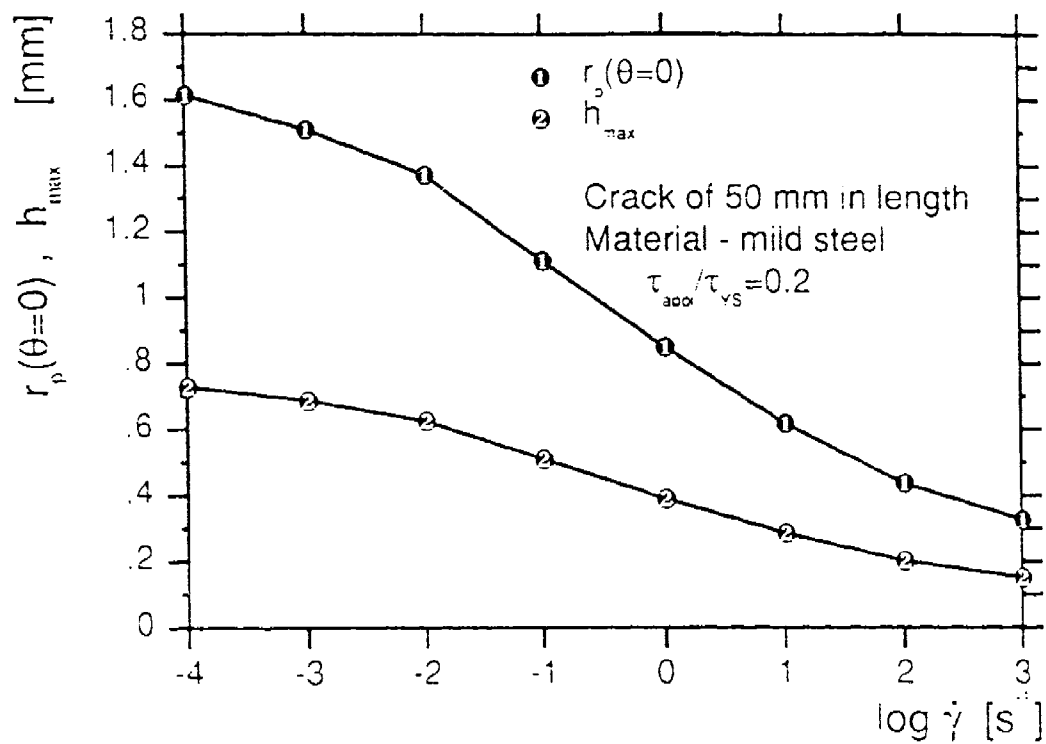
Figure 18a
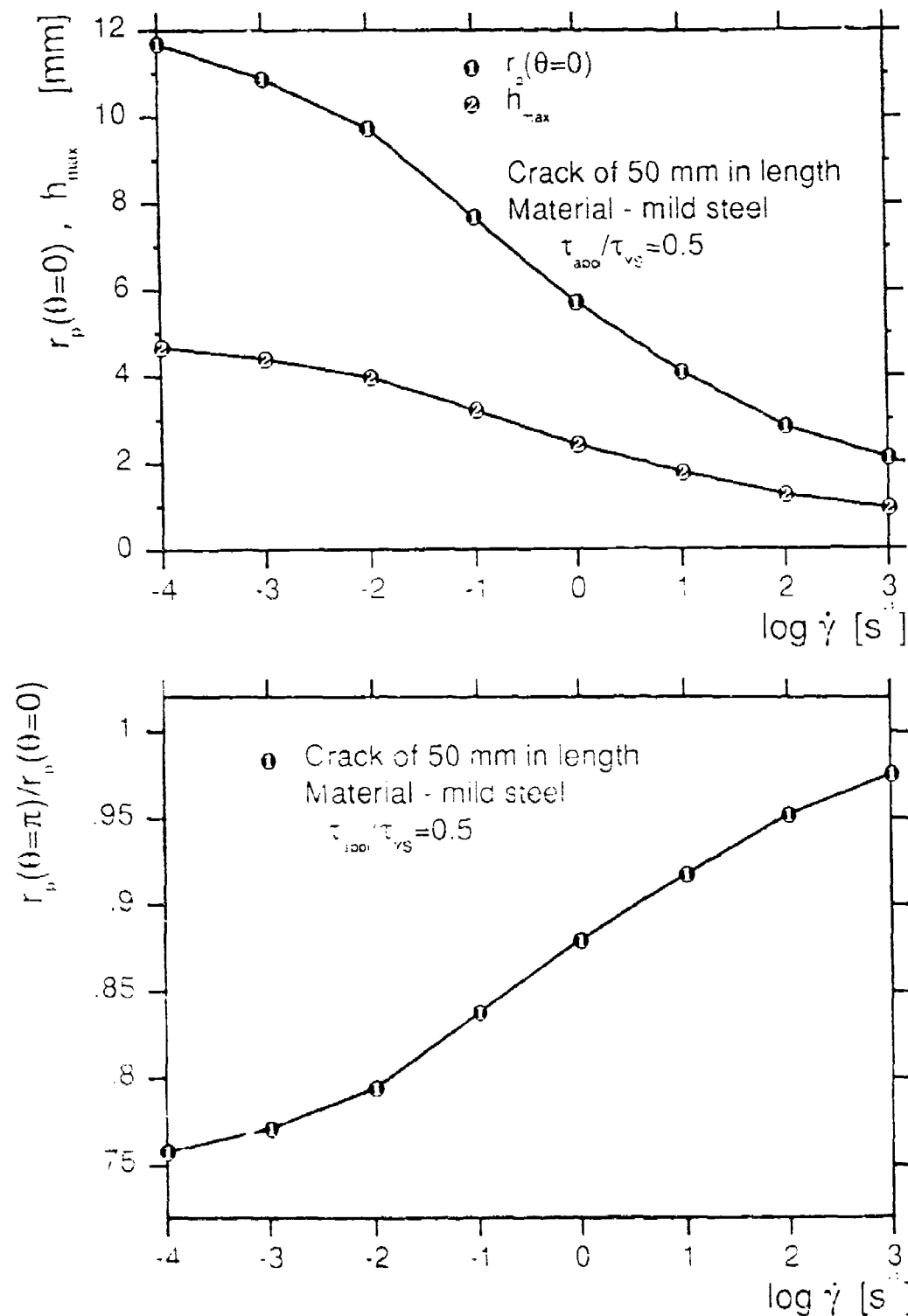
Figure 18b

Figure 18. Variation of parameters which characterize the geometry of plastic zone near the crack tip versus logarithm of strain rate for a finite length edge crack in mild steel: (a) $\tau_{appl}/\tau_{YS}=0.2$; (b) $\tau_{appl}/\tau_{YS}=0.5$.
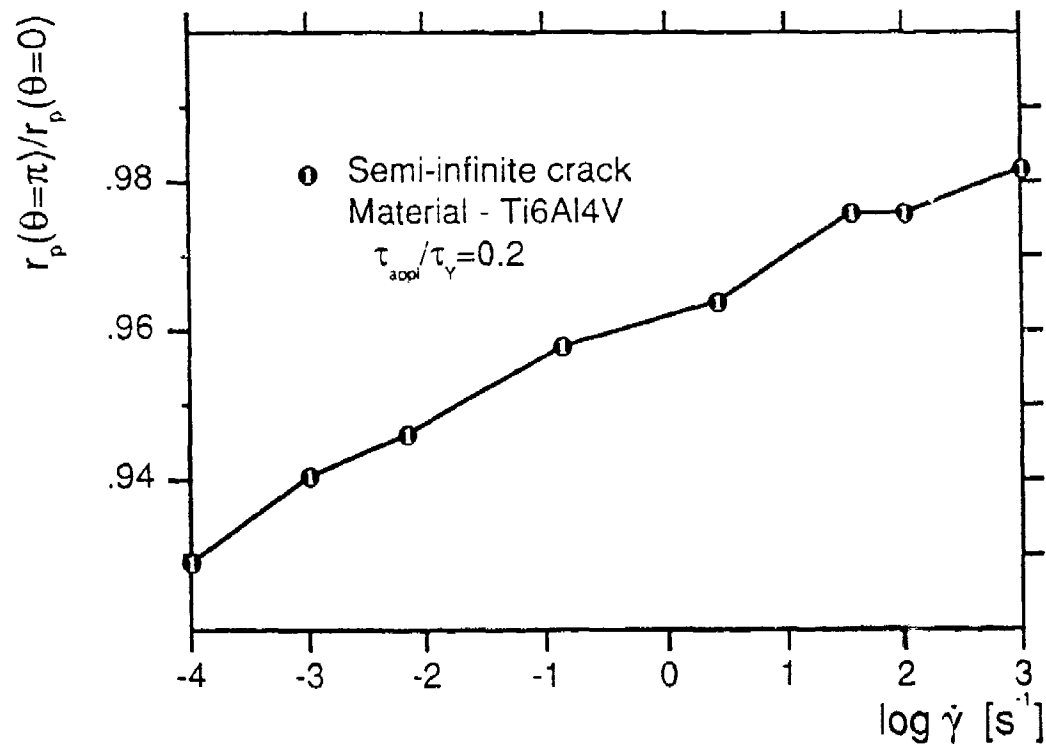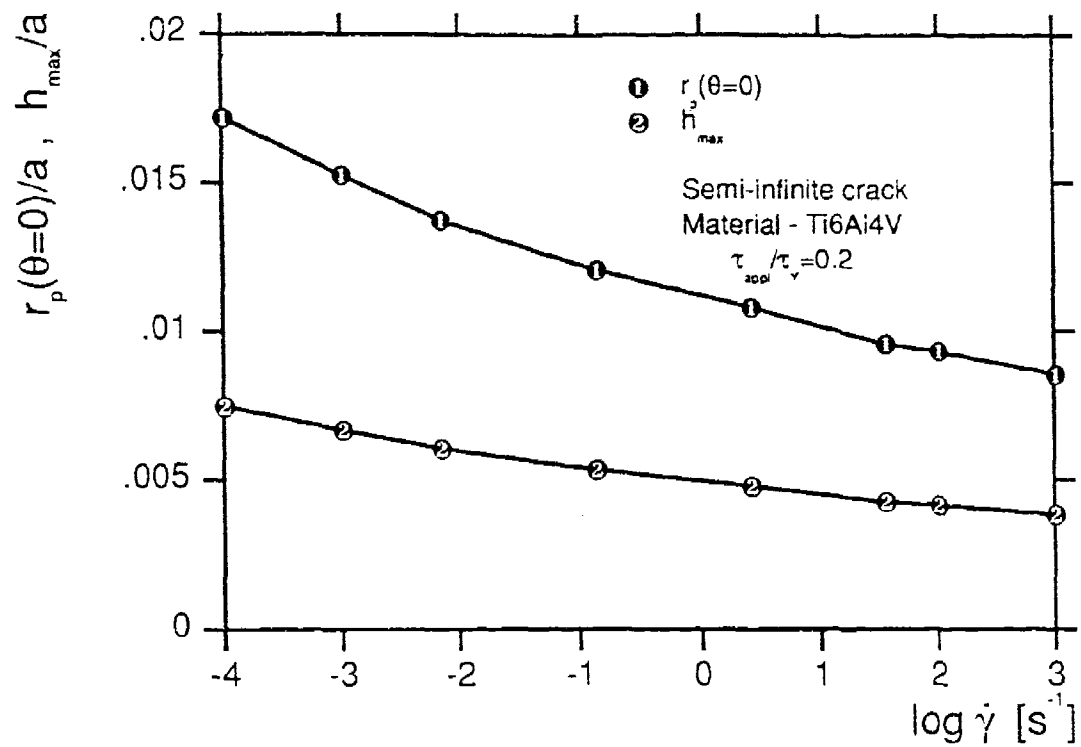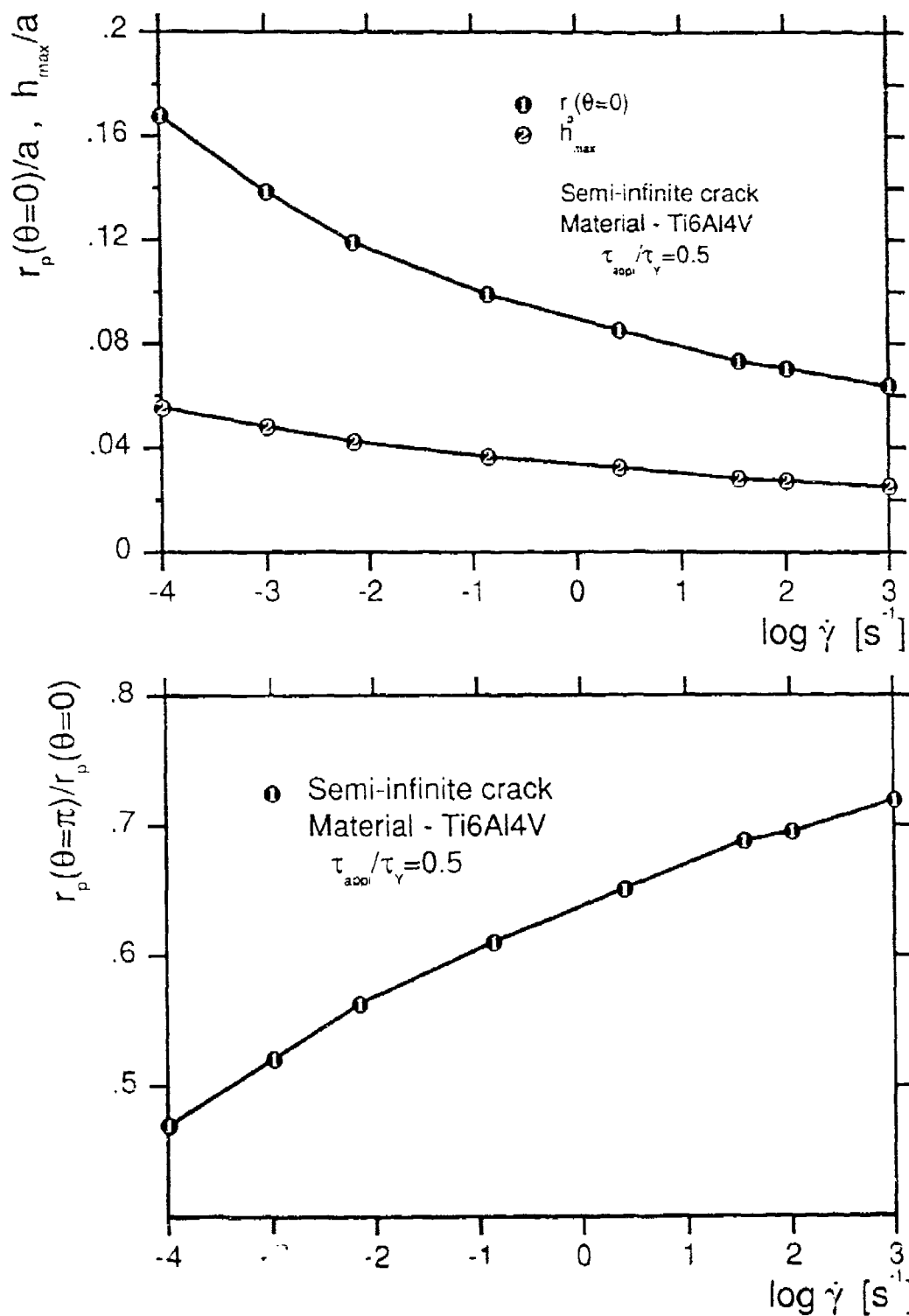
Figure 19a

**Figure 19b**

Figure 19. Variation of parameters which characterize the geometry of plastic zone near the crack tip versus logarithm of strain rate for a semi-infinite crack in Ti6Al4V alloy: (a) $\tau_{appl}/\tau_{YS}=0.2$; (b) $\tau_{appl}/\tau_{YS}=0.5$.
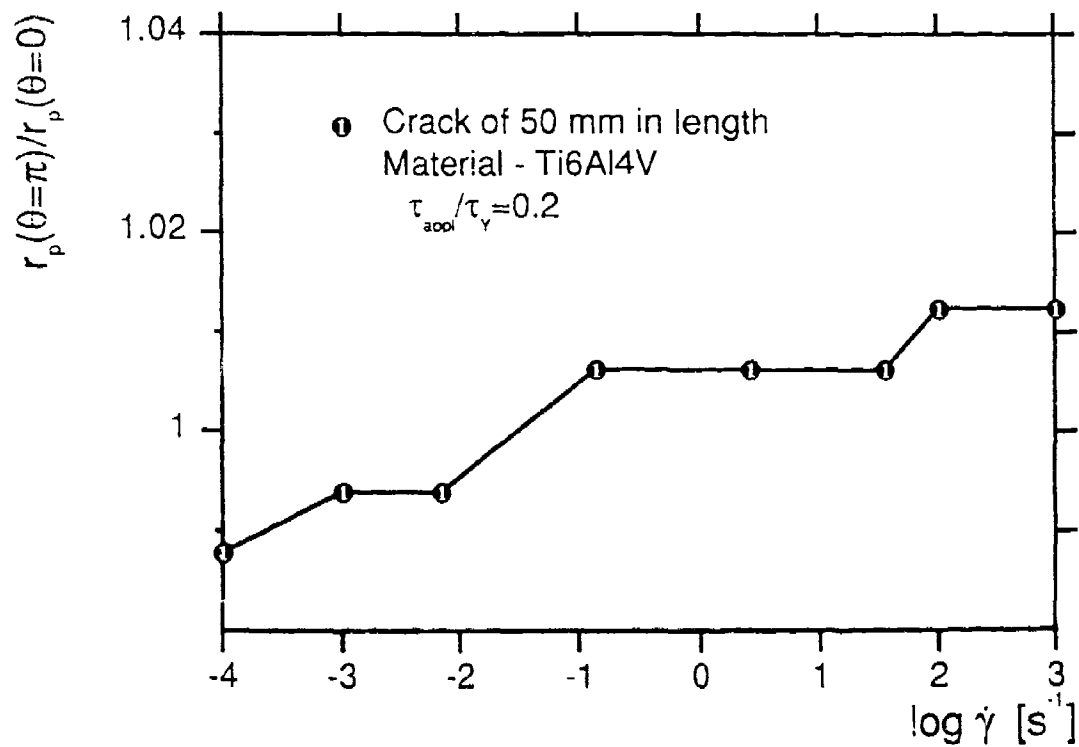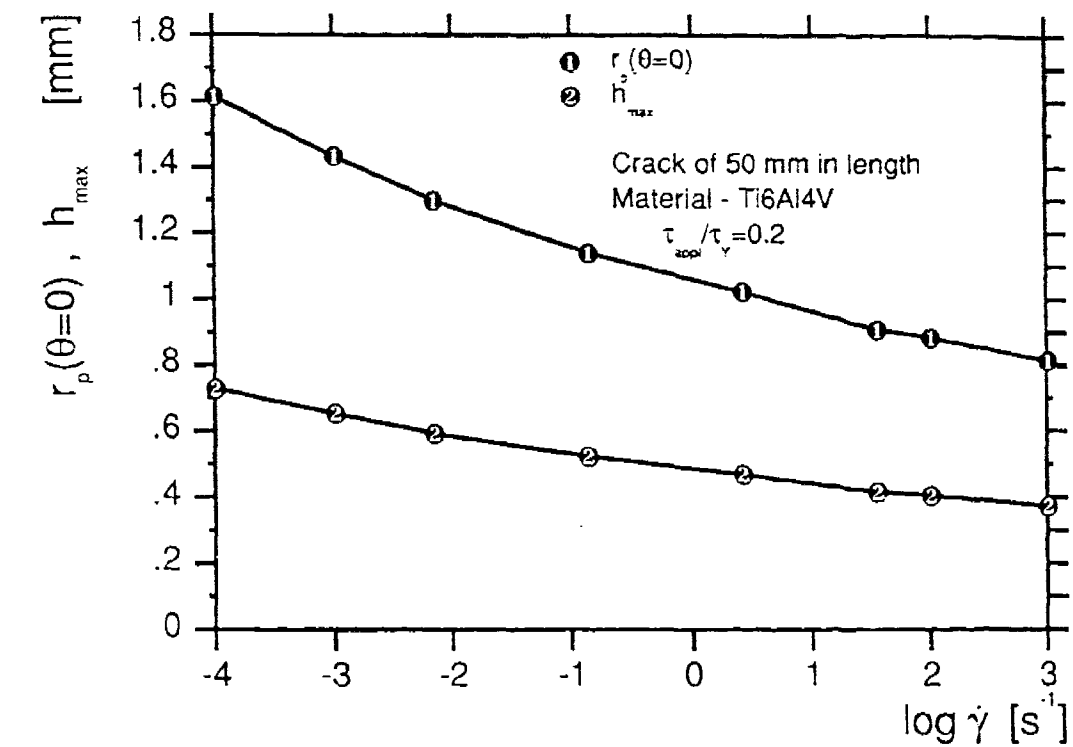
Figure 20a

Figure 20b

Figure 20. Variation of parameters which characterize the geometry of plastic zone near the crack tip versus logarithm of strain rate for a finite length edge crack in Ti6Al4V alloy: (a) $\tau_{appl}/\tau_{YS}=0.2$; (b) $\tau_{appl}/\tau_{YS}=0.5$.
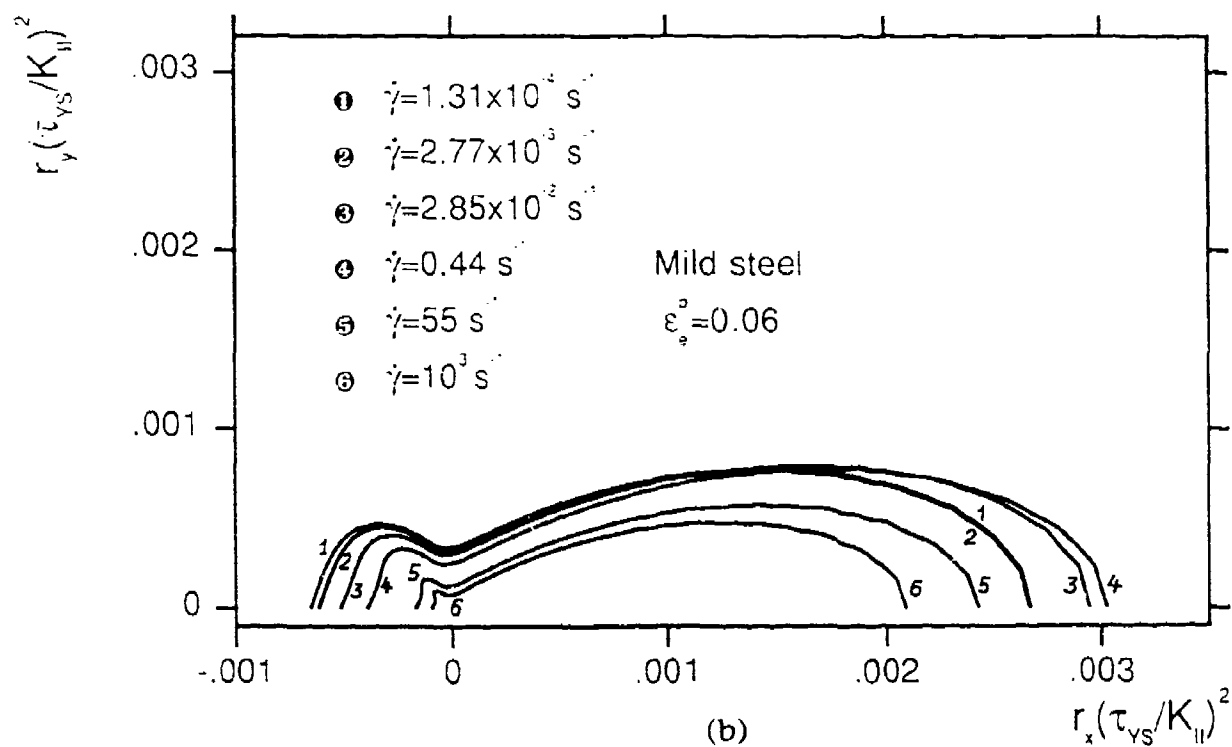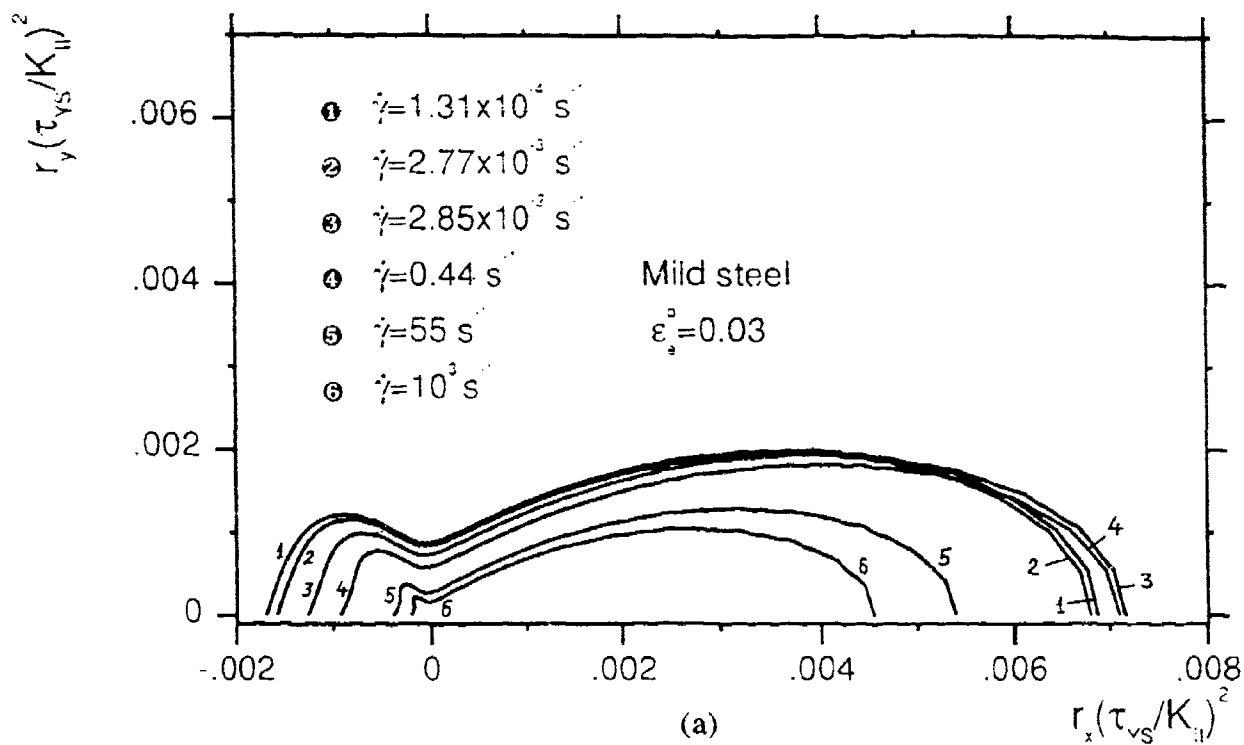
Figure 21. Boundaries of equal equivalent plastic strain at the crack tip in Mode II in mild steel versus strain rate: (a) $\varepsilon_e^p = 0.03$; (b) $\varepsilon_e^p = 0.06$.
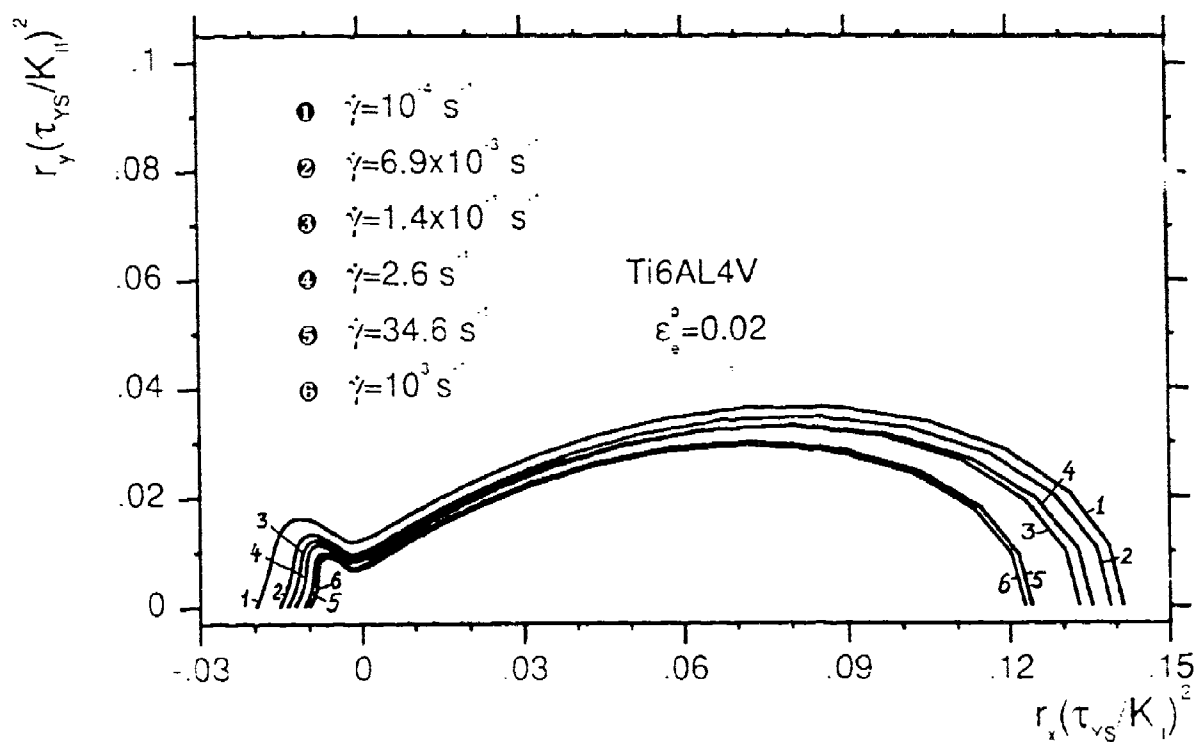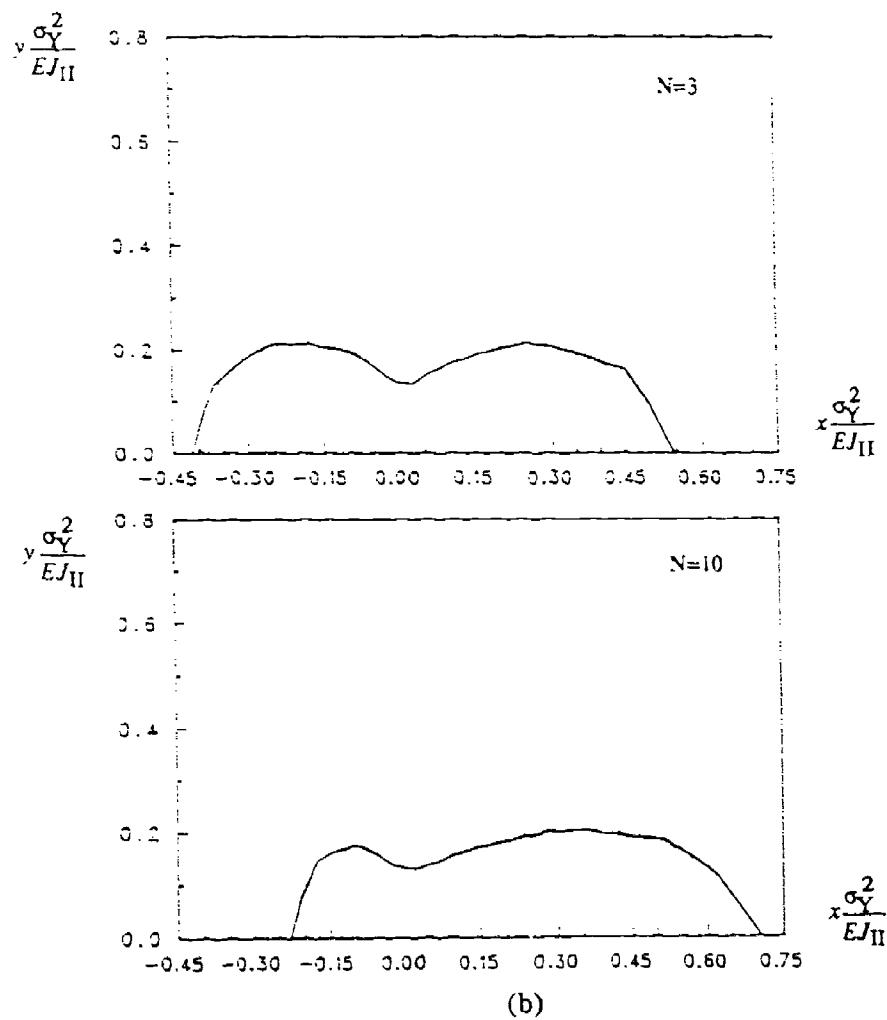
Figure 22. Boundaries of equal equivalent plastic strain at the crack tip in Mode II in Ti6Al4V alloy versus strain rate, $\varepsilon_e^p = 0.02$.
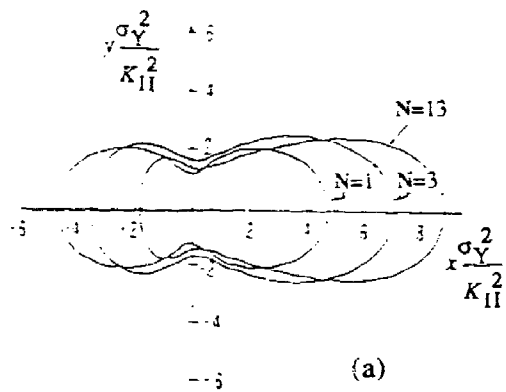
$y\dfrac{\sigma_Y^2}{K_{II}^2}$

$x\dfrac{\sigma_Y^2}{K_{II}^2}$

N=13

N=1   N=3

(a)

$y\dfrac{\sigma_Y^2}{EJ_{II}}$

N=3

$x\dfrac{\sigma_Y^2}{EJ_{II}}$

$y\dfrac{\sigma_Y^2}{EJ_{II}}$

N=10

$x\dfrac{\sigma_Y^2}{EJ_{II}}$

(b)

Figure 23. Finite-element solutions on variation of the plastic zone boundary versus strain hardening exponent at the crack tip in Mode II: (a) after Shih (1974); (b) after Pan and Shih (1990).
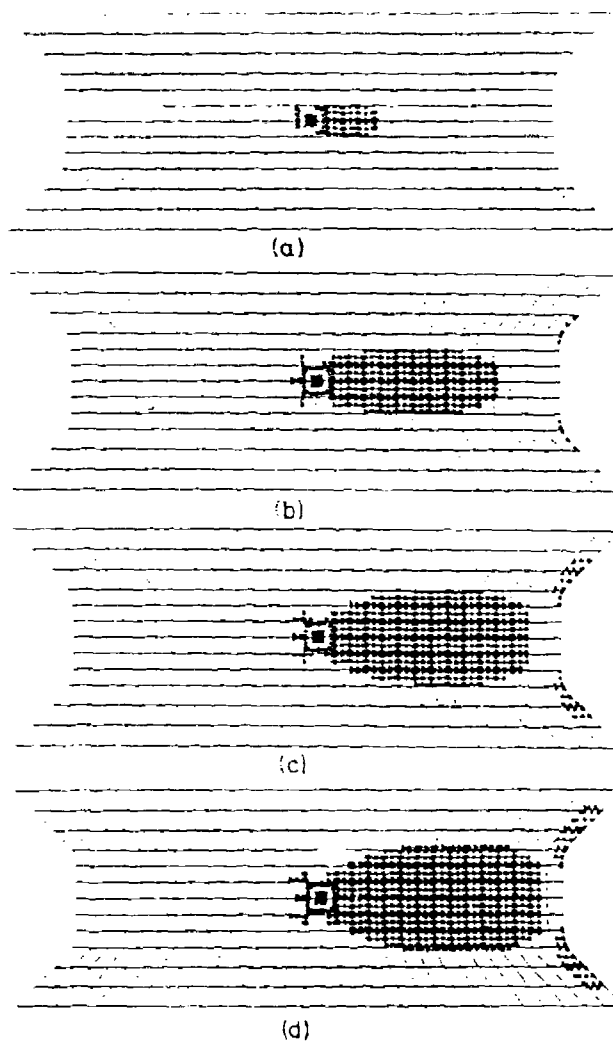
Figure 24. Finite-element solution on variation of the plastic zone boundary versus load level at the crack tip in Mode II (after Banks-Sills and Sherman, 1990): (a) $\tau_{appl}/\tau_{YS} = 0.35$; (b) $\tau_{appl}/\tau_{YS} = 0.45$; (c) $\tau_{appl}/\tau_{YS} = 0.48$; (d) $\tau_{appl}/\tau_{YS} = 0.52$.
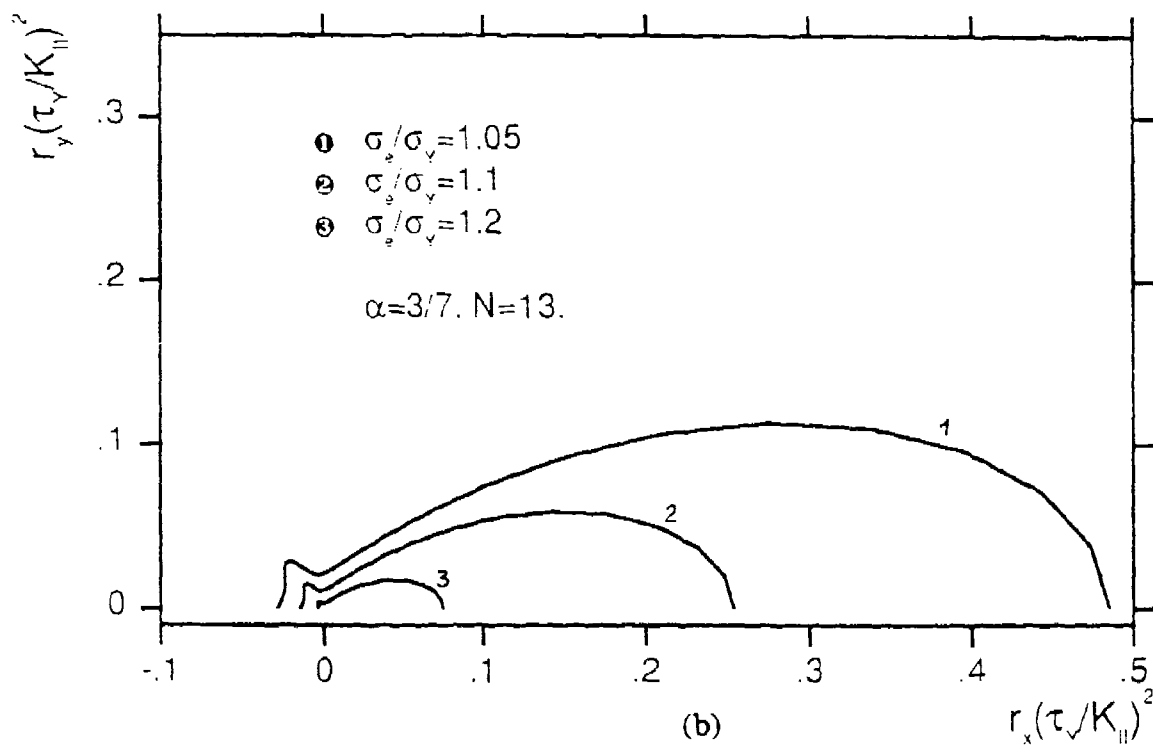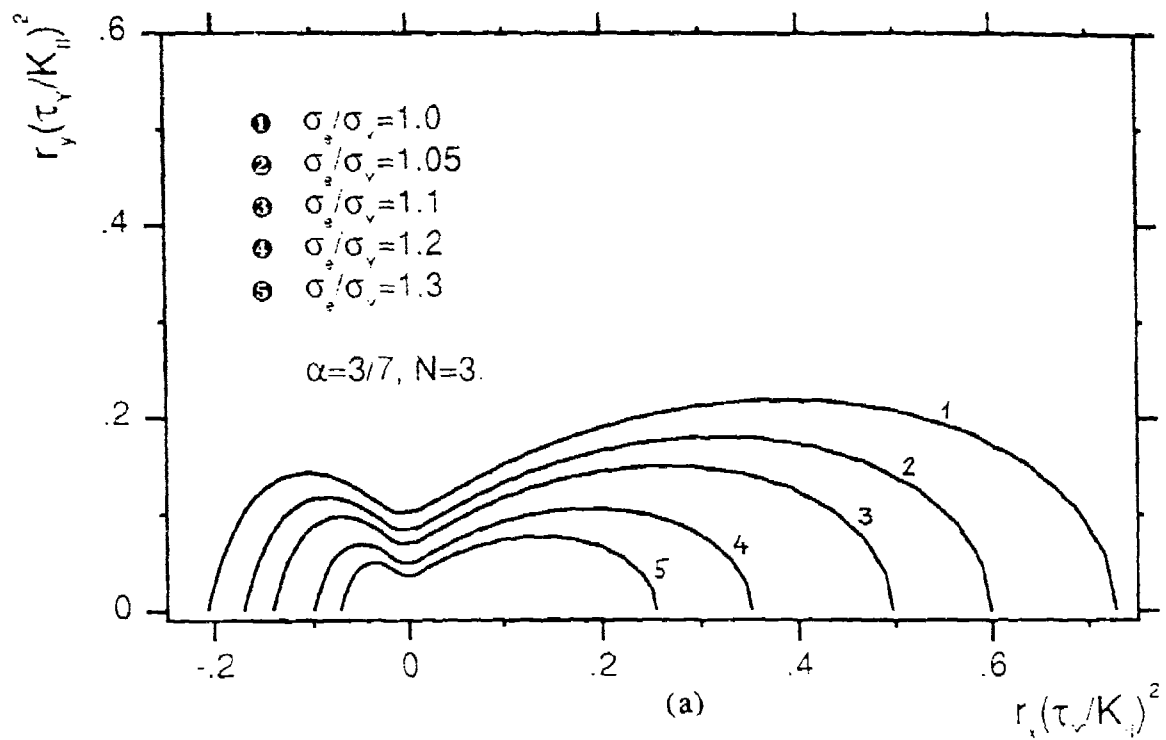
Figure 25. Boundaries of equal equivalent stress at the crack tip in Mode II for $\alpha=3/7$, N=3 (a) and N=13 (b).
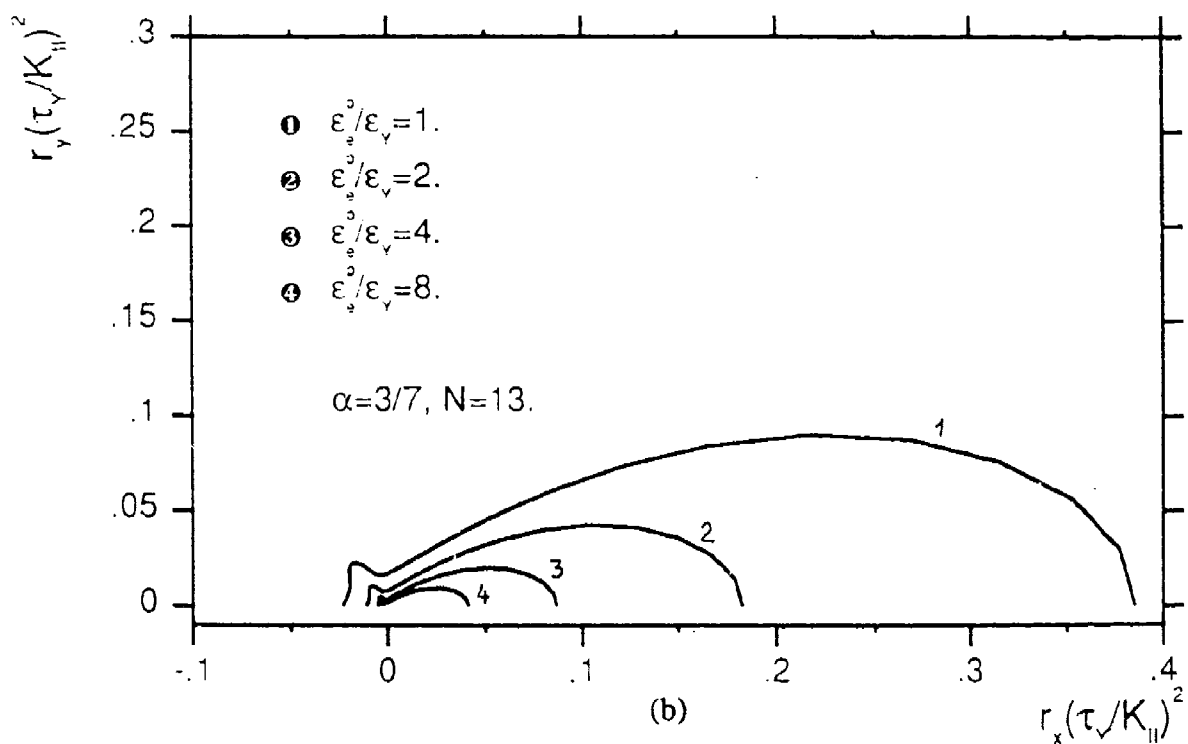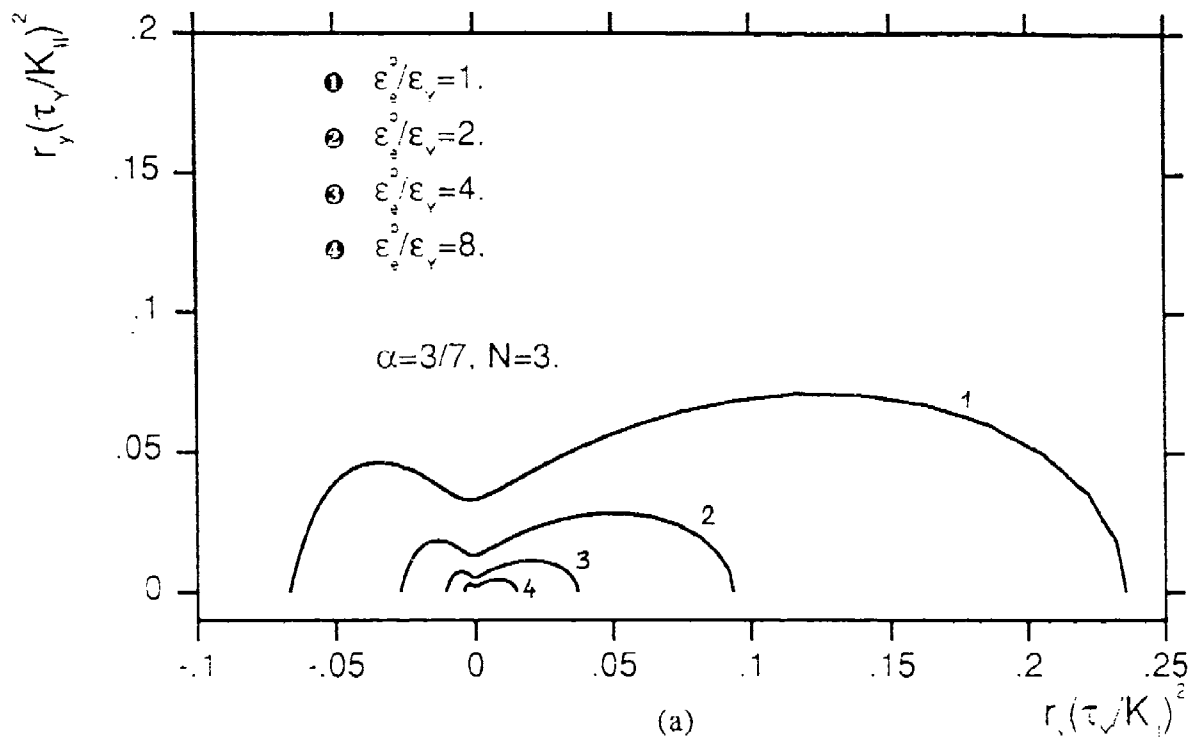
Figure 26. Boundaries of equal equivalent plastic strain at the crack tip in Mode II for $\alpha=3/7$, $N=3$ (a) and $N=13$ (b).